

Copy #32

NASA
UARL G910461-24

MI

SECOND ANNUAL PROGRESS REPORT

ANALYTICAL STUDY OF CATALYTIC REACTORS FOR HYDRAZINE DECOMPOSITION

GPO PRICE \$ _____
CFSTI PRICE(S) \$ _____
Hard copy (HC) 3.00
Microfiche (MF) .65

by
Arthur S. Kesten

ff 653 July 65

prepared for

NATIONAL AERONAUTICS AND SPACE ADMINISTRATION

May, 1968

CONTRACT NAS 7-458



United Aircraft Research Laboratories

UNITED AIRCRAFT CORPORATION
**U
A
C**
EAST HARTFORD, CONNECTICUT

68-36029
(ACCESSION NUMBER)
86 (PAGES)
CR-97097 (NASA CR OR TMX OR AD NUMBER)
CR-97097
(THRU) _____
(COPY) 28
(CATEGORY) _____
FACILITY FORM 602

NASA
UURL G910461-24

SECOND ANNUAL PROGRESS REPORT

**ANALYTICAL STUDY OF CATALYTIC
REACTORS FOR HYDRAZINE
DECOMPOSITION**

by
Arthur S. Kesten

prepared for
NATIONAL AERONAUTICS AND SPACE ADMINISTRATION

May, 1968

CONTRACT NAS 7-458

United Aircraft Research Laboratories

U
UNITED AIRCRAFT CORPORATION
A
EAST HARTFORD, CONNECTICUT

Analytical Study of Catalytic Reactors

for Hydrazine Decomposition

Second Annual Progress Report

April 15, 1967 - April 14, 1968

Contract No. NAS 7-458

TABLE OF CONTENTS

	<u>Page</u>
ABSTRACT	i
FOREWORD	ii
SUMMARY	1
INTRODUCTION	3
DISCUSSION	4
<u>Integral Analysis of Processes Occurring within Catalyst Particles</u>	4
<u>Use of Integral Analysis in One-Dimensional Steady State Model</u>	9
<u>One-Dimensional Steady-State Program</u>	11
<u>Two-Dimensional Steady-State Model</u>	12
<u>Results of Calculations Using the Two-Dimensional Steady State Program</u>	15
REFERENCES	19
LIST OF SYMBOLS	20
APPENDIX I	23
APPENDIX II	26
FIGURES	33-86

ABSTRACT

As part of a continuing effort under Contract NAS 7-458, an analytical study of catalyzed hydrazine decomposition reaction chambers was performed to assess the effects on the steady-state behavior of the system of nonuniform radial injection and of catalyst bed configurations exhibiting both radial and axial nonuniformities. Radial variations in mass flow rate or bed packing cause radial temperature and concentration gradients which lead to turbulent diffusion of heat and mass in the reactor system. A computer program was developed to calculate temperature and reactant concentration distributions as functions of axial and radial position in typical hydrazine reaction chambers. The program is based upon a model of the reactor system which includes treatment of the turbulent diffusion of heat and mass in the free-gas phase along with heat and mass diffusion within the catalyst particles and between the particles and the free-gas phase. Both thermal and catalytic decomposition of the reactants are considered. Included in this report are descriptions of the turbulent diffusion phenomena, the reactor model which treats these phenomena and typical results calculated on the basis of this model.

FOREWORD

This work was performed by United Aircraft Research Laboratories for the National Aeronautics and Space Administration under Contract NAS 7-458 initiated April 15, 1966.

Included among those who cooperated in performance of the work under Contract NAS 7-458 were Dr. A. S. Kesten, Program Manager, Dr. W. G. Burwell, Chief, Kinetics and Thermal Sciences Section, Mr. D. B. Smith, and Mrs. E. Smith of UARL.

This work was conducted under program management of the NASA Chief, Liquid Propulsion Experimental Engineering Systems, NASA Headquarters, Washington, D. C., and the Technical Manager was Mr. T. W. Price, Jet Propulsion Laboratory, Pasadena, California.

Analytical Study of Catalytic Reactors

for Hydrazine Decomposition

Second Annual Progress Report

April 15, 1967 - April 14, 1968

Contract No. NAS 7-458

SUMMARY

The Research Laboratories of United Aircraft Corporation under Contract NAS 7-458 with the National Aeronautics and Space Administration are performing an analytical study of catalytic reactors for hydrazine decomposition. This second annual technical report summarizes work performed under this continuing contract from April 15, 1967 to April 14, 1968. Work during this period has included the development of a computer program representing a two-dimensional steady-state model of a distributed-feed catalyzed hydrazine decomposition reaction chamber. This program was developed to assess the effects on the steady-state behavior of the system of nonuniform radial injection and of catalyst bed configurations exhibiting both radial and axial nonuniformities. The program is based upon a model of the reactor system which includes a treatment of the turbulent diffusion of heat and mass in the free-gas phase along with heat and mass diffusion within the catalyst particles and between the particles and the free-gas phase. Both thermal and catalytic decomposition of the reactants are considered. Calculations have been made of temperature and reactant concentration distributions as functions of axial and radial position in typical hydrazine reaction chambers for a number of injection profiles and catalyst bed configurations.

The integral equation method, developed during the first year of contract effort to describe the diffusional processes within the pores of the catalyst particles, has been modified to include the effects of heat and mass transfer from the bulk fluid, through a stagnant film surrounding the catalyst particles, and to the outside surface of the particles. An iterative procedure has been developed to solve the implicit integral equations describing reactant concentration and temperature profiles in the porous catalyst particles. A computer program representing this iterative procedure has been used as a subroutine in the two-dimensional steady-state program. This subroutine has also been used

in the one-dimensional program to define more precisely the kinetics of ammonia dissociation by comparing temperature and concentration profiles calculated using this program with available experimental information.

Empirical predictions have been developed of one-dimensional steady-state temperature and fractional ammonia dissociation profiles in hydrazine reactors packed with Shell 405 catalyst particles. The empirical correlations were developed on the basis of many runs made with the steady-state computer program developed during the first year of effort on the present contract. It was found that fractional ammonia dissociation and bulk fluid temperature are easily predicted for a broad range of operating conditions for cases in which most of the hydrazine decomposition occurs in the first few tenths of an inch of the reactor; this rapid hydrazine decomposition rate is associated with reactors packed with particles 25 mesh or smaller for approximately 0.2 inch of reactor bed length.

INTRODUCTION

Under Contract NAS 7-458, the Research Laboratories of United Aircraft Corporation are performing analytical studies to characterize the behavior of distributed-feed catalytic reactors for hydrazine decomposition. The specific objectives of this program are (a) to develop computer programs for predicting the temperature and concentration distributions in monopropellant hydrazine catalytic reactors in which hydrazine can be injected at arbitrary axial and radial locations in the reaction chamber and (b) to perform calculations using these computer programs to demonstrate the effects of various system parameters on the performance of the reactor.

Progress previously reported in the first annual report (Ref. 1) has included the development of computer programs which describe the steady-state and transient behavior of a reactor system in which complete radial mixing in the free-gas (or liquid) phase was assumed. These programs had been used to calculate temperature and reactant concentration distributions as functions of initial bed temperature, feed temperature, chamber pressure, mass flow rate, catalyst size distribution, and axial injector locations.

During the present reporting period attention has been focused on extending the steady-state model to include radial as well as axial variations in temperature and concentrations in order to permit an analysis of various injection schemes and catalyst bed configurations which exhibit radial nonuniformities. In addition, a refinement has been made of the method used in the one- and two-dimensional steady-state models to describe the effects of diffusional processes on reaction rates in porous catalyst particles and sample calculations using this modified film and pore diffusion model have been made. Effort during the second annual reporting period is described in detail in succeeding sections of this report.

DISCUSSION

The analysis of a hydrazine engine reaction system carried out to date pertains to a reaction chamber of arbitrary cross section packed with catalyst particles into which liquid hydrazine is injected at arbitrarily selected locations. Catalyst particles are represented as "equivalent" spheres with a diameter taken as a function of the particle size and shape. Both thermal and catalytic vapor phase decomposition of hydrazine and ammonia are considered in developing equations describing the concentration distributions of these reactants. Diffusion of reactants from the free-gas phase to the outside surface of the catalyst pellets is taken into account. Since the catalyst material is impregnated on the interior and exterior surfaces of porous particles, the diffusion of reactants into the porous structure must also be considered. In addition, the conduction of heat within the porous particles must be taken into account since the decomposition reactions are accompanied by the evolution or absorption of heat.

Included in succeeding sections of this report are detailed descriptions of (a) the development of an integral equation method describing the effects of film and pore diffusion of heat and mass on reaction rates in porous catalyst particles, (b) the use of a computer program representing this integral equation method as a subroutine in the one-dimensional steady-state model of the reactor system to define more precisely the kinetics of ammonia dissociation by comparing temperature and concentration profiles calculated using this program with available experimental information, (c) the use of the one-dimensional steady-state program to develop empirical correlations to predict axial temperature and fractional ammonia dissociation profiles in hydrazine reactors packed with Shell 405 catalyst particles, (d) the development of computer program representing the two-dimensional steady-state model of the reactor system, and (e) the use of the two-dimensional program to calculate the effects on steady-state temperature and reactant concentration distributions of nonuniform radial injection and of catalyst bed configurations exhibiting both radial and axial nonuniformities.

Integral Analysis of Processes Occurring within Catalyst Particles

Catalytic reaction of hydrazine on Shell 405 catalyst particles is so fast (Ref. 1) that, even at low temperatures, the rate of decomposition of hydrazine vapor is controlled by the rate of diffusion of hydrazine from the bulk vapor through a stagnant gas film surrounding the catalyst particles to the outside surface of the particles. In the case of ammonia, however, film diffusion is rapid relative to the rate of dissociation of ammonia within the particles. The concentration of ammonia at the surface of the catalyst particles, $(c_p)_s^{NH_3}$, is therefore fairly close to the ammonia concentrations in the bulk vapor phase, $c_i^{NH_3}$. The surface concentration can be calculated, along with the concentration

profile in the porous particles, at any axial location in the reaction chamber by solving simultaneously the equations representing film and pore diffusion of heat and mass. In describing the diffusion of mass within a porous pellet, it is assumed that changes in the mass density of fluid within the particle are negligible relative to changes in concentration of the reacting species. In addition, pressure changes within the particle resulting from nonequimolar diffusion are neglected, as is heat transported by pore diffusion of mass. Assuming constant diffusion coefficients, D_p , and thermal conductivities, K_p , the equations describing heat and mass transfer within a catalyst particle may be written as

$$D_p^{NH_3} \nabla^2 C_p^{NH_3} - r_{het}^{NH_3} = 0 \quad (1)$$

$$K_p \nabla^2 T_p - H^{NH_3} r_{het}^{NH_3} = 0 \quad (2)$$

The boundary conditions which consider diffusion of heat and mass through a film surrounding a spherical particle are

$$D_p^{NH_3} \left(\frac{dC_p}{dx} \right)_S^{NH_3} = k_c^{NH_3} \left[C_i^{NH_3} - (C_p)_S^{NH_3} \right] \quad (3)$$

and

$$(H k_c c_i)^{N_2H_4} + H^{NH_3} D_p^{NH_3} \left(\frac{dC_p}{dx} \right)_S^{NH_3} = h_c [T_i - (T_p)_S] \quad (4)$$

where $(k_c c_i)^{N_2H_4}$ represents the rate of diffusion of hydrazine to the particle surface. It should be noted here that $(c_p)_S^{N_2H_4}$ is approximately zero, reflecting the fact that the catalytic decomposition of hydrazine vapor is quite rapid.

As in the particle diffusion model developed in Ref. 1 which neglected film diffusion (assuming equal surface and interstitial temperatures and ammonia concentrations), the temperature and ammonia concentration within a catalyst particle are related by (Ref. 2)

$$T_p - (T_p)_s = - \frac{H^{NH_3} D_p^{NH_3}}{K_p} \left[(c_p)_s^{NH_3} - c_p^{NH_3} \right] \quad (5)$$

The use of this relationship enables the reaction rate, $r_{het}^{NH_3}$, to be written as a function of concentration alone instead of concentration and temperature. In this case, however, the reaction rate is a function of two parameters, $(T_p)_s$ and $(c_p)_s^{NH_3}$, which are yet to be determined. Equation (1) can be solved for the concentration at any point in the porous particle in terms of the reaction rate, $r_{het}^{NH_3}$, and the interstitial concentration, $c_i^{NH_3}$. The solution is derived in Appendix I as an implicit integral equation given by

$$c_p(x)^{NH_3} = c_i^{NH_3} - \left[\frac{1}{x} - \frac{\alpha k_c^{NH_3} D_p^{NH_3}}{a^2 k_c^{NH_3}} \right] \int_0^x \xi^2 \frac{r_{het}^{NH_3}(c_p)}{D_p^{NH_3}} d\xi \\ - \int_x^a \left[\frac{1}{\xi} - \frac{\alpha k_c^{NH_3} D_p^{NH_3}}{a^2 k_c^{NH_3}} \right] \xi^2 \frac{r_{het}^{NH_3}(c_p)}{D_p^{NH_3}} d\xi \quad (6)$$

In order to determine the particle ammonia concentration profile directly in terms of the interstitial temperature and reactant concentrations it is necessary to solve Eqs. (3), (4), and (6) simultaneously. Numerical methods to accomplish this have been developed and programmed for machine computation.*

In the special case of negligible film resistance to heat and mass transfer (i.e., $(T_p)_s = T_i$ and $(c_p)_s = c_i$), Eq. (6) can be written, for any reacting species, as

$$c_p(x) = c_i - \left[\frac{1}{x} - \frac{1}{a} \right] \int_0^x \xi^2 \frac{r_{het}(c_p)}{D_p} d\xi \\ - \int_x^a \left[\frac{1}{\xi} - \frac{1}{a} \right] \xi^2 \frac{r_{het}(c_p)}{D_p} d\xi \quad (7)$$

It is Eq. (7) which is used to describe the hydrazine concentration profiles within the catalyst particles located in the liquid region of the reaction chamber. In this liquid region it is assumed that liquid hydrazine wets the outside surface of the catalyst particles so that $(c_p)_s^{N_2H_4} = c_i^{N_2H_4}$, where $c_i^{N_2H_4}$ is the vapor concentration in equilibrium with liquid hydrazine at temperature T_i .

*These methods are described in detail in a computer manual describing to potential users the operation of the computer programs representing the one- and two-dimensional steady-state models of the reactor system. This manual is being prepared as part of the third year of effort under the present contract.

Sample calculations of ammonia concentration and temperature profiles within a porous catalyst particle have been made with and without hydrazine in the interstitial fluid. An illustrative example was considered for the case without hydrazine for which the parameters are

T_i	=	2024 deg R
P	=	100 psia
Mole Fractions in Bulk Fluid	}	NH_3 = 0.19
		H_2 = 0.51
		N_2 = 0.30
$D_p^{NH_3}$	=	0.35×10^{-4} ft ² /sec
H^{NH_3}	=	1405 Btu/lb
$k_c^{NH_3}$	=	5.0 ft/sec
h_c	=	0.29 Btu/ft ² -sec-deg R
K_p	=	0.40×10^{-4} Btu/ft-sec-deg R
a	=	10^{-3} ft

The temperature and ammonia concentration profiles within the catalyst particle were calculated by simultaneous solution of Eqs. (3), (4), and (6) using the expression for r_{het} cited in Ref. 1. These profiles are plotted for this case in Fig. 1. The flux at the particle surface, $D_p(dc_p/dx)_s$ or $k_c [c_i - (c_p)_s]$, is easily calculated once the concentration profile is known. For the ammonia dissociation case discussed above, the mass flux of ammonia into the catalyst particle, normalized by dividing by $(k_c c_i)^{NH_3}$, is plotted as a function of bulk fluid temperature in Fig. 2. The reactant concentration profile and then the mass flux at the particle surface were obtained for temperatures between 1700 and 2700 deg R; all other parameters were fixed at the same values used in computing the profiles shown in Fig. 1. The normalizing factor, $(k_c c_i)^{NH_3}$, is the ammonia mass flux which would be obtained if the reaction were controlled by the film diffusion of heat and mass. For comparison purposes, normalized fluxes are also plotted in Fig. 2 for the case in which film resistance to heat and mass transfer is negligible (i.e., $(c_p)_s = c_i$ and $(T_p)_s = T_i$) and for the case where film and pore diffusion are sufficiently rapid so that the system is controlled by the rate of chemical reaction on the catalytic surfaces (i.e., $c_p(x) = c_i$ and $T_p(x) = T_i$). For the case of negligible film resistance to heat

and mass transfer, Eq. (7) was used to determine the ammonia concentration distribution within the particle and then the flux at the particle surface. For the chemical reaction-controlled system, the flux was computed as $(a/3)r_{\text{het}}^{\text{NH}_3}(c_i, T_i)$. As shown in Fig. 2, these two cases represent low-temperature asymptotes for the general case where the effects of film and pore diffusion on catalytic reaction rates are considered. At high temperature this flux asymptotically approaches the flux which would be obtained if the reaction were controlled by the film diffusion of heat and mass.

Equations (3), (4), and (6) have also been solved simultaneously for the temperature and ammonia concentration profiles in a porous catalyst particle for a case in which hydrazine is present in the bulk fluid and the parameters are

	T_i	= 2000 deg R
	P	= 100 psia
Mole Fractions in Bulk Fluid	$\left\{ \begin{array}{l} \text{N}_2\text{H}_4 \\ \text{NH}_3 \\ \text{H}_2 \\ \text{N}_2 \end{array} \right.$	= 0.43
		= 0.11
		= 0.23
		= 0.23
	$D_p^{\text{NH}_3}$	= 0.34×10^{-4} ft ² /sec
	H^{NH_3}	= 1404 Btu/lb
	$H^{\text{N}_2\text{H}_4}$	= -1928 Btu/lb
	$k_c^{\text{NH}_3}$	= 4.4 ft/sec
	$k_c^{\text{N}_2\text{H}_4}$	= 3.0 ft/sec
	h_c	= 0.29 Btu/ft ² -sec-deg R
	K_p	= 0.40×10^{-4} Btu/ft-sec-deg R
	a	= 10^{-3} ft

Both the temperature and the ammonia concentration distributions are plotted for this case in Fig. 3. Similar concentration profiles were calculated for bulk fluid temperatures between 1700 and 2700 deg R; all other parameters were fixed at the same values used in computing the profiles shown in Fig. 3. The

flux of ammonia at the particle surface was then calculated, normalized by dividing by $(k_c c_i)^{\text{NH}_3}$, and plotted as a function of bulk fluid temperature in Fig. 4. Here again, at high temperature, the flux asymptotically approaches the values which would be obtained if the reaction were controlled by the film diffusion of heat and mass. At low temperature, in this case, film resistance to heat transfer remains important because of the heat generated at the particle surface by the decomposition of hydrazine.

Use of Integral Analysis in One-Dimensional Steady-State Model

A computer program representing the integral analysis was used as a subroutine in the one-dimensional steady-state program to define more precisely the kinetics of ammonia dissociation by comparing temperature and concentration profiles calculated using this program with available experimental information. The rate of catalytic dissociation of ammonia can be expressed as (Ref. 1)

$$r_{\text{net}}^{\text{NH}_3} = \alpha^{\text{NH}_3} \frac{C_p^{\text{NH}_3}}{(C_p^{\text{H}_2})^{1.6}} e^{-50,000/T_p} \quad \text{lb / ft}^3\text{-sec} \quad (8)$$

where the concentrations are expressed in lb/ft^3 and T_p is in deg R. A value of 0.3×10^{11} for α^{NH_3} was obtained in Ref. 1 by comparing experimental data with calculated steady-state temperature and concentration profiles. However, in the model used to calculate these profiles it was assumed that the temperature at the surface of the catalyst pellet is equal to the interstitial (bulk fluid) temperature at the same axial location. Using the more sophisticated integral method described above, the same cases were rerun with the one-dimensional steady-state program. The use of this method changes the predicted steady-state behavior of the reactor most significantly in regions of the reactor system where the bulk vapor temperature is low and the heat generated at the catalyst particle surfaces by the decomposition of hydrazine results in large differences between the bulk vapor temperature and the particle surface temperature. High temperatures at the particle surface result in rapid ammonia decomposition which leads to low peak temperatures in the bulk vapor phase. Apart from lowering the predicted peak temperatures and ammonia concentrations, the use of the modified film and pore diffusion model did not result in any appreciable difference between the recalculated temperature and mole-fraction profiles and those presented in Ref. 1. The value of α^{NH_3} which yielded closest agreement with experimental data was $1 \times 10^{11} (\text{lb/ft}^3)^{1.6} (\text{sec})^{-1}$. The results of calculations using this value are shown in Figs. 5 through 14.* For each of these cases the catalyst bed packing was taken to consist of 25-30 mesh catalyst particles for the first 0.2 in. and $1/8 \times 1/8$ in. cylindrical

*The sensitivity of these results to changes in α^{NH_3} is very similar to the sensitivity to this rate constant of the results reported in Ref. 1.

pellets for the remainder of the bed. This configuration is referred to in the figures as the "standard bed configuration." The reactor operating conditions of chamber pressure and mass flow rate were varied, as was the feed temperature, T_F , although, in each of these cases, T_F was between approximately 510 and 530 deg R.

Temperature distributions are plotted in Fig. 5 for a case in which the reactor operating conditions were taken as $G = 3.12$ lb/ft²-sec and $P = 479.5$ psia. Also shown in Fig. 5 are temperature measurements obtained by Rocket Research Corporation (Ref. 3) during the course of engine firings under the same operating conditions. The calculated mole-fraction profiles for this case, together with experimental values of mole fractions, are shown in Fig. 6. The results of similar calculations made for $G = 2.43$ lb/ft²-sec and $P = 1042$ psia are shown in Figs. 7 and 8; those made for $G = 6.29$ lb/ft²-sec and $P = 974$ psia are shown in Figs. 9 and 10; those made for $G = 1.52$ lb/ft²-sec and $P = 217.9$ psia are shown in Figs. 11 and 12, and those made for $G = 1.51$ lb/ft²-sec and $P = 111.4$ psia are shown in Figs. 13 and 14.

As noted in Ref. 1, the heat transfer coefficients used in this model were estimated using correlations developed for nonreacting systems. In regions where significant chemical reaction takes place, such as the zones in which both hydrazine and ammonia are decomposing, actual heat transfer rates are considerably higher than those calculated in this model. Precise accounting of this increase in rate would lead to a value of α^{NH_3} somewhat less than 1×10^{11} .

The effects of various reactor operating conditions on steady-state temperature profiles are illustrated more specifically in Figs. 15 through 18. A reference case was chosen in which the operating conditions were $G = 3.0$ lb/ft²-sec, $P = 100$ psia, and $T_F = 530$ R, and the catalyst bed configuration was the "standard bed configuration." Chamber pressure, mass flow rate, catalyst bed configuration and axial injection profile were then varied in turn and the resulting temperature distributions were plotted. In Fig. 15 temperature distributions are plotted for chamber pressures of 100, 500 and 1000 psia with all other conditions taken as those of the reference case. Increasing pressure causes the peak temperature to rise and shift slightly toward the inlet of the reactor. This is due to the inhibiting action of hydrogen on the rate of ammonia dissociation. Temperature profiles are shown in Fig. 16 for mass flow rates of 1.5, 3.0 and 6.0 lb/ft²-sec. Increasing flow rate causes the peak temperature to rise and shift slightly away from the reactor inlet. The effect of changing the catalyst bed configuration on the temperature distribution is shown in Fig. 17. Temperature profiles are plotted for beds packed with all 25-30 mesh particles, all 1/8 in. x 1/8 in. cylindrical pellets, and the standard nonuniform particle size distribution. It is apparent that the larger particles slow down the rates of the catalytic decomposition reactions. The effects of distributed injectors on temperature profiles are illustrated in Fig. 18. Temperature distributions are plotted

for the reference case, for the case in which 2/3 of the hydrazine is injected at the inlet and the remaining 1/3 is injected uniformly over the first 1/2 in. of the reactor, and for the case in which 1/3 of the hydrazine is injected at the inlet and the remaining 2/3 is injected uniformly over the first 1/2 in. of the reactor. In these cases the bed was taken to be packed with all 25-30 mesh particles.

One-Dimensional Steady-State Program

A series of runs was made with the one-dimensional steady-state computer program in order to develop empirical correlations to predict axial temperature and fractional ammonia dissociation profiles in hydrazine reactors packed with Shell 405 catalyst particles. Empirical correlations were developed on the basis of about 65 runs representing different combinations of mass flow rates, pressures and catalyst bed configurations. It was found that fractional ammonia dissociation and bulk fluid temperature could be predicted using the equations

$$1 - \text{Fractional Ammonia Dissociation} = \Phi \quad (9)$$

and

$$T_i = 1020 \left\{ \Phi + [0.075 (P/1000)] \right\} + 1535 \quad (10)$$

where

$$\Phi = (0.66) (G/z)^{0.28} \left\{ \left[(0.55 a^{0.17} - 0.17) (1000/P)^{0.22} \right] + 0.17 \right\} \quad (11)$$

and z and a are expressed in ft, G in $\text{lb/ft}^2\text{-sec}$, P in psia, and T_i in deg R. Here, as in Ref. 1, fractional ammonia dissociation is determined on the basis that, with no ammonia dissociation, one mole each of hydrogen and nitrogen are formed for every two moles of hydrazine decomposed. Results obtained using these equations are illustrated in Figs. 19 and 20, respectively, for cases in which most of the hydrazine decomposition occurs in the first few tenths of an inch of the reactor; this rapid hydrazine decomposition rate is associated with reactors packed with particles 25 mesh or smaller for approximately 0.2 in. of bed length. For these cases the correlations depicted in Figs. 19 and 20 work well for axial distances greater than one inch and for values of pressure, P , between 10 and 1000 psia, mass flow rate, G , between 1.44 and 14.4 $\text{lb/ft}^2\text{-sec}$ (0.01 and 0.1 $\text{lb/in.}^2\text{-sec}$, respectively) and equivalent spherical radius, a , between 0.001 and 0.01 ft. For a reactor packed with small (≤ 25 mesh) particles for the first few tenths of an inch and larger particles thereafter, the particle radius, a , refers to the larger particles.

In Figs. 19 and 20, Rocket Research experimental data (Ref. 3) are plotted along with the empirical predictions and the results of sample cases run using the one-dimensional steady-state program. Values of fractional ammonia dissociation obtained from the steady-state program are plotted for axial locations between 1 and 6 inches while values of bulk fluid temperature obtained from the program are plotted only for axial locations between 3 and 6 inches. Calculated values of temperature for axial locations between 1 and 3 inches scatter slightly about the predicted line in Fig. 20 in the same manner as the corresponding values of fractional ammonia dissociation scatter about the predicted line in Fig. 19.

It should be emphasized that these empirical correlations do not correctly predict the behavior of reactors in which hydrazine decomposition is slow, for example, reactors which are uniformly packed with large catalyst particles, such as 1/8 in. x 1/8 in. cylinders. The correlations work quite well though for catalyst bed configurations consisting of 25-30 mesh particles for the first 0.2 in. and 1/8 in. x 1/8 in. cylindrical pellets for the remainder of the bed.

Two-Dimensional Steady-State Model

In developing the two-dimensional model of a hydrazine reactor system the temperature and reactant concentrations in the bulk fluid phase are permitted to vary with radial and axial position in the reaction chamber. In the entrance region of the reactor, where the temperature is low enough to permit the existence of liquid hydrazine, radial mixing between adjacent layers of liquid is neglected. The equations representing the change in liquid enthalpy and temperature with axial distance at any radial position are the same as those developed for the one-dimensional model described in Ref. 1. As in the one-dimensional model, catalytic reaction is assumed to be fast enough to keep liquid hydrazine from wetting the pores of the particles; the hydrazine concentration at the surface of the catalyst particles at any location in the entrance region is then computed from the vapor pressure of liquid hydrazine in the interstitial phase at the same location.

In the vapor regions of the reaction chamber, turbulent diffusion of heat and mass is considered as a mechanism for radial mixing. Radial heat and mass fluxes are computed as functions of temperature and reactant concentration gradients. Heat is being supplied to the system by homogeneous as well as heterogeneous decomposition of hydrazine, and is being removed from the system by the catalytic decomposition of ammonia. The change in enthalpy with axial distance at any radial location is related to the reactant concentrations in the interstitial phase and at the surface of the porous catalyst particles by

$$\frac{\partial h_i}{\partial z} = -\frac{1}{G} \left\{ F(h_i - h_F) + A_P h_c [T_i - (T_P)_S] + H^{N_2H_4} r_{hom}^{N_2H_4} \delta + \frac{\partial q_r}{\partial r} \delta + \frac{q_r}{r} \delta + \frac{\partial T_i}{\partial r} \delta \sum N_r^J C_f^J \right\} \quad (12)^*$$

The changes in reactant weight fractions in the interstitial phase with axial distance at any radial location are related to the reactant concentrations in the interstitial phase and at the surface of the porous catalyst particles by

$$\frac{\partial w_i^{N_2H_4}}{\partial z} = \frac{1}{G} \left\{ F - r_{hom}^{N_2H_4} \delta - A_P (k_C C_i)^{N_2H_4} - \frac{\partial N_r^{N_2H_4}}{\partial r} \delta - \frac{N_r^{N_2H_4}}{r} \delta - F \left(\frac{C_i}{\rho_i} \right)^{N_2H_4} \right\} \quad (13)$$

$$\frac{\partial w_i^{NH_3}}{\partial z} = \frac{1}{G} \left\{ r_{hom}^{N_2H_4} \delta \frac{M^{NH_3}}{M^{N_2H_4}} + A_P (k_C C_i)^{N_2H_4} \frac{M^{NH_3}}{M^{N_2H_4}} - A_P (k_C [C_i - (C_P)_S])^{NH_3} - \frac{\partial N_r^{NH_3}}{\partial r} \delta - \frac{N_r^{NH_3}}{r} \delta - F \left(\frac{C_i}{\rho_i} \right)^{NH_3} \right\} \quad (14)$$

$$\frac{\partial w_i^{N_2}}{\partial z} = \frac{1}{G} \left\{ \frac{1}{2} r_{hom}^{N_2H_4} \delta \frac{M^{N_2}}{M^{N_2H_4}} + \frac{A_P}{2} (k_C C_i)^{N_2H_4} \frac{M^{N_2}}{M^{N_2H_4}} + \frac{A_P}{2} (k_C [C_i - (C_P)_S])^{NH_3} \frac{M^{N_2}}{M^{NH_3}} - \frac{\partial N_r^{N_2}}{\partial r} \delta - \frac{N_r^{N_2}}{r} \delta - F \left(\frac{C_i}{\rho_i} \right)^{N_2} \right\} \quad (15)$$

$$\frac{\partial w_i^{H_2}}{\partial z} = \frac{1}{G} \left\{ \frac{1}{2} r_{hom}^{N_2H_4} \delta \frac{M^{H_2}}{M^{N_2H_4}} + \frac{A_P}{2} (k_C C_i)^{N_2H_4} \frac{M^{H_2}}{M^{N_2H_4}} + \frac{3A_P}{2} (k_C [C_i - (C_P)_S])^{NH_3} \frac{M^{H_2}}{M^{NH_3}} - \frac{\partial N_r^{H_2}}{\partial r} \delta - \frac{N_r^{H_2}}{r} \delta - F \left(\frac{C_i}{\rho_i} \right)^{H_2} \right\} \quad (16)$$

*Equations of this type are presented in somewhat different form in Ref. 4. The last term on the right-hand side of the equation reflects the heat transferred by the radial diffusion of mass.

where

$$q_r = -\lambda (\partial T_i / \partial r) \quad (17)$$

$$N_r^J = -\epsilon (\partial c_i^J / \partial r)_r \quad (18)$$

$$h_c = 0.74 \left[\frac{G}{A_P \mu} \right]^{-0.41} \left[\frac{\bar{C}_f G}{\rho_i} \right] \quad (19)$$

$$k_c^J = \left[\frac{0.61 G}{\rho_i} \right] \left[\frac{\mu}{\rho_i D_i^J} \right]^{-0.667} \left[\frac{G}{A_P \mu} \right]^{-0.41} \quad (20)$$

The eddy conductivity and diffusivity may be estimated from (Ref. 5)

$$\lambda = \frac{\alpha \bar{C}_f G}{5\delta} \quad \text{and} \quad \epsilon = \frac{\alpha G}{5\rho_i} \quad (21)$$

The changes in reactant concentrations with axial distance are then given by

$$\frac{\partial c_i^J}{\partial z} = \rho_i \frac{\partial w_i^J}{\partial z} + \frac{c_i^J}{\rho_i} \frac{\partial \rho_i}{\partial z} \quad (22)$$

where

$$\frac{\partial \rho_i}{\partial z} = \rho_i \left[\frac{1}{\bar{M}} \frac{\partial \bar{M}}{\partial z} - \frac{1}{T_i} \frac{\partial T_i}{\partial z} + \frac{1}{P} \frac{dP}{dz} \right] \quad (23)$$

$$\frac{1}{\bar{M}} \frac{\partial \bar{M}}{\partial z} = - \frac{1}{\sum_J (w_i^J / M^J)} \sum_J \frac{1}{M^J} \frac{\partial w_i^J}{\partial z} \quad (24)$$

and the pressure drop may be estimated from the Ergun equation (Ref. 4) as

$$\frac{dP}{dz} = - \left(\frac{1-\delta}{\delta^3} \right) \left(1.75 + \frac{150(1-\delta)}{2\alpha G/\mu} \right) \left(\frac{G^2}{2\alpha \rho_1 g_c} \right) \quad (25)$$

The mass flow rate, G , is computed as a function of the rate of feed of liquid hydrazine from the distributed injectors into the system. Radial pressure gradients, caused by particle-fluid viscous interaction, are neglected. Such pressure gradients would lead to recirculating flow patterns in the reaction chamber. This bulk radial flow is neglected in this analysis. It is assumed, therefore, that downstream of the injectors the mass flow rate profile remains unchanged.

The equations representing the two-dimensional model have been programmed for digital computation. A computer manual containing a detailed description of the operating characteristics of the program is currently being prepared as part of the third year of effort under the present contract.

Results of Calculations Using the Two-Dimensional Steady-State Program

A series of calculations was made using the two-dimensional steady-state computer program in order to examine the effectiveness of the two-dimensional model and to evaluate the effects on system performance of nonuniform radial injection and of catalyst bed configurations exhibiting both radial and axial nonuniformities. The calculated results illustrated in Figs. 21 through 54 refer to a reactor 3 in. in diameter into which liquid hydrazine is injected at a temperature of 530 deg R.

Axial temperature profiles at various radial locations are plotted in Fig. 21 for a case in which a radial nonuniformity in mass flow rate, G , is represented as a step function (see Fig. 21). In this case the upstream chamber pressure was taken as 100 psia and the catalyst bed packing was taken to consist of 25-30 mesh catalyst particles for the first 0.2 in. and $1/8 \times 1/8$ in. cylindrical pellets for the remainder of the bed. This configuration is referred to in the figures as the "standard bed configuration". Turbulent diffusion of heat, which tends to reduce radial temperature gradients, is more pronounced in the downstream end of the reactor. Here the catalyst particle size is larger, and both eddy conductivity and eddy diffusivity are directly proportional to particle size. The consequences of radial heat conduction are complicated somewhat by the simultaneous turbulent diffusion of mass. Higher temperatures are associated with more hydrazine decomposition; thus high temperature regions may lose heat by radial conduction, but may gain hydrazine from adjoining low temperature regions by radial diffusion of mass. Subsequent decomposition of this hydrazine may lead to even higher temper-

atures. In these same regions the ammonia produced by the decomposition of hydrazine may exist at higher concentration than in adjacent low temperature regions. In the absence of radial diffusion the ammonia in these high-temperature regions would decompose and lower the temperature. With radial diffusion, however, the concentration of ammonia available for decomposition may be lowered considerably. For the case considered here, these combined effects lead to the temperature distribution shown in Fig. 21*. For comparison purposes, the axial temperature profile corresponding to a radially uniform mass flow rate of $3.0 \text{ lb/ft}^2\text{-sec}$ is also plotted in Fig. 21. This is the average mass flow rate calculated by averaging the actual mass flow rate profile over the cross-sectional area of the reactor. The mole-fraction distributions of hydrazine and ammonia associated with the temperature distribution shown in Fig. 21 are illustrated in Figs. 22 and 23 respectively.

The results of similar calculations made for two different upstream chamber pressures are shown in Figs. 24 through 29. The calculated temperature, mole fraction of hydrazine, and mole fraction of ammonia distributions are plotted in Figs. 24 through 26 respectively for a pressure of 200 psia and the same mass flow rate profile and bed configuration used in the calculations presented in Figs. 21 through 23. These calculations were repeated for a chamber pressure of 1000 psia; the results are shown in Figs. 27 through 29.

Retaining the catalyst bed configuration and step function injection profile discussed above, and taking the upstream chamber pressure as 200 psia, similar calculations were made for two other average mass flow rates. The calculated temperature, mole fraction of hydrazine, and mole fraction of ammonia profiles are plotted in Figs. 30 through 32 respectively for an average mass flow rate of $1.0 \text{ lb/ft}^2\text{-sec}$ and in Figs. 33 through 35 respectively for an average mass flow rate of $6.0 \text{ lb/ft}^2\text{-sec}$.

The results of calculations made for two other injection profiles are shown in Figs. 36 through 41. These calculations were made for the "standard bed configuration," an upstream chamber pressure of 100 psia, and an average mass flow rate of $3.0 \text{ lb/ft}^2\text{-sec}$. The temperature and mole-fraction distributions associated with the injection profile illustrated in Fig. 36 are plotted in Figs. 36 through 38 and those associated with the continuously varying injection profile illustrated in Fig. 39 are shown in Figs. 39 through 41.

*The effects of radial diffusion can be more clearly illustrated with cross-plots showing radial temperature profiles at various axial locations in the reactor. While radial profiles were not plotted for this case, they were plotted for another case discussed later in this section.

The effects on temperature and reactant concentration distributions of two catalyst bed configurations exhibiting both radial and axial nonuniformities are illustrated in Figs. 42 through 47. For both of these configurations the mass flow rate was taken as uniform at $3.0 \text{ lb/ft}^2\text{-sec}$ and the upstream chamber pressure was taken as 100 psia. The calculated temperature, mole fraction of hydrazine, and mole fraction of ammonia distributions corresponding to the bed configuration shown in Fig. 42 are plotted in Figs. 42 through 44 respectively. Similar calculations corresponding to the bed configuration shown in Fig. 45 are plotted in Figs. 45 through 47.

The effects of the simultaneous turbulent diffusion of heat and mass on temperature and reactant concentration profiles are more clearly indicated for a case in which hydrazine injection is uniform across the inlet face of the reactor but additional hydrazine is introduced into the reactor through injectors imbedded in the catalyst bed. Calculations were made for an injection profile of this type, illustrated in Fig. 48, where the chamber pressure was taken as 100 psia and the bed configuration as "standard". In this case the buried injectors were taken to distribute hydrazine uniformly for $0 \leq r/R \leq 0.7$ over the first $1/2$ in. of the reactor. The calculated temperatures are plotted as a function of axial position at various radial positions in Fig. 48. Hydrazine diffusion from low to high temperature regions results in unusually high temperatures at the interface between the high and low flow rate regions. This results in the formation of a "thermal sheath" which is more clearly illustrated in Fig. 49 which is a cross-plot of the results presented in Fig. 48. Here temperature is plotted as a function of radial position at various axial locations in the reactor. For comparison purposes, the radial temperature profile at the exit of a 3 in. bed with a step function (all inlet) injection profile is also plotted in Fig. 49. The mole fraction of hydrazine and ammonia distributions associated with the temperature profiles shown in Figs. 48 and 49 are plotted in Figs. 50 and 51 respectively.

The effects of various reactor operating conditions on radial temperature profiles at the exit of a 3 in. bed are illustrated in Figs. 52 through 54 for the standard bed configuration and for hydrazine injection at the reactor inlet only. The effect of upstream chamber pressure on exit radial temperature profile is shown in Fig. 52 for a step function injection profile with an average mass flow rate of $3.0 \text{ lb/ft}^2\text{-sec}$. Very little effect is noted over a ten-fold pressure range. A marked effect of average mass flow rate on radial temperature profile is shown in Fig. 53 for the same step function injection profile and an upstream chamber pressure of 200 psia. The effect of inlet injection profile on radial temperature distribution is illustrated in Fig. 54 for an average mass flow rate of $3.0 \text{ lb/ft}^2\text{-sec}$ and an upstream chamber pressure of 100 psia.

It should be noted here that the injection profiles and catalyst bed configurations discussed in this section were chosen simply to illustrate the two-dimensional effects which can occur in the hydrazine reactor. No attempt was made to perform an exhaustive study of the effects of radial variations in reactor operating and design parameters on the steady-state behavior of the reactor system. It is apparent, however, that a one-dimensional model of the system, based on parameters averaged over the reactor cross-section, is not adequate to describe the behavior of a reactor which exhibits significant radial variations in injection profile or bed configuration. For these systems, it is necessary to use the two-dimensional model to effectively predict, for example, the locations of very high temperature regions such as "thermal sheaths".

REFERENCES

1. Kesten, A. S.: Analytical Study of Catalytic Reactors for Hydrazine Decomposition. United Aircraft Research Laboratories Report F910461-12, First Annual Progress Report, Contract NAS 7-458, May 1967.
2. Prater, D. C.: The Temperature Produced by Heat of Reaction in the Interior of Porous Particles. Chemical Engineering Science, Vol. 8, 1958, pp. 284-286.
3. Rocket Research Corporation: Development of Design and Scaling Criteria for Monopropellant Hydrazine Reactors Employing Shell 405 Spontaneous Catalyst. RRC-66-R-76, January 1967.
4. Bird, R. B., W. E. Stewart, and E. N. Lightfoot: Transport Phenomena. John Wiley & Sons, Inc., New York, 1960.
5. Argo, W. B., and J. M. Smith: Heat Transfer in Packed Beds, Chemical Engineering Progress, 49, 1953, pp. 443-451.
6. Irving, J., and N. Millieux: Mathematics in Physics and Engineering. Academic Press, Inc., New York, 1959, p. 731.

LIST OF SYMBOLS

a	Radius of spherical particle, ft
A_p	Total external surface of catalyst particle per unit volume of bed, ft^{-1}
c_i	Reactant concentration in interstitial fluid, lb/ft^3
c_p	Reactant concentration in gas phase within the porous particle, lb/ft^3
c_p^*	Equals $c_p - (c_p)_s$, lb/ft^3
C_F	Specific heat of fluid in the interstitial phase, $\text{Btu}/\text{lb} - \text{deg R}$
\bar{C}_F	Average specific heat of fluid in the interstitial phase, $\text{Btu}/\text{lb} - \text{deg R}$
C_s	Specific heat of catalyst particle, $\text{Btu}/\text{lb} - \text{deg R}$
D_i	Diffusion coefficient of reactant gas in the interstitial fluid, ft^2/sec
D_p	Diffusion coefficient of reactant gas in the porous particle, ft^2/sec
F	Rate of feed of hydrazine from distributed injectors into the system, $\text{lb}/\text{ft}^3\text{-sec}$
g_c	Conversion factor, $(\text{lb}_m/\text{lb}_f) \text{ft}/\text{sec}^2$
G	Mass flow rate, $\text{lb}/\text{ft}^2\text{-sec}$
h	Enthalpy, Btu/lb
h_c	Heat transfer coefficient, $\text{Btu}/\text{ft}^2\text{-sec-deg R}$
H	Heat of reaction (negative for exothermic reaction), Btu/lb
k_c	Mass transfer coefficient, ft/sec
K_p	Thermal conductivity of the porous catalyst particle, $\text{Btu}/\text{ft-sec-deg R}$
M	Molecular weight, $\text{lb}/\text{lb mole}$
\bar{M}	Average molecular weight, $\text{lb}/\text{lb mole}$
N_r	Radial mass flux, $\text{lb}/\text{ft}^2\text{-sec}$
p	Chamber pressure, psia

q_r	Radial heat flux, Btu/ft ² -sec
r	Radial distance, ft
r_{het}	Rate of (heterogeneous) chemical reaction on the catalyst surfaces, lb/ft ³ -sec
r_{hom}	Rate of (homogeneous) chemical reaction in the interstitial phase, lb/ft ³ -sec
R	Gas constant, equals 10.73 psia - ft ³ /lb mole - deg R, or, Radius of reactor
t	Time, sec
t^*	Actual time minus time required, under steady-state conditions, for liquid hydrazine to flow from the reactor inlet to the interface between the liquid-vapor and vapor regions, sec
T	Temperature, deg R
w_i	Weight fraction of reactant in interstitial phase
x	Radial distance from the center of the spherical catalyst particle, ft
z	Axial distance, ft
α	Preexponential factor in rate equation
δ	Interparticle void fraction
ϵ	Eddy diffusivity, ft ² /sec
λ	Eddy conductivity, Btu/ft-sec-deg R
μ	Viscosity of interstitial fluid, lb/ft - sec
ρ_i	Density of interstitial fluid, lb/ft ³
ρ_s	Bulk density of catalyst particle, lb/ft ³
ϕ	Defined by Eq. (11)

Subscripts

F	Refers to feed
i	Refers to interstitial phase

P Refers to gas within the porous catalyst particle

s Refers to surface of catalyst particle

Superscripts

J Refers to chemical species

L Refers to liquid at vaporization temperature

V Refers to vapor at vaporization temperature

APPENDIX I

DERIVATION OF INTEGRAL EQUATIONS REPRESENTING THE CONCENTRATION
PROFILE OF A REACTANT WITHIN A POROUS CATALYST PARTICLE
SURROUNDED BY A STAGNANT GAS FILM

In this section equations are developed to describe the steady-state concentration profile of a reactant within a porous catalyst particle which is surrounded by a stagnant gas film. The reactant concentration profile in the porous particle at any location can be found as a solution to:

$$D_p \nabla^2 c_p - r_{het}(c_p) = 0 \quad (I-1)$$

If the catalyst particles are taken to be "equivalent" spheres of radii a , and if concentration c_p^* is defined such that $c_p^* = c_p - c_i$, Eq. (I-1) can be written as

$$D_p \left[\frac{1}{x^2} \frac{d}{dx} \left(x^2 \frac{dc_p^*}{dx} \right) \right] - r_{het} = 0 \quad (I-2)$$

where x is the radial distance from the center of a sphere. The boundary conditions associated with Eq. (I-2) are

$$\frac{dc_p^*}{dx} = 0 \quad \text{AT} \quad x = 0 \qquad \frac{dc_p^*}{dx} = - \frac{k_c}{D_p} c_p^* \quad \text{AT} \quad x = a \quad (I-3)$$

Equation (I-2) can be rearranged to get

$$\frac{d}{dx} \left(x^2 \frac{dc_p^*}{dx} \right) = \frac{r_{het} x^2}{D_p} = \phi(x, c_p^*) \quad (I-4)$$

The solution to Eq. (I-4) is most easily obtained by converting it into a Fredholm integral equation (see Ref. 6) of the form

$$c_p^*(x) = \frac{1}{x^2 [u(x)v'(x) - u'(x)v(x)]} \int_0^a G(x, \xi) \cdot \phi(\xi, c_p^*) d\xi \quad (I-5)$$

where $u(x)$ is a solution of

$$\frac{d}{dx} \left(x^2 \frac{du}{dx} \right) = 0 \quad (\text{I-6})$$

subject to the condition that

$$\left[u \frac{dc_p^*}{dx} - \frac{du}{dx} c_p^* \right]_{x=0} = 0 \quad (\text{I-7})$$

and $v(x)$ is a solution of

$$\frac{d}{dx} \left(x^2 \frac{dv}{dx} \right) = 0 \quad (\text{I-8})$$

subject to the condition that

$$\left[v \frac{dc_p^*}{dx} - \frac{dv}{dx} c_p^* \right]_{x=a} = 0 \quad (\text{I-9})$$

The Green's function, $G(x, \xi)$ is given by

$$G(x, \xi) = \begin{cases} u(\xi) v(x) & \text{FOR } 0 \leq \xi \leq x \\ u(x) v(\xi) & \text{FOR } x \leq \xi \leq a \end{cases} \quad (\text{I-10})$$

The function $u(x)$ can be determined by first integrating Eq. (I-6) to get

$$u = -\frac{A_1}{x} + B_1 \quad (\text{I-11})$$

Applying Eq. (I-7) together with the first of boundary conditions (I-3) to Eq. (I-11), it is found that $A_1 = 0$ and

$$u = B_1 \quad (\text{I-12})$$

The function $v(x)$ can be determined in a similar manner by first integrating Eq. (I-8) to get

$$v = -\frac{A_2}{x} + B_2 \quad (\text{I-13})$$

and then applying Eq. (I-9) and the second of boundary conditions (I-3) to Eq. (I-13) to get

$$v = A_2 \left[\frac{ak_c - D_p}{a^2 k_c} - \frac{1}{x} \right] \quad (\text{I-14})$$

Equations (I-10), (I-12), and (I-14) can now be combined to get

$$G(x, \xi) = \begin{cases} A_2 B_1 \left[\frac{ak_c - D_p}{a^2 k_c} - \frac{1}{x} \right] & \text{FOR } 0 \leq \xi \leq x \\ A_2 B_1 \left[\frac{ak_c - D_p}{a^2 k_c} - \frac{1}{\xi} \right] & \text{FOR } x \leq \xi \leq a \end{cases} \quad (\text{I-15})$$

In addition,

$$x^2 \left[u(x) v'(x) - u'(x) v(x) \right] = A_2 B_1 \quad (\text{I-16})$$

Equations (I-15) and (I-16) can now be substituted into Eq. (I-5) to get

$$c_p^*(x) = \left[\frac{ak_c - D_p}{a^2 k_c} - \frac{1}{x} \right] \int_0^x \phi(\xi, c_p^*) d\xi + \int_x^a \left[\frac{ak_c - D_p}{a^2 k_c} - \frac{1}{\xi} \right] \phi(\xi, c_p^*) d\xi \quad (\text{I-17})$$

or

$$c_p(x) = c_i - \left[\frac{1}{x} - \frac{ak_c - D_p}{a^2 k_c} \right] \int_0^x \xi^2 \frac{r_{het}(c_p)}{D_p} d\xi - \int_x^a \left[\frac{1}{\xi} - \frac{ak_c - D_p}{a^2 k_c} \right] \xi^2 \frac{r_{het}(c_p)}{D_p} d\xi \quad (\text{I-18})$$

Equation (I-18) is an implicit integral equation which can be solved numerically to determine the concentration at any point in a porous particle in terms of c_i , the concentration in the bulk fluid.

APPENDIX II

DISTRIBUTION LIST FOR SECOND ANNUAL PROGRESS REPORT

G910461-24

<u>Addressee</u>	<u>Copies</u>	<u>Addressee</u>	<u>Copies</u>
National Aeronautics & Space Administration Washington, D. C. 20546 Attn: Chief, Liq. Prop. Res. & Tech., RPL	1	NASA Lewis Research Center 21000 Brookpark Road Cleveland, Ohio 44135 Attn: Mr. I. A. Johnsen	1
National Aeronautics & Space Administration Washington, D. C. 20546 Attn: Chief, Liq. Prop. Exp. Systems, RPX	10	Marshall Space Flight Center Huntsville, Alabama 35812 Attn: Mr. Kieth Coates	1
National Aeronautics & Space Administration Washington, D. C. 20546 Attn: Dir., Launch Vehicles & Prop., SV	1	Department of Chemical Engineering University of British Columbia Vancouver 8, Canada Attn: Dr. J. Lielmezs	1
National Aeronautics & Space Administration Washington, D. C. 20546 Attn: Dir., Advanced Manned Missions, MT	1	NASA Ames Research Center Moffett Field, California 94035 Attn: Technical Librarian	2
Air Force Rocket Propulsion Laboratory Research and Technology Division Air Force System Command Edwards, California 93523 Attn: Mr. K. Rimer	1	NASA Ames Research Center Moffett Field, California 94035 Attn: Mr. Harold Hornby Mission Analysis Division	Ltr. Only
Air Force Rocket Propulsion Laboratory Research and Technology Division Air Force System Command Edwards, California 93523 Attn: Capt. Noyce/32725	1	NASA Ames Research Center Moffett Field, California 94035 Attn: Mr. Clarence A. Syvertson	Ltr. Only
U. S. Naval Ordnance Test Station China Lake, California 93553 Attn: Mr. Duane Williams	1	NASA Goddard Space Flight Center Greenbelt, Maryland 20771 Attn: Technical Librarian	2
U. S. Naval Ordnance Test Station China Lake, California 93553 Attn: Mr. James Dake	1	NASA Goddard Space Flight Center Greenbelt, Maryland 20771 Attn: Mr. Merland L. Moseson, Code 620	Ltr. Only
U. S. Naval Ordnance Test Station China Lake, California 93553 Attn: Mr. David Oliver	1	NASA Goddard Space Flight Center Greenbelt, Maryland 20771 Attn: Mr. D. Grant	Ltr. Only
Jet Propulsion Laboratory 4800 Oak Grove Drive Pasadena, California 91103 Attn: Mr. Theodore W. Price	10	Jet Propulsion Laboratory California Institute of Technology 4800 Oak Grove Drive Pasadena, California 91103 Attn: Technical Librarian	2
NASA Pasadena Office 4800 Oak Grove Drive Pasadena, California 91103 Attn: Contracting Officer	1	Jet Propulsion Laboratory California Institute of Technology 4800 Oak Grove Drive Pasadena, California 91103 Attn: Mr. Henry Burlage, Jr. Propulsion Div., 38	Ltr. Only
NASA Pasadena Office 4800 Oak Grove Drive Pasadena, California 91103 Attn: Office of Tech. Information & Patent Matters	1	NASA Langley Research Center Langley Station Hampton, Virginia 23365 Attn: Technical Librarian	2
Scientific & Technical Information Facility P. O. Box 5700 Bethesda, Maryland 20014 Attn: NASA Rep., Code CRT	2	NASA Langley Research Center Langley Station Hampton, Virginia 23365 Attn: Mr. David Carter	1
NASA Lewis Research Center 21000 Brookpark Road Cleveland, Ohio 44135 Attn: Mr. Paul N. Herr	3	NASA Langley Research Center Langley Station Hampton, Virginia 23365 Attn: Dr. Floyd L. Thompson, Dir.	Ltr. Only

<u>Addressee</u>	<u>Copies</u>	<u>Addressee</u>	<u>Copies</u>
NASA Langley Research Center Langley Station Hampton, Virginia 23365 Attn: Mr. R. Hook	Ltr. Only	Air Force Missile Development Center Holloman Air Force Base, New Mexico 88330 Attn: Maj. R. E. Bracken, Code MDGRT	Ltr. Only
NASA Lewis Research Center 21000 Brookpark Road Cleveland, Ohio 44135 Attn: Technical Librarian	2	Air Force Missile Test Center Patrick Air Force Base, Florida Attn: Technical Librarian	1
NASA Lewis Research Center 21000 Brookpark Road Cleveland, Ohio 44135 Attn: Dr. Abe Silverstein, Dir.	Ltr. Only	Air Force Missile Test Center Patrick Air Force Base, Florida Attn: Mr. L. J. Ullian	Ltr. Only
NASA Lewis Research Center 21000 Brookpark Road Cleveland, Ohio 44135 Attn: Mr. Steve Cohen	Ltr. Only	Air Force Systems Division Air Force Unit Post Office Los Angeles 45, California 90045 Attn: Technical Librarian	1
NASA Marshall Space Flight Center Huntsville, Alabama 35812 Attn: Technical Librarian	2	Air Force Systems Division Air Force Unit Post Office Los Angeles 45, California 90045 Attn: Col. Clark, Tech. Data Center	Ltr. Only
NASA Marshall Space Flight Center Huntsville, Alabama 35812 Attn: Mr. Hans G. Paul, Code R-P+VED	Ltr. Only	Technical Library AFFTC (FTBPP-2) Edwards AFB, California 93523 Attn: Technical Librarian	2
NASA Marshall Space Flight Center Huntsville, Alabama 35812 Attn: Mr. Werner Voss, R-P&VE-FM	Ltr. Only	Arnold Engineering Development Center Arnold Air Force Station Tullahoma, Tennessee 37388 Attn: Technical Librarian	1
NASA Manned Spacecraft Center Houston, Texas 77001 Attn: Technical Librarian	2	Arnold Engineering Development Center Arnold Air Force Station Tullahoma, Tennessee 37388 Attn: Dr. H. K. Doetsch	Ltr. Only
NASA Manned Spacecraft Center Houston, Texas 77001 Attn: Dr. Robert R. Gilruth, Dir.	Ltr. Only	Bureau of Naval Weapons Department of the Navy Washington, D. C. 20546 Attn: Technical Librarian	1
NASA Manned Spacecraft Center Houston, Texas 77001 Attn: Mr. H. Pohl	Ltr. Only	Bureau of Naval Weapons Department of the Navy Washington, D. C. 20546 Attn: Mr. J. Kay, RIMS-41	Ltr. Only
NASA John F. Kennedy Space Center Cocoa Beach, Florida 32931 Attn: Technical Librarian	2	Defense Documentation Center Headquarters Cameron Station, Building 5 5010 Duke Street Alexandria, Virginia 22314 Attn: Technical Librarian	1
NASA John F. Kennedy Space Center Cocoa Beach, Florida 32931 Attn: Dr. Kurt H. Debus	Ltr. Only	Defense Documentation Center Headquarters Cameron Station, Building 5 5010 Duke Street Alexandria, Virginia 22314 Attn: TISIA	Ltr. Only
NASA Test Facility Propulsion Engineering Office White Sands, New Mexico Attn: Technical Librarian	1	Headquarters, U. S. Air Force Washington, D. C. 20546 Attn: Technical Librarian	1
NASA Test Facility Propulsion Engineering Office White Sands, New Mexico Attn: Mr. I. D. Smith, Staff Chemist	Ltr. Only	Headquarters, U. S. Air Force Washington, D. C. 20546 Attn: Col. C. K. Stambaugh, AFRST	Ltr. Only
Aeronautical Systems Division Air Force Systems Command Wright-Patterson Air Force Base Dayton, Ohio 45433 Attn: Technical Librarian	1	Picatiny Arsenal Dover, New Jersey 07801 Attn: Technical Librarian	1
Aeronautical Systems Division Air Force Systems Command Wright-Patterson Air Force Base Dayton, Ohio 45433 Attn: Mr. D. L. Schmidt, Code ASRCNC-2	Ltr. Only	Picatiny Arsenal Dover, New Jersey 07801 Attn: Mr. I. Forsten, Chief Liquid Propulsion Lab., SMUPA-DL	Ltr. Only
Air Force Missile Development Center Holloman Air Force Base, New Mexico 88330 Attn: Technical Librarian	1		

<u>Addressee</u>	<u>Copies</u>	<u>Addressee</u>	<u>Copies</u>
Air Force Rocket Propulsion Laboratory Research and Technology Division Air Force Systems Command Edwards, California 93523 Attn: Technical Librarian	1	Aeronutronic Division Philco Corporation Ford Road Newport Beach, California 92663 Attn: Technical Librarian	1
Air Force Rocket Propulsion Laboratory Research and Technology Division Air Force Systems Command Edwards, California 93523 Attn: Mr. H. Main, RPRR	Ltr. Only	Aeronutronic Division Philco Corporation Ford Road Newport Beach, California 92663 Attn: Mr. N. Stern	Ltr. Only
U. S. Atomic Energy Commission Technical Information Services Box 62 Oak Ridge, Tennessee 37830 Attn: Technical Librarian	1	Aerospace Corporation 2400 East El Segundo Boulevard P. O. Box 95085 Los Angeles, California 90045 Attn: Technical Librarian	1
U. S. Atomic Energy Commission Technical Information Services Box 62 Oak Ridge, Tennessee 37830 Attn: Mr. A. P. Huber Oak Ridge Gaseous Diffusion Plant (ORGDP) P. O. Box P	Ltr. Only	Aerospace Corporation 2400 East El Segundo Boulevard P. O. Box 95085 Los Angeles, California 90045 Attn: Mr. M. J. Russi	Ltr. Only
U. S. Army Missile Command Redstone Arsenal, Alabama 35809 Attn: Technical Librarian	1	Aerospace Corporation 2400 East El Segundo Boulevard P. O. Box 95085 Los Angeles, California 90045 Attn: Mr. H. Greer, Propulsion Dept.	Ltr. Only
U. S. Army Missile Command Redstone Arsenal, Alabama 35809 Attn: Dr. Walter Wharton	Ltr. Only	Arthur D. Little, Incorporated 20 Acorn Park Cambridge, Massachusetts 02140 Attn: Technical Librarian	1
U. S. Naval Ordnance Test Station China Lake, California 93557 Attn: Technical Librarian	1	Arthur D. Little, Incorporated 20 Acorn Park Cambridge, Massachusetts 02140 Attn: Mr. E. Karl Bastress	Ltr. Only
U. S. Naval Ordnance Test Station China Lake, California 93557 Attn: Code 4562 Chief, Missile Propulsion Division	Ltr. Only	Astropower Laboratory Douglas Aircraft Company 2121 Paularino Newport Beach, California 92663 Attn: Technical Librarian	1
Chemical Propulsion CPIA Information Agency Applied Physics Laboratory 8621 Georgia Avenue Silver Spring, Maryland 20910 Attn: Technical Librarian	1	Astropower Laboratory Douglas Aircraft Company 212 Paularino Newport Beach, California 92663 Attn: Dr. George Moc, Dir. Research	Ltr. Only
Chemical Propulsion CPIA Information Agency Applied Physics Laboratory 8621 Georgia Avenue Silver Spring, Maryland 20910 Attn: Mr. P. Martin	Ltr. Only	Astrosystems International, Incorporated 1275 Bloomfield Avenue Fairfield, New Jersey 07007 Attn: Technical Librarian	1
Aerojet-General Corporation P. O. Box 296 Azusa, California 91703 Attn: Technical Librarian	1	Astrosystems International, Incorporated 1275 Bloomfield Avenue Fairfield, New Jersey 07007 Attn: Mr. A. Mendenhall	Ltr. Only
Aerojet-General Corporation P. O. Box 296 Azusa, California 91703 Attn: Mr. L. F. Kohrs	Ltr. Only	Atlantic Research Corporation Edsall Road and Shirley Highway Alexandria, Virginia 22314 Attn: Technical Librarian	1
Aerojet-General Corporation P. O. Box 1947 Technical Library, Bldg. 2015, Dept. 2410 Sacramento, California 95809 Attn: Technical Librarian	1	Atlantic Research Corporation Edsall Road and Shirley Highway Alexandria, Virginia 22314 Attn: Mr. A. Scurlock	Ltr. Only
Aerojet-General Corporation P. O. Box 1947 Sacramento, California 95809 Attn: Dr. C. B. McGough	Ltr. Only	Beech Aircraft Corporation Boulder Division Box 631 Boulder, Colorado 80302 Attn: Technical Librarian	1

<u>Addressee</u>	<u>Copies</u>	<u>Addressee</u>	<u>Copies</u>
Beech Aircraft Corporation Boulder Division Box 631 Boulder, Colorado 80302 Attn: Mr. J. H. Rodgers	Ltr. Only	Missile and Space Systems Division Douglas Aircraft Company, Incorporated 3000 Ocean Park Boulevard Santa Monica, California 90406 Attn: Mr. R. W. Hallet, Chief Engineer Advanced Space Tech.	Ltr. Only
Bell Aerosystems Company P. O. Box 1 Buffalo, New York 14240 Attn: Technical Librarian	1	Missile and Space Systems Division Douglas Aircraft Company, Incorporated 3000 Ocean Park Boulevard Santa Monica, California 90406 Attn: Mr. A. Pisciotto, Jr.	Ltr. Only
Bell Aerosystems Company P. O. Box 1 Buffalo, New York 14240 Attn: Mr. N. Safeer	Ltr. Only	Aircraft Missiles Division Fairchild Hiller Corporation Hagerstown, Maryland 21740 Attn: Technical Librarian	1
Bell Aerosystems Company P. O. Box 1 Buffalo, New York 14240 Attn: Mr. N. R. Roth	Ltr. Only	Aircraft Missiles Division Fairchild Hiller Corporation Hagerstown, Maryland 21740 Attn: Mr. J. S. Kerr	Ltr. Only
Bell Aerosystems Company P. O. Box 1 Buffalo, New York 14240 Attn: Mr. J. Flanagan	Ltr. Only	General Dynamics Convair Division 5001 Kearny Villa Road P. O. Box 1628 San Diego, California 92112 Attn: Technical Librarian	1
Bendix Systems Division Bendix Corporation 3300 Plymouth Road Ann Arbor, Michigan 48105 Attn: Technical Librarian	1	General Dynamics Convair Division 5001 Kearny Villa Road P. O. Box 1628 San Diego, California 92112 Attn: Mr. E. R. Peterson V.P., Research and Eng.	Ltr. Only
Bendix Systems Division Bendix Corporation 3300 Plymouth Road Ann Arbor, Michigan 48105 Attn: Mr. John M. Brueger	Ltr. Only	General Dynamics Convair Division 5001 Kearny Villa Road P. O. Box 1628 San Diego, California 92112 Attn: Mr. Frank Dore	Ltr. Only
Boeing Company P. O. Box 3707 Seattle, Washington 98124 Attn: Technical Librarian	1	Missile and Space Systems Center General Electric Company Valley Forge Space Technology Center P. O. Box 8555 Philadelphia, Pennsylvania Attn: Technical Librarian	1
Boeing Company P. O. Box 3707 Seattle, Washington 98124 Attn: Mr. J. D. Alexander	Ltr. Only	Missile and Space Systems Center General Electric Company Valley Forge Space Technology Center P. O. Box 8555 Philadelphia, Pennsylvania Attn: Mr. F. Mezger	Ltr. Only
Missile Division Chrysler Corporation P. O. Box 2628 Detroit, Michigan 48231 Attn: Technical Librarian	1	Missile and Space Systems Center General Electric Company Valley Forge Space Technology Center P. O. Box 8555 Philadelphia, Pennsylvania Attn: Mr. R. E. Emmer	Ltr. Only
Missile Division Chrysler Corporation P. O. Box 2628 Detroit, Michigan 48231 Attn: Mr. John Gates	Ltr. Only	Missile and Space Systems Center General Electric Company Valley Forge Space Technology Center P. O. Box 8555 Philadelphia, Pennsylvania Attn: Mr. B. H. Caldwell	Ltr. Only
Wright Aeronautical Division Curtiss-Wright Corporation Wood-Ridge, New Jersey 07075 Attn: Technical Librarian	1	Advanced Engine & Technology Department General Electric Company Cincinnati, Ohio 45215 Attn: Technical Librarian	1
Wright Aeronautical Division Curtiss-Wright Corporation Wood-Ridge, New Jersey 07075 Attn: Mr. G. Kelley	Ltr. Only		
Missile and Space Systems Division Douglas Aircraft Company, Incorporated 3000 Ocean Park Boulevard Santa Monica, California 90406 Attn: Technical Librarian	1		

<u>Addressee</u>	<u>Copies</u>	<u>Addressee</u>	<u>Copies</u>
Advanced Engine & Technology Department General Electric Company Cincinnati, Ohio 45215 Attn: Mr. D. Suichu	Ltr. Only	The Marquardt Corporation 16555 Saricoy Street Van Nuys, California 91409 Attn: Mr. Warren P. Boardman, Jr.	Ltr. Only
Grumman Aircraft Engineering Corporation Bethpage, Long Island, New York 11714 Attn: Technical Librarian	1	The Marquardt Corporation 16555 Saricoy Street Van Nuys, California 91409 Attn: Mr. R. Knox	Ltr. Only
Grumman Aircraft Engineering Corporation Bethpage, Long Island, New York 11714 Attn: Mr. Joseph Gavin	Ltr. Only	Baltimore Division Martin Marietta Corporation Baltimore, Maryland 21203 Attn: Technical Librarian	1
Hughes Aircraft Company Aerospace Group Centinela and Teale Streets Culver City, California Attn: Technical Librarian	1	Baltimore Division Martin Marietta Corporation Baltimore, Maryland 21203 Attn: Mr. John Calathes (3214)	Ltr. Only
Hughes Aircraft Company Aerospace Group Centinela and Teale Streets Culver City, California Attn: Mr. E. H. Meier, V.P. & Div. Mgr. Research and Dev. Div.	Ltr. Only	Denver Division Martin Marietta Corporation P. O. Box 179 Denver, Colorado 80201 Attn: Technical Librarian	1
Walter Kidde & Company, Incorporated 675 Main Street Belleville, New Jersey 07109 Attn: Technical Librarian	1	Denver Division Martin Marietta Corporation P. O. Box 179 Denver, Colorado 80201 Attn: Mr. J. D. Goodlette (A-241)	Ltr. Only
Walter Kidde & Company, Incorporated 675 Main Street Belleville, New Jersey 07109 Attn: Mr. K. A. Traynelis	Ltr. Only	Denver Division Martin Marietta Corporation P. O. Box 179 Denver, Colorado 80201 Attn: Mr. A. J. Kullas	Ltr. Only
Ling-Temco-Vought Corporation Astronautics P. O. Box 5907 Dallas, Texas 75222 Attn: Technical Librarian	1	Orland Division Martin Marietta Corporation Box 5837 Orlando, Florida Attn: Technical Librarian	1
Ling-Temco-Vought Corporation Astronautics P. O. Box 5907 Dallas, Texas 75222 Attn: Mr. Garland Whisenhunt	Ltr. Only	Orland Division Martin Marietta Corporation Box 5837 Orlando, Florida Attn: Mr. J. Ferm	Ltr. Only
Lockheed Missiles and Space Company Attn: Technical Information Center P. O. Box 504 Sunnyvale, California 94088 Attn: Technical Librarian	1	McDonnell Aircraft Corporation P. O. Box 516 Municipal Airport St. Louis, Missouri 63166 Attn: Technical Librarian	1
Lockheed Missiles and Space Company Attn: Technical Information Center P. O. Box 504 Sunnyvale, California 94088 Attn: Mr. Y. C. Lee	Ltr. Only	McDonnell Aircraft Corporation P. O. Box 516 Municipal Airport St. Louis, Missouri 63166 Attn: Mr. R. A. Herzmark	Ltr. Only
Lockheed Propulsion Company P. O. Box 111 Redlands, California 92374 Attn: Technical Librarian	1	McDonnell Aircraft Corporation P. O. Box 516 Municipal Airport St. Louis, Missouri 63166 Attn: Mr. P. Kelley	Ltr. Only
Lockheed Propulsion Company P. O. Box 111 Redlands, California 92374 Attn: Mr. H. L. Thackwell	Ltr. Only	Rocket Research Corporation 520 South Portland Street Seattle, Washington 98108 Attn: Technical Librarian	1
Lockheed Propulsion Company P. O. Box 111 Redlands, California 92374 Attn: Mr. J. E. Fitzgerald	Ltr. Only	Rocket Research Corporation 520 South Portland Street Seattle, Washington 98108 Attn: Mr. Foy McCullough, Jr.	Ltr. Only
The Marquardt Corporation 16555 Saricoy Street Van Nuys, California 91409 Attn: Technical Librarian	1		

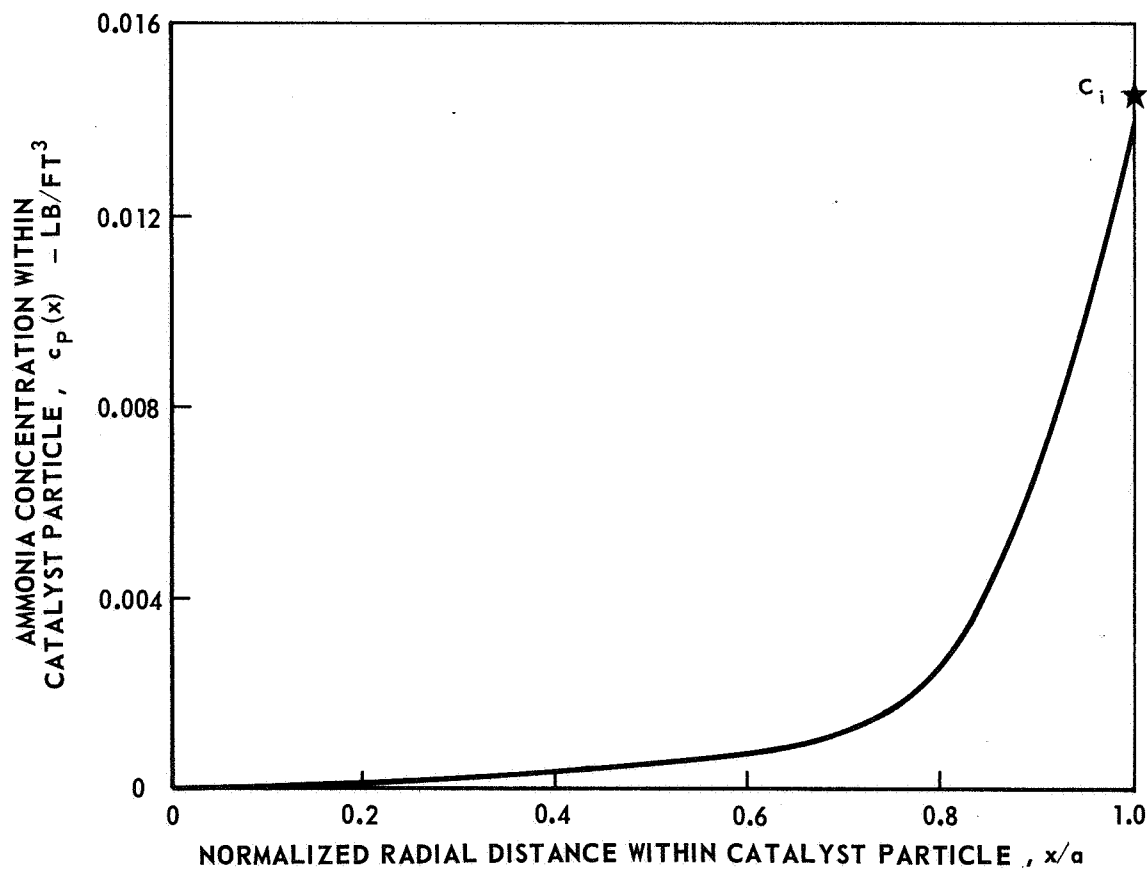
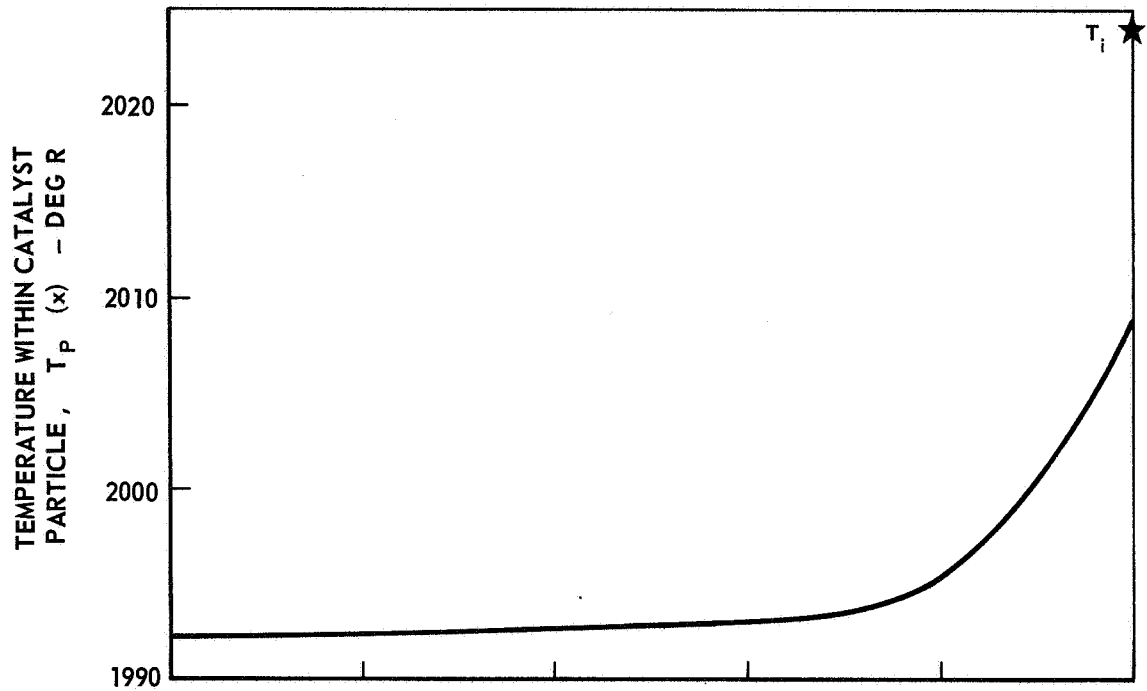
<u>Addressee</u>	<u>Copies</u>	<u>Addressee</u>	<u>Copies</u>
Rocket Research Corporation 520 South Portland Street Seattle, Washington 98108 Attn: Mr. Bruce Schmitz	Ltr. Only	Republic Aviation Corporation Farmingdale, Long Island, New York Attn: Technical Librarian	1
Rocket Research Corporation 520 South Portland Street Seattle, Washington 98108 Attn: Dr. Duane Williams	Ltr. Only	Republic Aviation Corporation Farmingdale, Long Island, New York Attn: Dr. William O'Donnell	Ltr. Only
Space & Information Systems Division North American Aviation, Incorporated 12214 Lakewood Boulevard Downey, California 90241 Attn: Technical Librarian	1	Space General Corporation 9200 East Flair Avenue El Monte, California 91734 Attn: Technical Librarian	1
Space & Information Systems Division North American Aviation, Incorporated 12214 Lakewood Boulevard Downey, California 90241 Attn: Mr. H. Storms	Ltr. Only	Space General Corporation 9200 East Flair Avenue El Monte, California 91734 Attn: Mr. C. E. Roth	Ltr. Only
Rocketdyne (Library 586-306) North American Aviation, Incorporated 6633 Canoga Avenue Canoga Park, California 91304 Attn: Technical Librarian	1	Stanford Research Institute 333 Ravenswood Avenue Menlo Park, California 94025 Attn: Technical Librarian	1
Rocketdyne (Library 586-306) North American Aviation, Incorporated 6633 Canoga Avenue Canoga Park, California 91304 Attn: Mr. E. B. Monteath	Ltr. Only	Stanford Research Institute 333 Ravenswood Avenue Menlo Park, California 94025 Attn: Mr. Lionel Dickinson	Ltr. Only
Rocketdyne (Library 586-306) North American Aviation, Incorporated 6633 Canoga Avenue Canoga Park, California 91304 Attn: Mr. E. V. Zettle	Ltr. Only	TRW Systems One Space Park Redondo Beach, California 90278 Attn: Technical Librarian	1
Rocketdyne (Library 586-306) North American Aviation, Incorporated 6633 Canoga Avenue Canoga Park, California 91304 Attn: Mr. N. Rodewald	Ltr. Only	TRW Systems One Space Park Redondo Beach, California 90278 Attn: Mr. D. Lee	Ltr. Only
Northrop Space Laboratories 3401 West Broadway Hawthorne, California 90250 Attn: Technical Librarian	1	TRW Systems One Space Park Redondo Beach, California 90278 Attn: Mr. V. Moseley	Ltr. Only
Northrop Space Laboratories 3401 West Broadway Hawthorne, California 90250 Attn: Dr. William Howard	Ltr. Only	Tapco Division TRW, Incorporated 23555 Euclid Avenue Cleveland, Ohio 44117 Attn: Technical Librarian	1
Astro-Electronics Division Radio Corporation of America Princeton, New Jersey 08540 Attn: Technical Librarian	1	Tapco Division TRW, Incorporated 23555 Euclid Avenue Cleveland, Ohio 44117 Attn: Mr. P. T. Angell	Ltr. Only
Astro-Electronics Division Radio Corporation of America Princeton, New Jersey 08540 Attn: Mr. S. Fairweather	Ltr. Only	Thiokol Chemical Corporation Huntsville Division Huntsville, Alabama 35807 Attn: Technical Librarian	1
Reaction Motors Division Thiokol Chemical Corporation Denville, New Jersey 07832 Attn: Technical Librarian	1	Thiokol Chemical Corporation Huntsville Division Huntsville, Alabama 34807 Attn: Mr. John Goodloe	Ltr. Only
Reaction Motors Division Thiokol Chemical Corporation Denville, New Jersey 07832 Attn: Mr. Arthur Sherman	Ltr. Only	United Technology Center 587 Methilda Avenue P. O. Box 358 Sunnyvale, California 94088 Attn: Technical Librarian	1
Reaction Motors Division Thiokol Chemical Corporation Denville, New Jersey 07832 Attn: Mr. Robert Gere	Ltr. Only	United Technology Center 587 Methilda Avenue P. O. Box 358 Sunnyvale, California 94088 Attn: Mr. B. Adelman	Ltr. Only

<u>Addressee</u>	<u>Copies</u>	<u>Addressee</u>	<u>Copies</u>
Florida Research & Development Center Pratt & Whitney Aircraft United Aircraft Corporation P. O. Box 2691 West Palm Beach, Florida 33402 Attn: Technical Librarian	1	Brooklyn Polytechnic Institute Department of Chemical Engineering 333 Jay Street Brooklyn, New York 11201 Attn: Prof. I. Miller	Ltr. Only
Florida Research & Development Center Pratt & Whitney Aircraft United Aircraft Corporation P. O. Box 2691 West Palm Beach, Florida 33402 Attn: Mr. R. J. Coar	Ltr. Only		
Vickers Incorporated Box 302 Troy, Michigan Attn: Technical Librarian	1		
Sunstrand Aviation 2421 11th Street Rockford, Illinois 61101 Attn: Technical Librarian	1		
Sunstrand Aviation 2421 11th Street Rockford, Illinois 61101 Attn: Mr. R. W. Reynolds	Ltr. Only		
Hamilton Standard Division United Aircraft Corporation Windsor Locks, Connecticut 06096 Attn: Technical Librarian	1		
Hamilton Standard Division United Aircraft Corporation Windsor Locks, Connecticut 06096 Attn: Mr. R. Hatch	Ltr. Only		
Technical Library Air Research Manufacturing Company 9851 Sepulveda Boulevard Los Angeles, California 90009 Attn: Technical Librarian	1		
Air Research Manufacturing Company 9851 Sepulveda Boulevard Los Angeles, California 90009 Attn: Mr. C. S. Coe	Ltr. Only		
Air Research Manufacturing Company 9851 Sepulveda Boulevard Los Angeles, California 90009 Attn: Mr. A. C. Standiffe	Ltr. Only		
Shell Development Company 1400 53rd Street Emeryville, California 94608 Attn: Technical Librarian	1		
Shell Development Company 1400 53rd Street Emeryville, California 94608 Attn: Dr. H. Voge	Ltr. Only		
Shell Development Company 1400 53rd Street Emeryville, California 94608 Attn: Dr. T. J. Jennings	Ltr. Only		
Brooklyn Polytechnic Institute Department of Chemical Engineering 333 Jay Street Brooklyn, New York 11201 Attn: Technical Librarian	1		

TEMPERATURE AND AMMONIA CONCENTRATION PROFILES WITHIN CATALYST PARTICLE

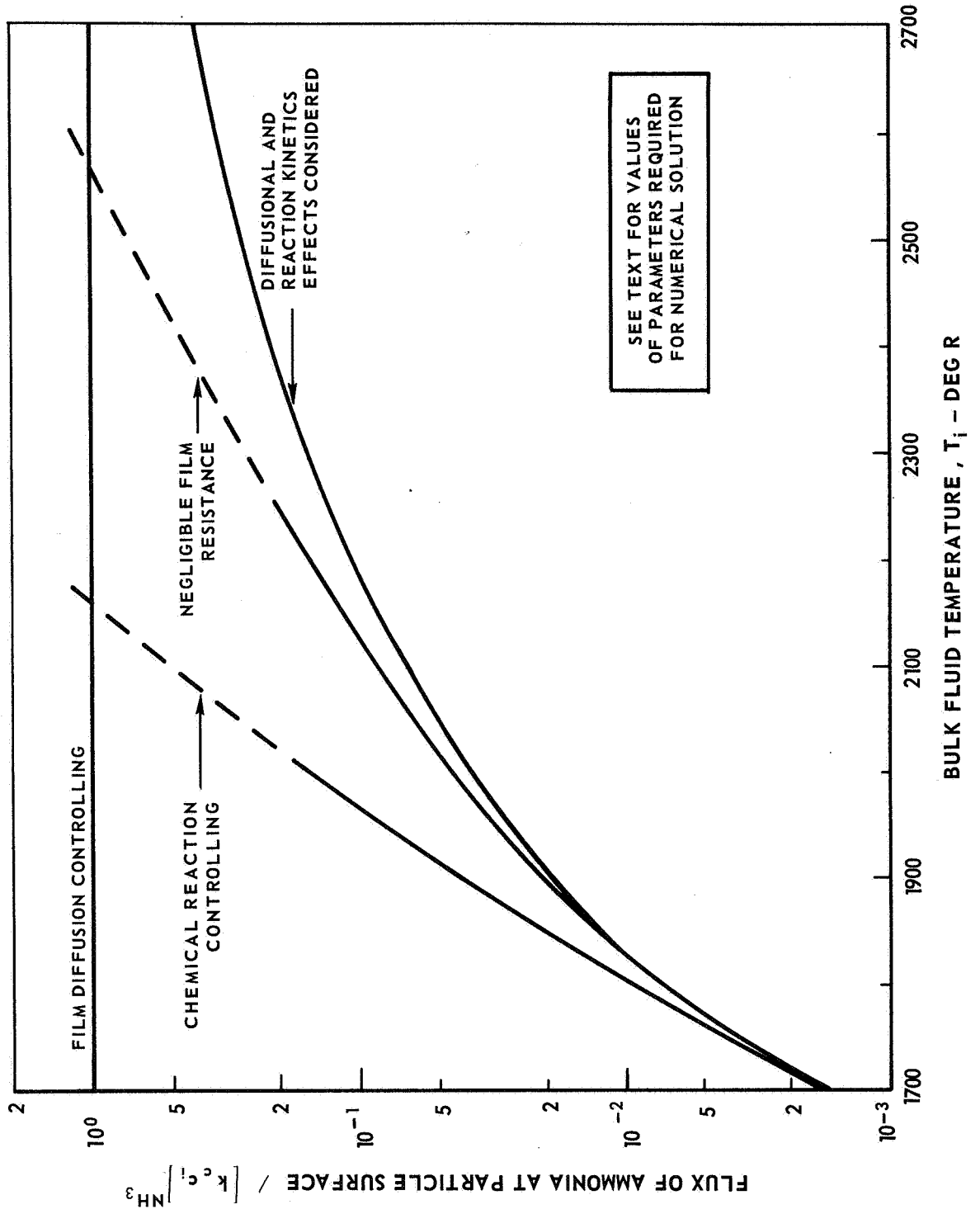
NO HYDRAZINE PRESENT IN BULK FLUID

SEE TEXT FOR VALUES OF PARAMETERS REQUIRED FOR NUMERICAL SOLUTION



EFFECT OF BULK FLUID TEMPERATURE ON MASS FLUX OF AMMONIA AT SURFACE OF CATALYST PARTICLE

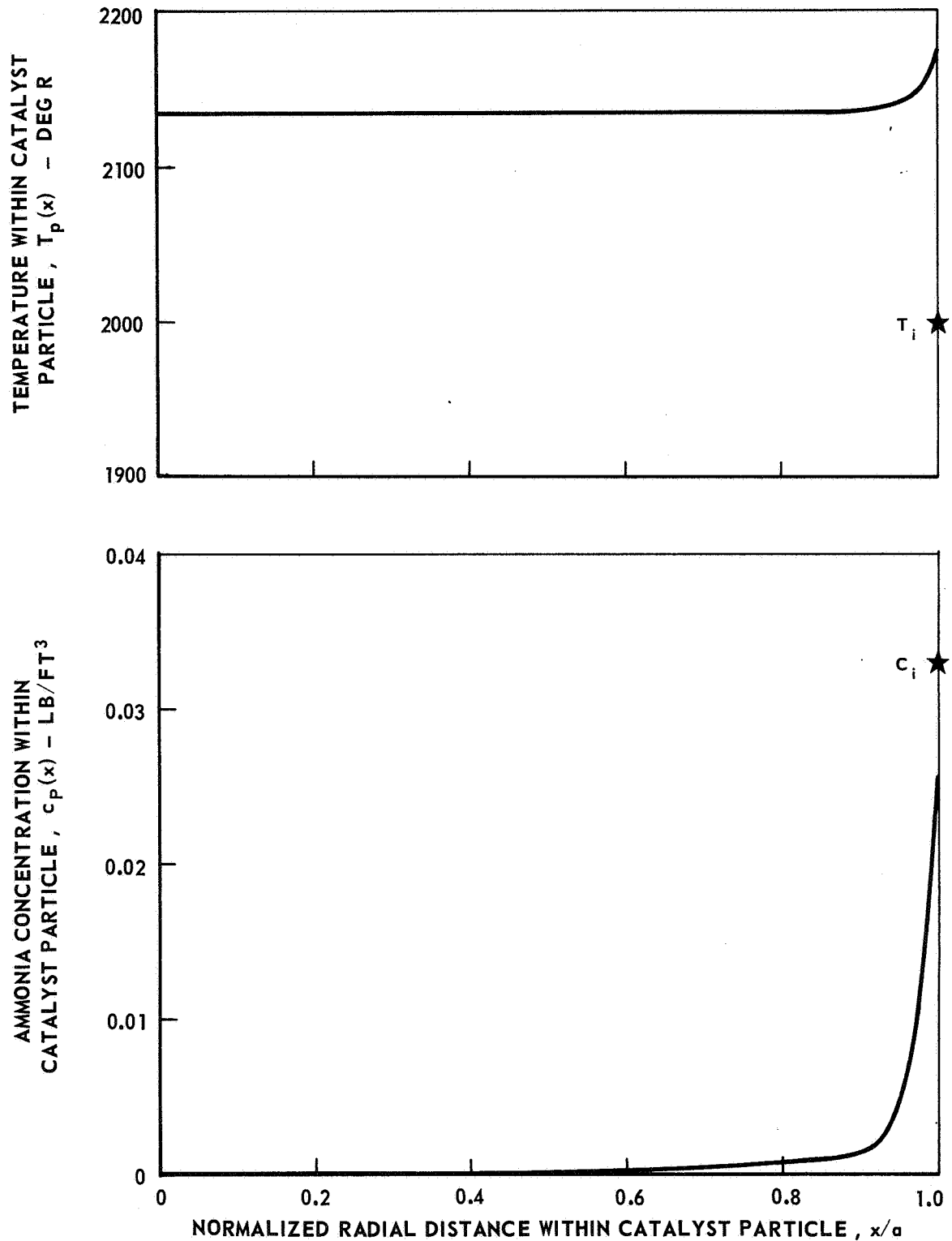
NO HYDRAZINE PRESENT IN BULK FLUID



TEMPERATURE AND AMMONIA CONCENTRATION PROFILES WITHIN CATALYST PARTICLE

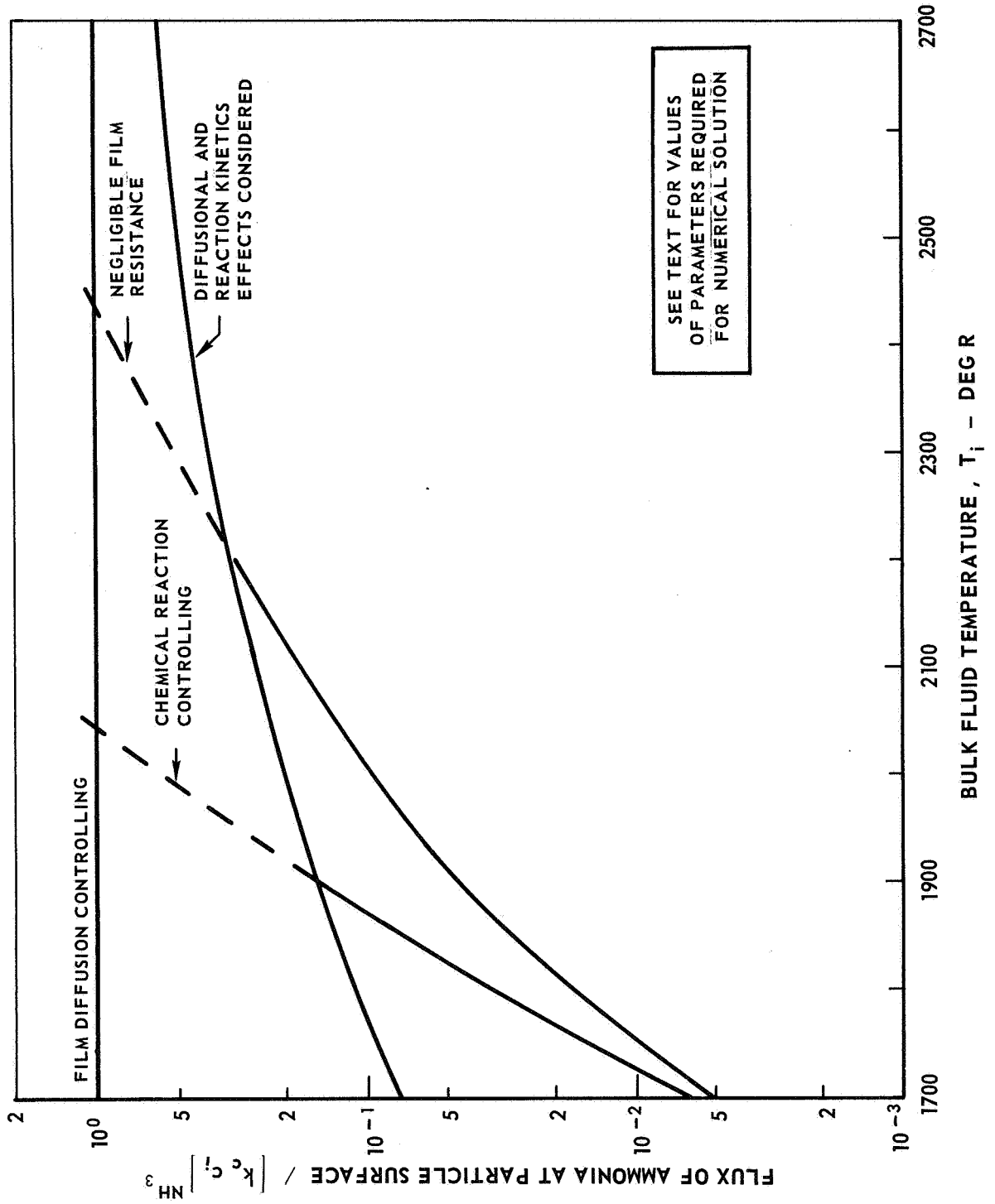
HYDRAZINE PRESENT IN BULK FLUID

SEE TEXT FOR VALUES OF PARAMETERS REQUIRED FOR NUMERICAL SOLUTION



EFFECT OF BULK FLUID TEMPERATURE ON MASS FLUX OF AMMONIA AT SURFACE OF CATALYST PARTICLE

HYDRAZINE PRESENT IN BULK FLUID

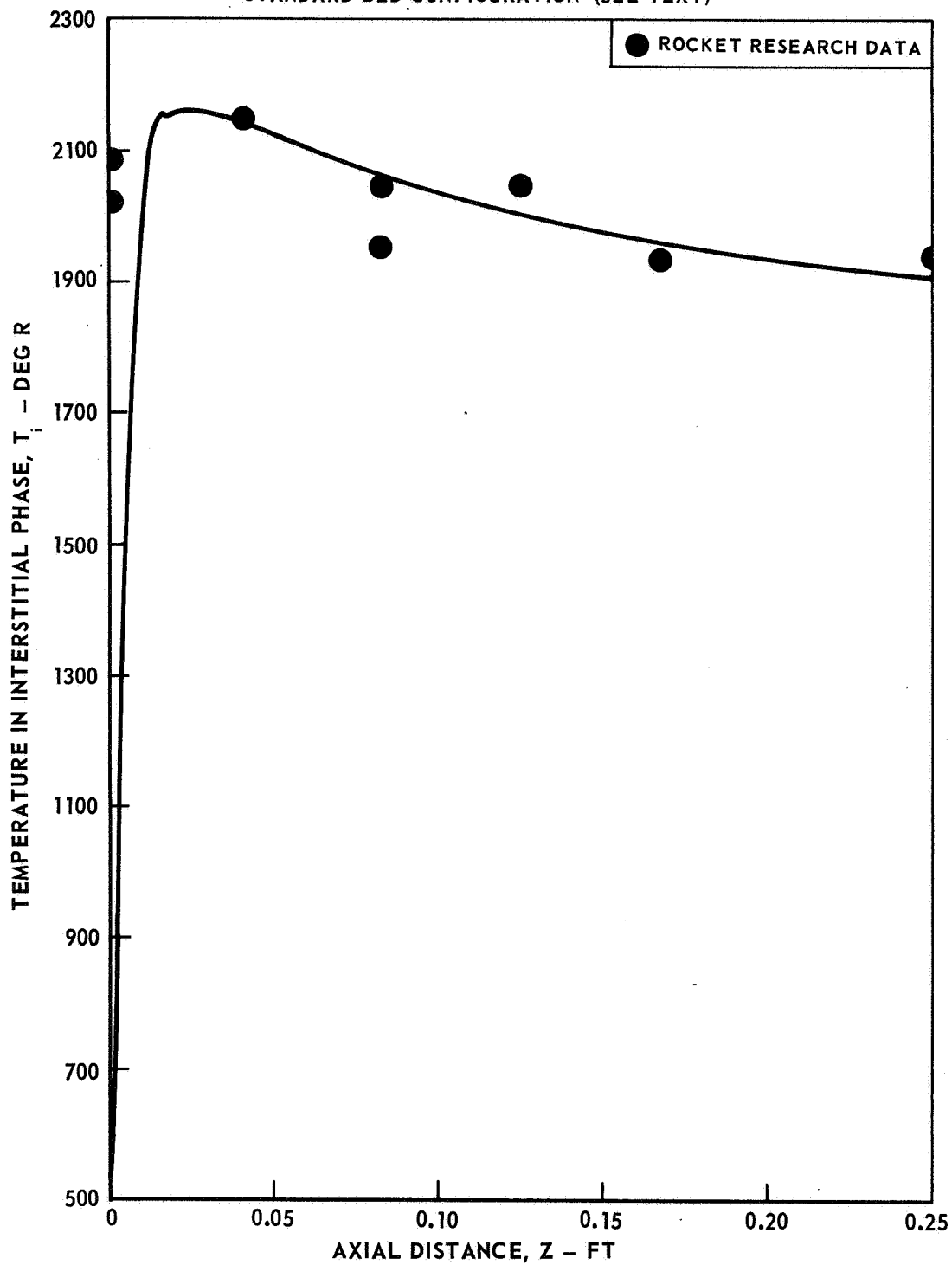


STEADY-STATE AXIAL TEMPERATURE PROFILE USING MODIFIED FILM AND PORE DIFFUSION MODEL

$P = 479.5$ PSIA

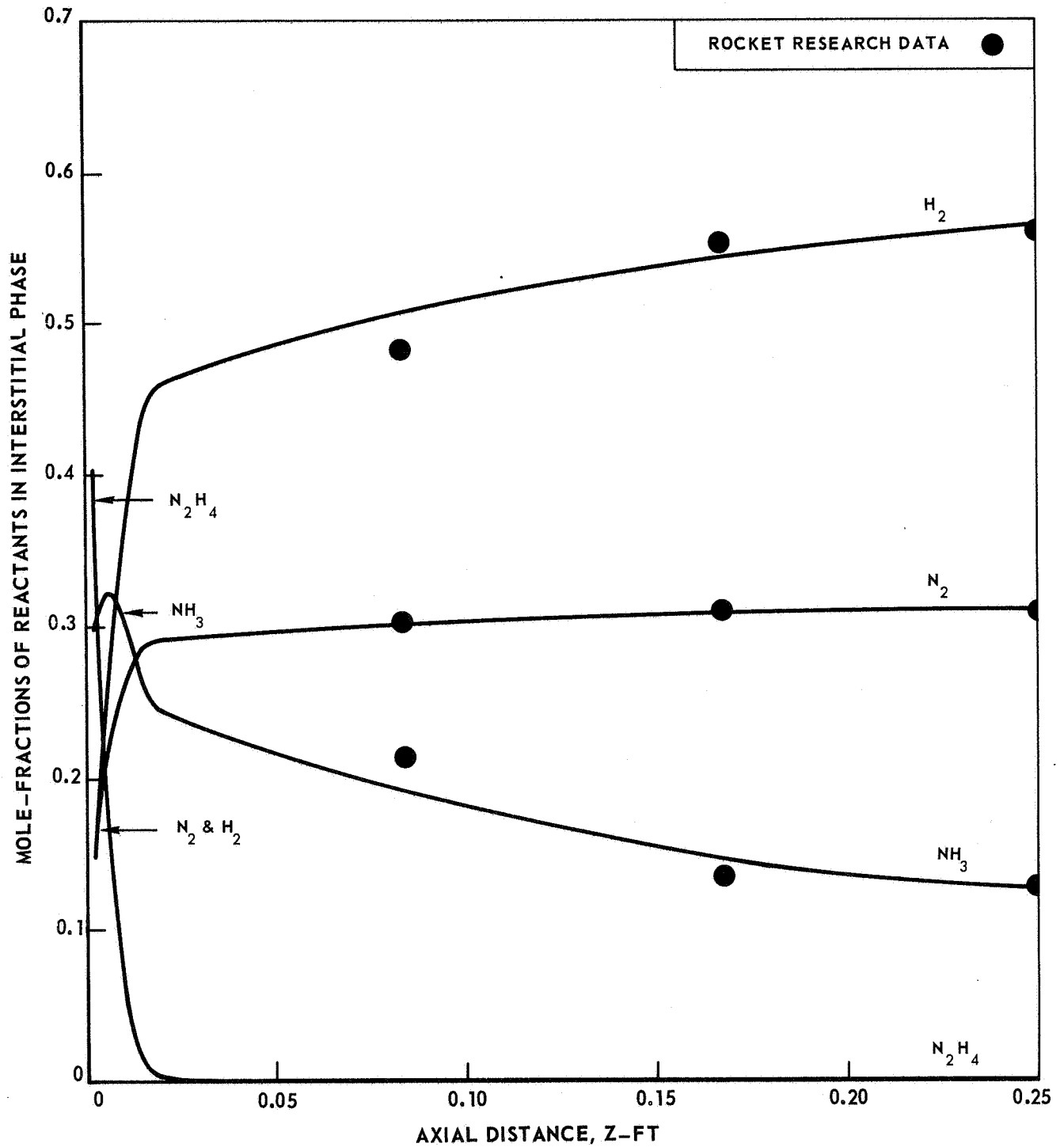
$G = 3.12$ LB/FT² - SEC

STANDARD BED CONFIGURATION (SEE TEXT)



STEADY-STATE AXIAL PROFILES
OF MOLE-FRACTIONS OF REACTANTS
USING MODIFIED FILM AND PORE DIFFUSION MODEL

P = 479.5 PSIA
G = 3.12 LB/FT²-SEC
STANDARD BED CONFIGURATION (SEE TEXT)

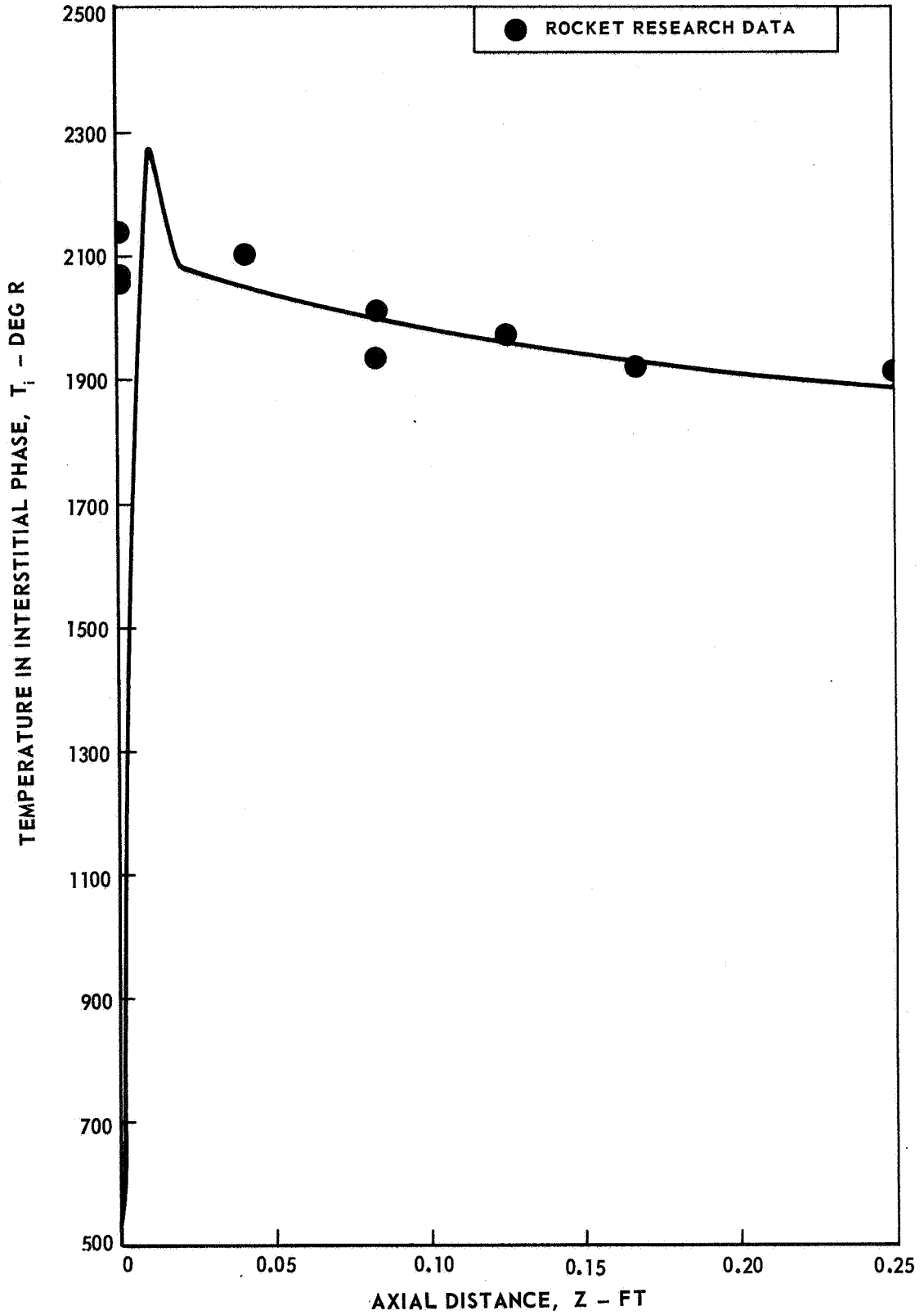


STEADY-STATE AXIAL TEMPERATURE PROFILE USING MODIFIED FILM AND PORE DIFFUSION MODEL

P = 1042 PSIA

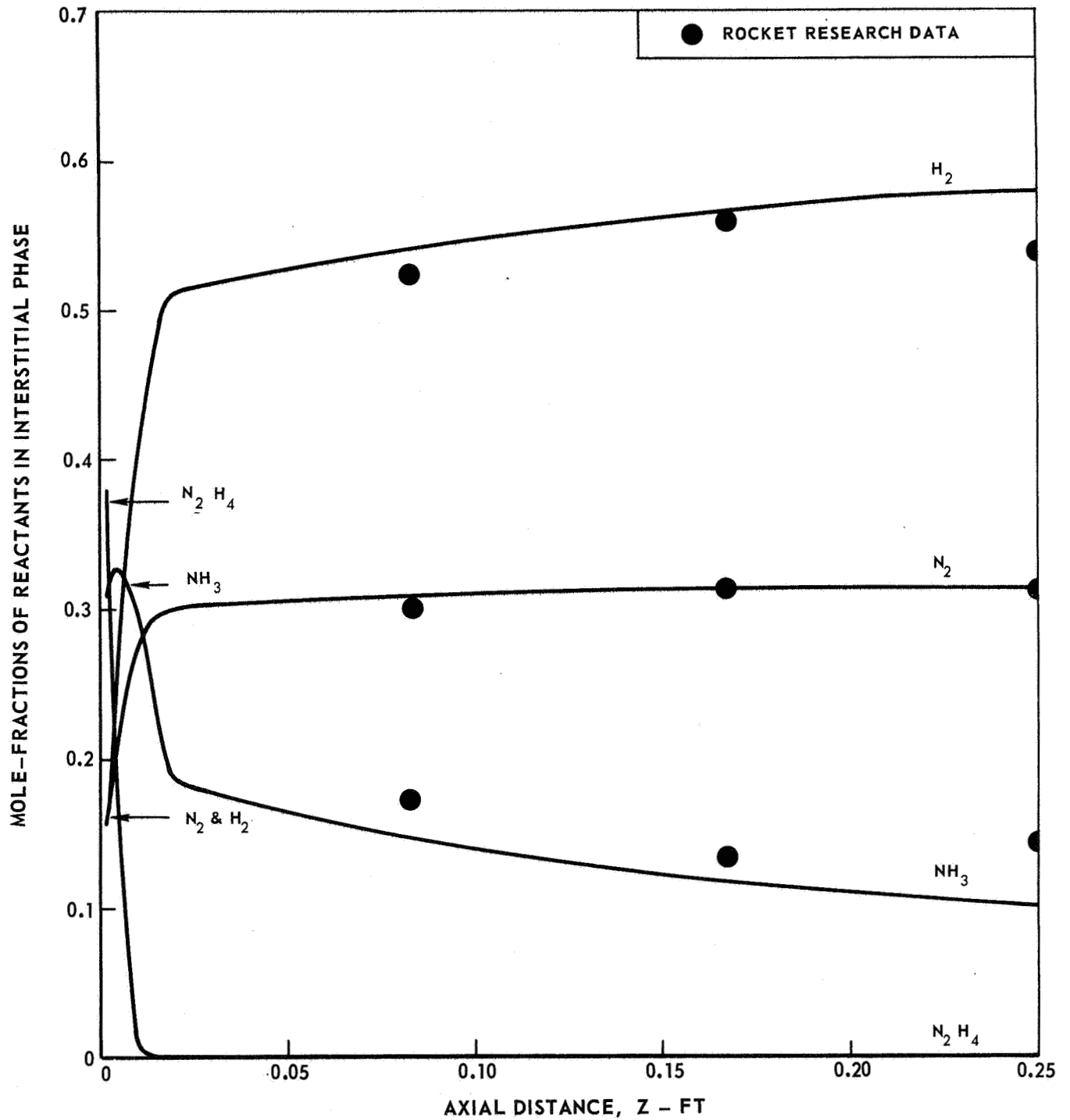
G = 2.43 LB/FT² - SEC

STANDARD BED CONFIGURATION (SEE TEXT)



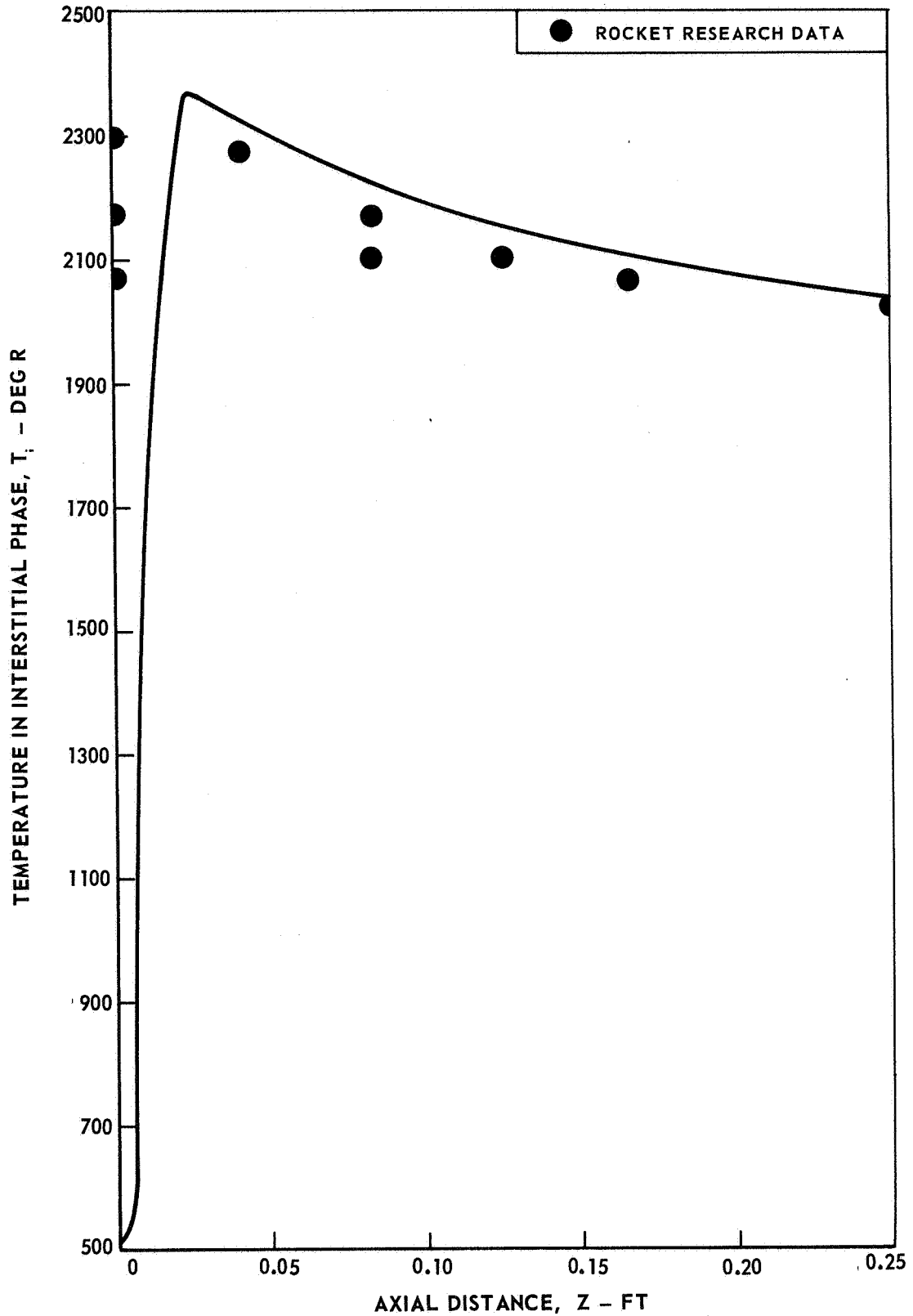
STEADY-STATE AXIAL PROFILES
OF MOLE-FRACTIONS OF REACTANTS
USING MODIFIED FILM AND PORE DIFFUSION MODEL

P = 1042 PSIA .
G = 2.43 LB/FT²- SEC
STANDARD BED CONFIGURATION (SEE TEXT)



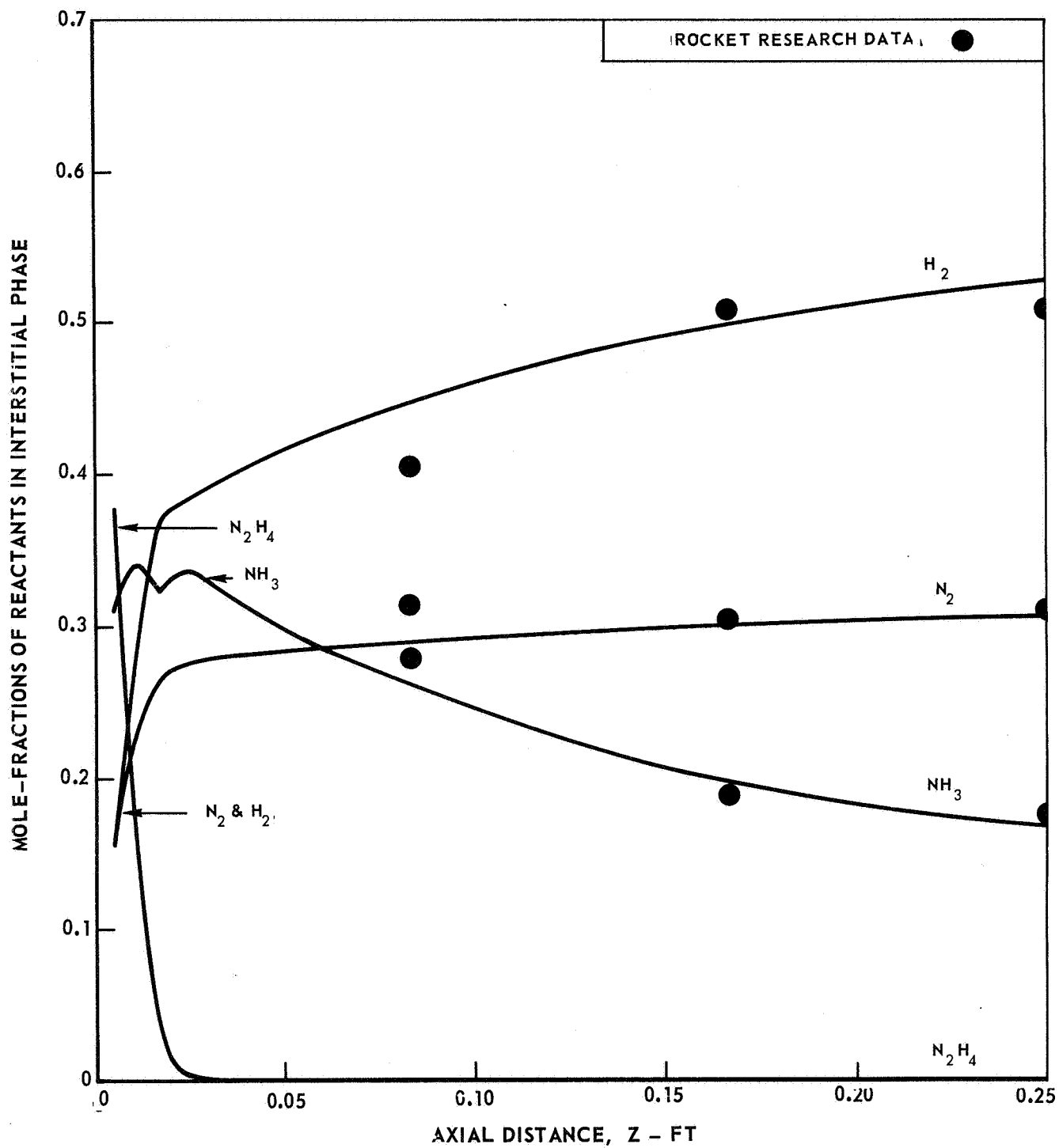
STEADY-STATE AXIAL TEMPERATURE PROFILE OF FILE USING MODIFIED FILM AND PORE DIFFUSION MODEL

P = 974 PSIA
G = 6.29 LB/FT²-SEC
STANDARD BED CONFIGURATION (SEE TEXT)



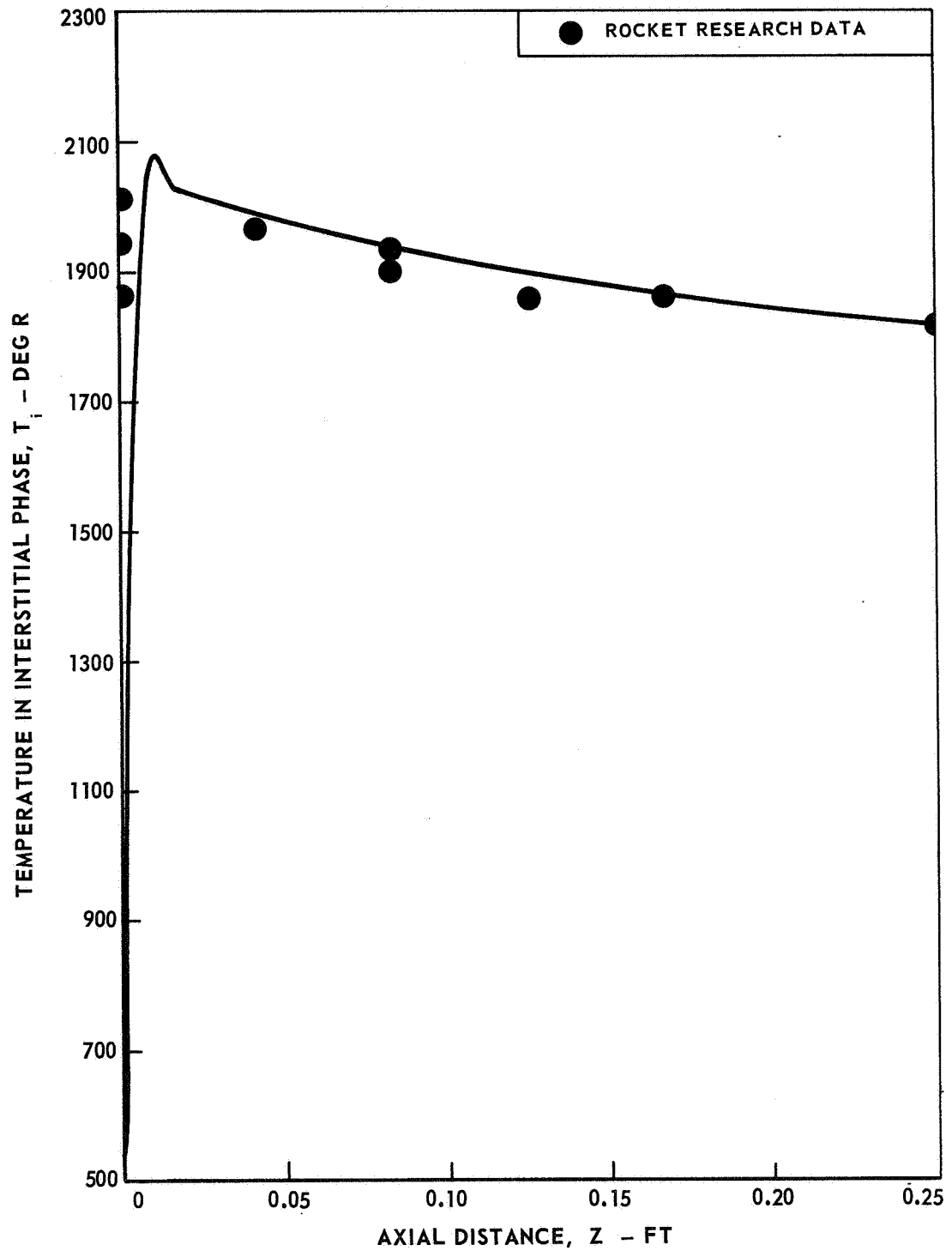
STEADY-STATE AXIAL PROFILES
OF MOLE-FRACTIONS OF REACTANTS
USING MODIFIED FILM AND PORE DIFFUSION MODEL

$P = 974$ PSIA
 $G = 6.29$ LB/FT² - SEC
STANDARD BED CONFIGURATION (SEE TEXT)



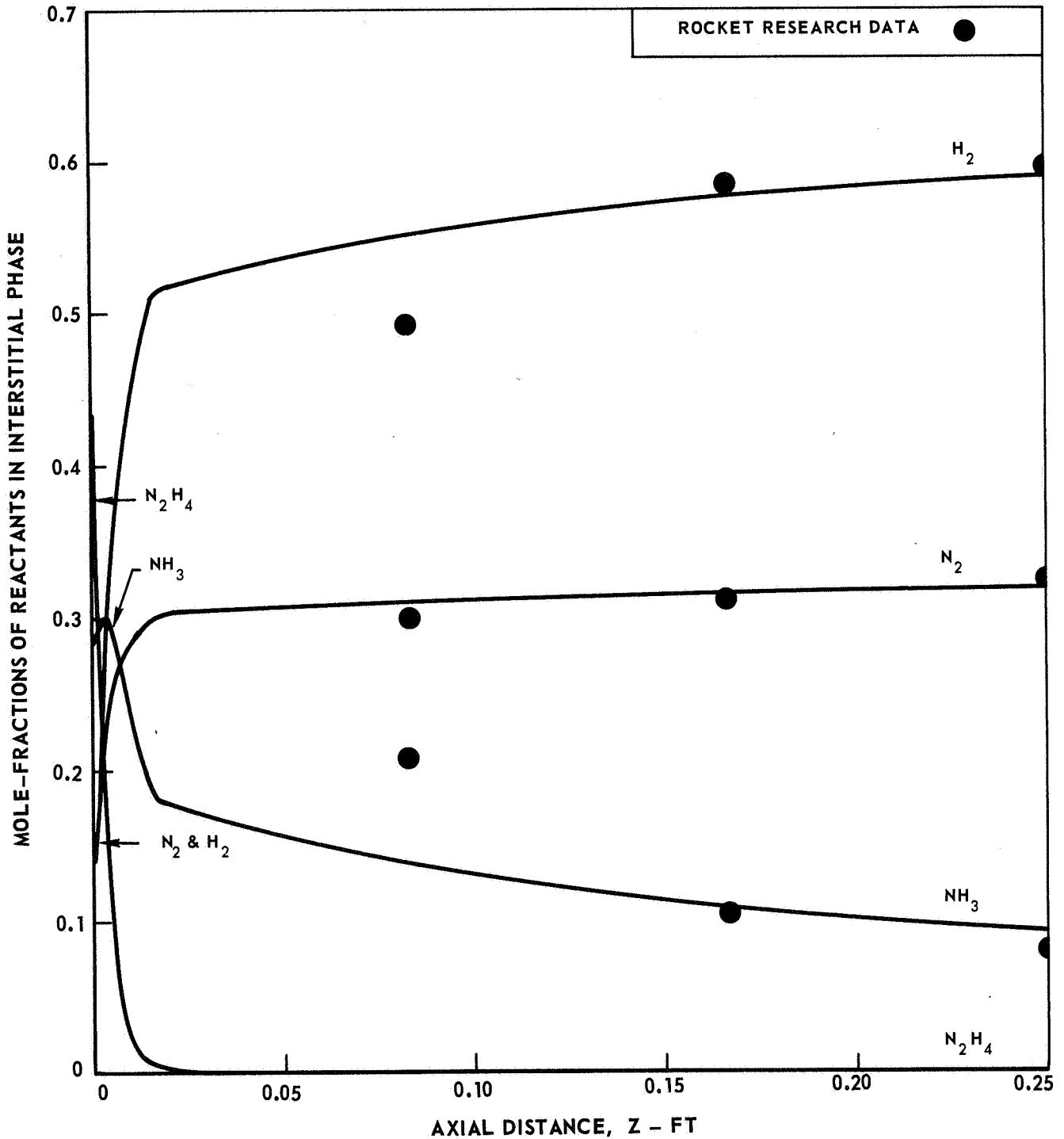
STEADY-STATE AXIAL TEMPERATURE PROFILE
USING MODIFIED FILM AND PORE DIFFUSION MODEL

P = 217.9 PSIA A
G = 1.52 LB/FT² - SEC SEC
STANDARD BED CONFIGURATION (SEE TEXT) TEXT)



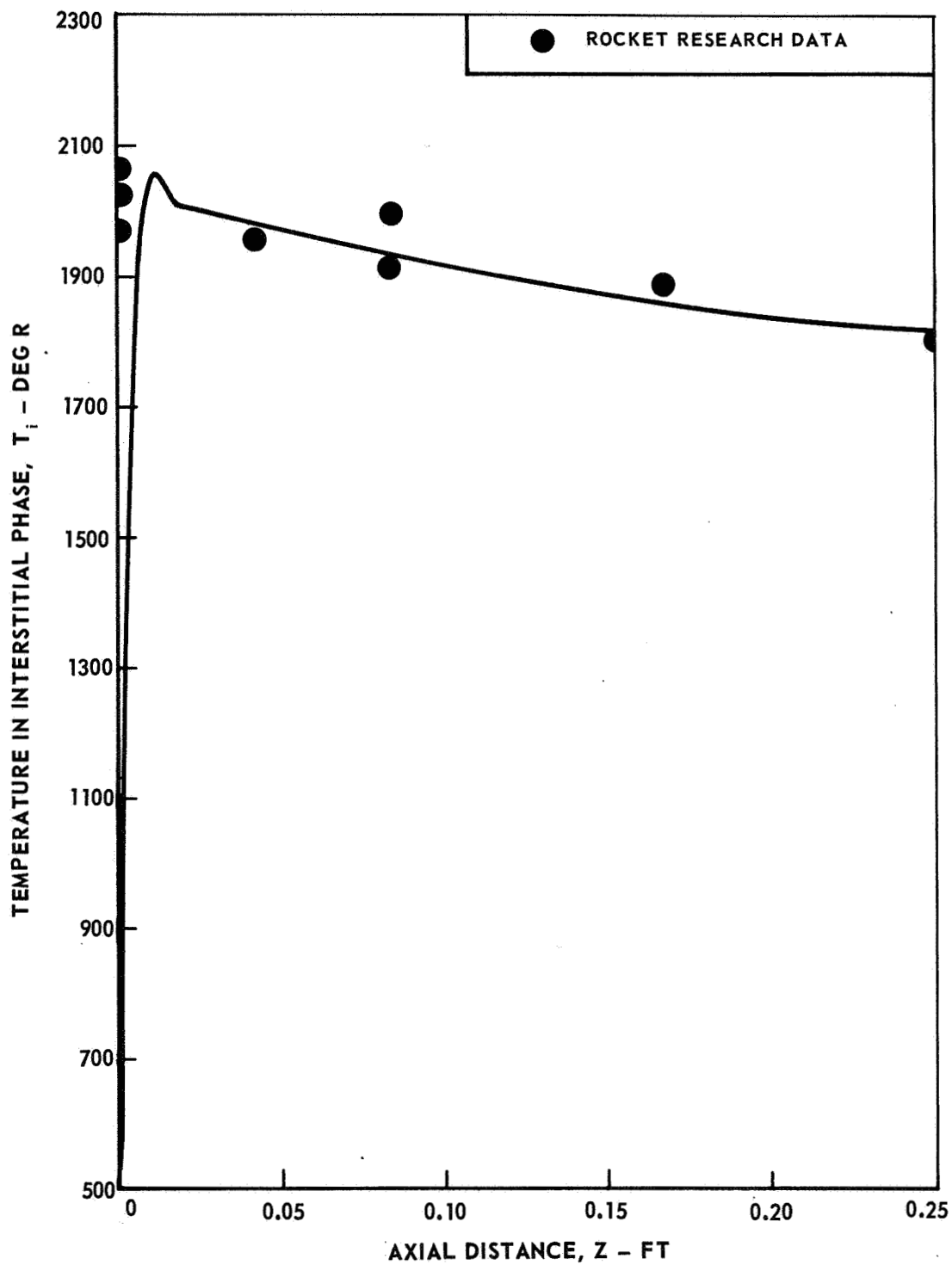
STEADY-STATE AXIAL PROFILES
OF MOLE-FRACTIONS OF REACTANTS
USING MODIFIED FILM AND PORE DIFFUSION MODEL

P = 217.9 PSIA
G = 1.52 LB/FT² - SEC
STANDARD BED CONFIGURATION (SEE TEXT)



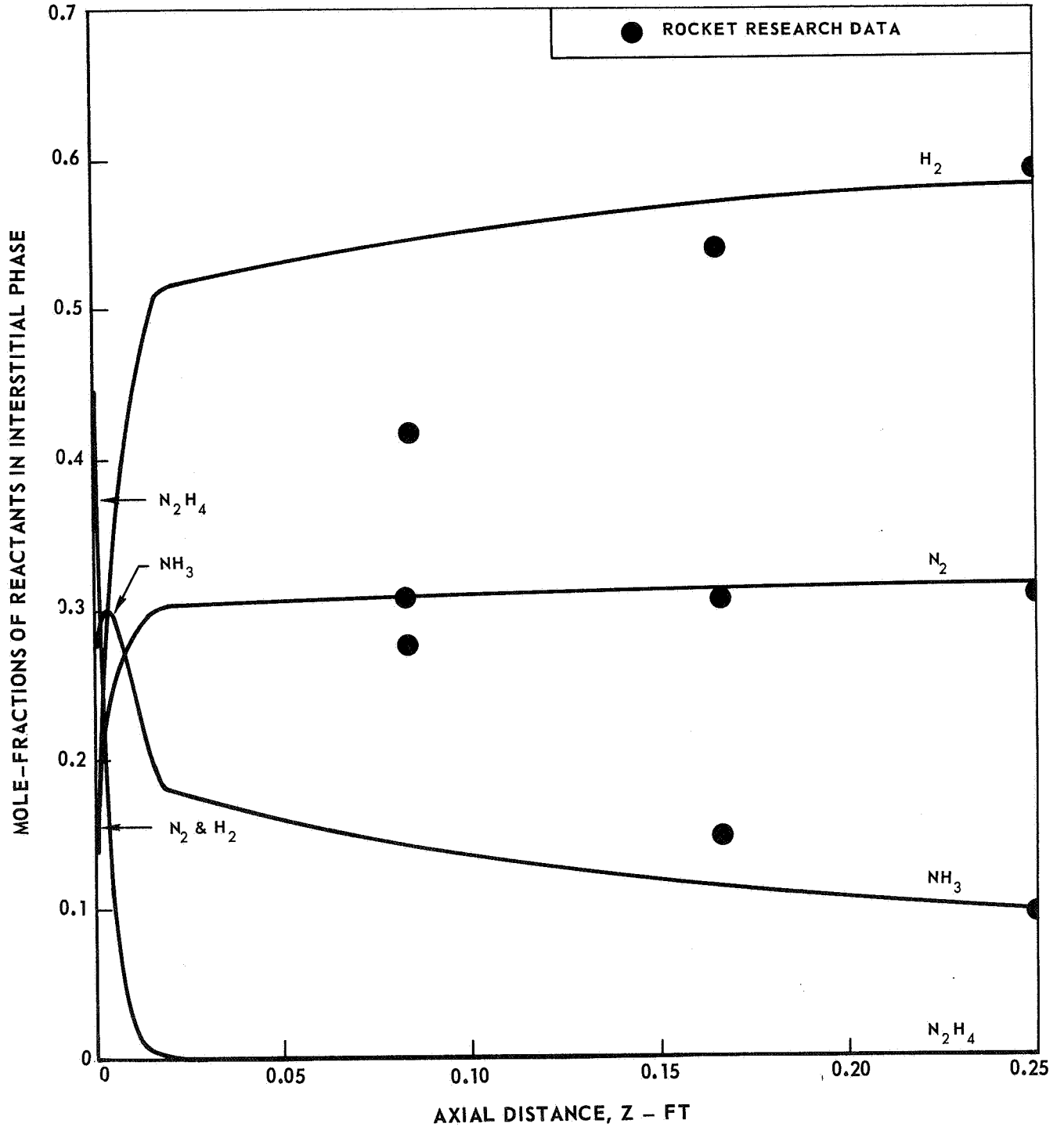
STEADY-STATE AXIAL TEMPERATURE PROFILE USING MODIFIED FILM AND PORE DIFFUSION MODEL

P = 111.4 PSIA
G = 1.51 LB/FT² - SEC
STANDARD BED CONFIGURATION (SEE TEXT)



STEADY-STATE AXIAL PROFILES
OF MOLE-FRACTIONS OF REACTANTS
USING MODIFIED FILM AND PORE DIFFUSION MODEL

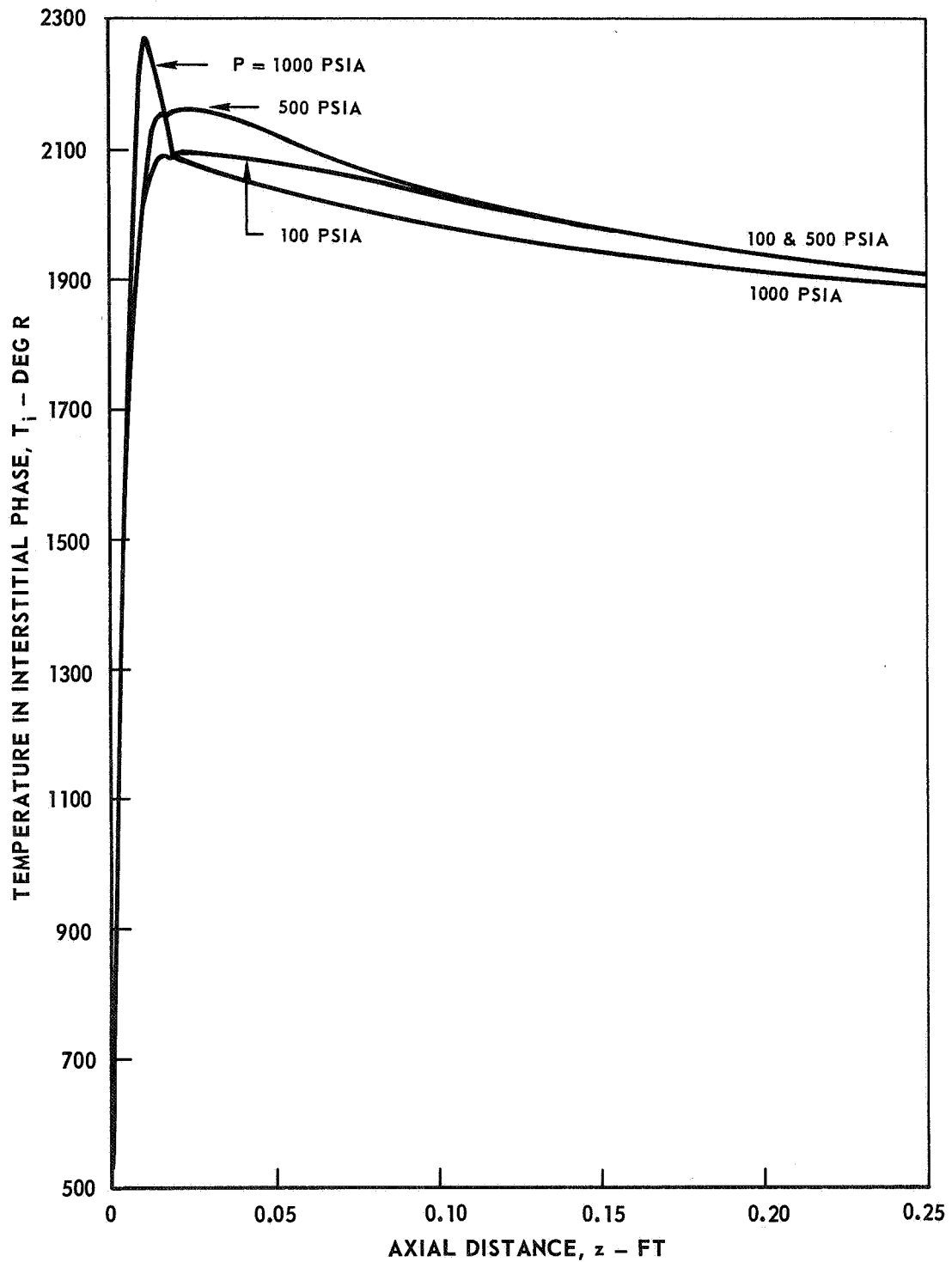
P = 111.4 PSIA
G = 1.51 LB/FT²-SEC
STANDARD BED CONFIGURATION (SEE TEXT)



STEADY - STATE AXIAL TEMPERATURE PROFILES
FOR VARIOUS CHAMBER PRESSURES
USING MODIFIED FILM AND PORE DIFFUSION MODEL

$$G = 3.0 \text{ LB/FT}^2\text{-SEC}$$

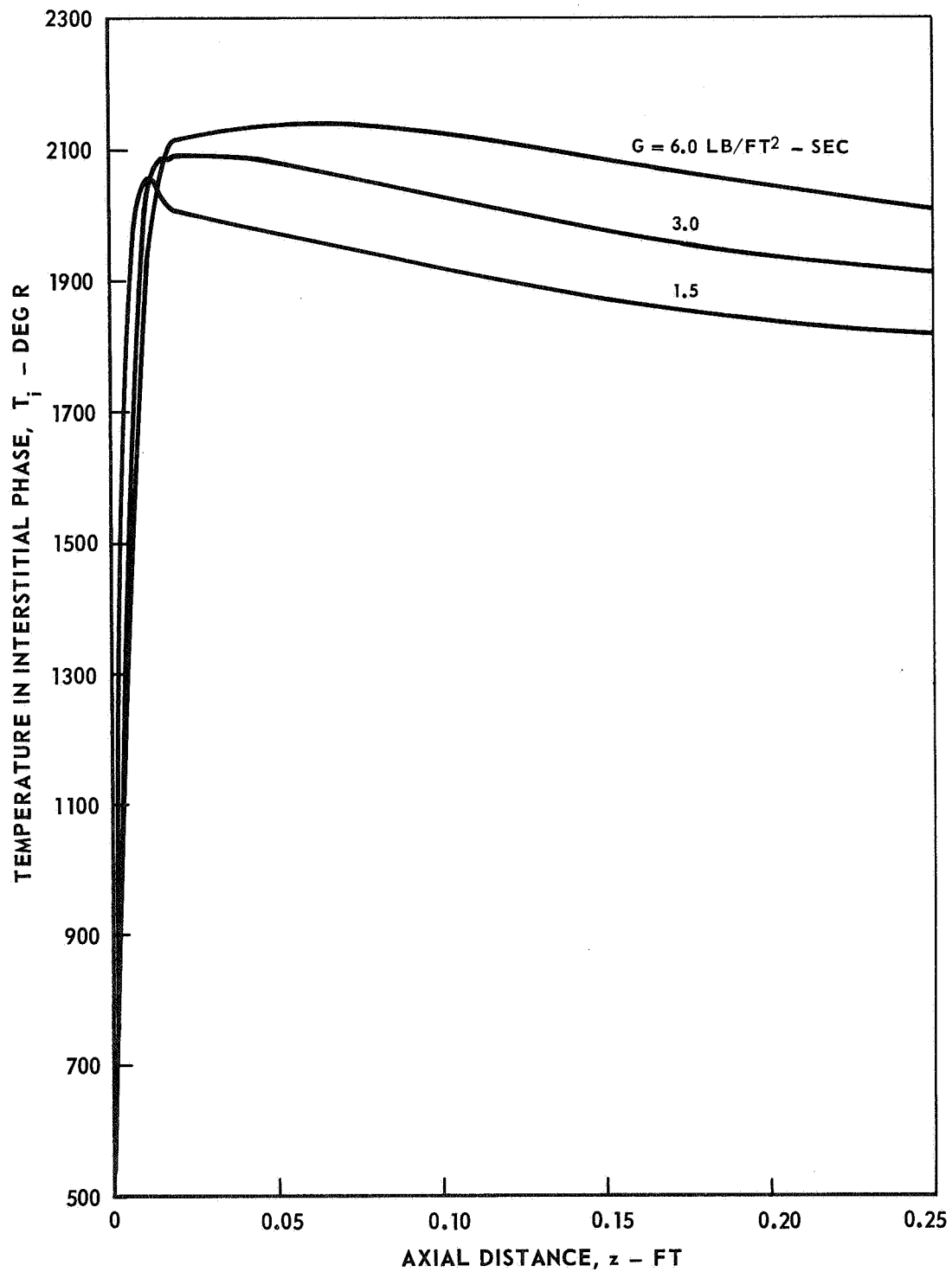
STANDARD BED CONFIGURATION (SEE TEXT)



STEADY - STATE AXIAL TEMPERATURE PROFILES
FOR VARIOUS MASS FLOW RATES
USING MODIFIED FILM AND PORE DIFFUSION MODEL

P = 100 PSIA

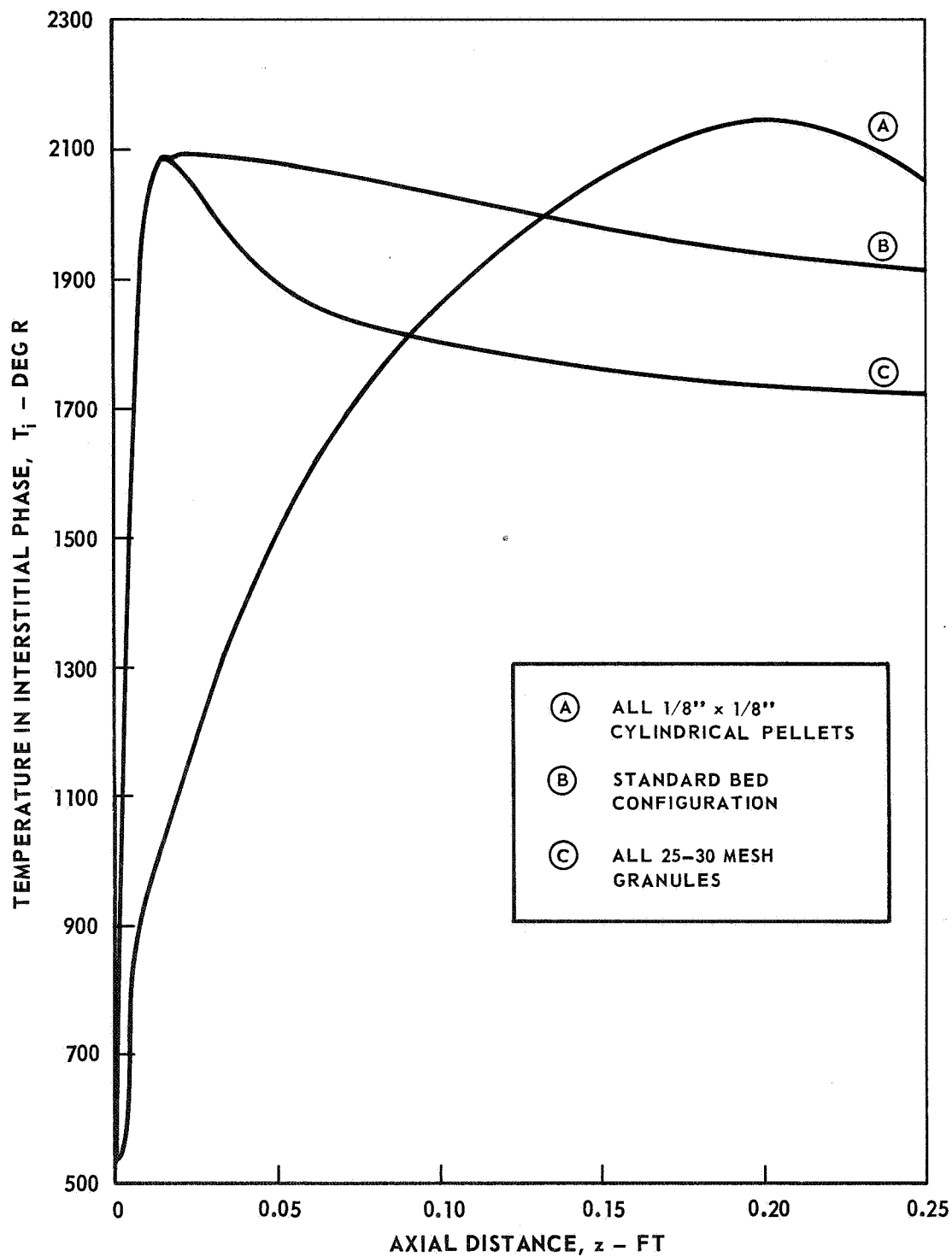
STANDARD BED CONFIGURATION (SEE TEXT)



STEADY - STATE AXIAL TEMPERATURE PROFILES
FOR VARIOUS CATALYTIC BED CONFIGURATIONS
USING MODIFIED FILM AND PORE DIFFUSION MODEL

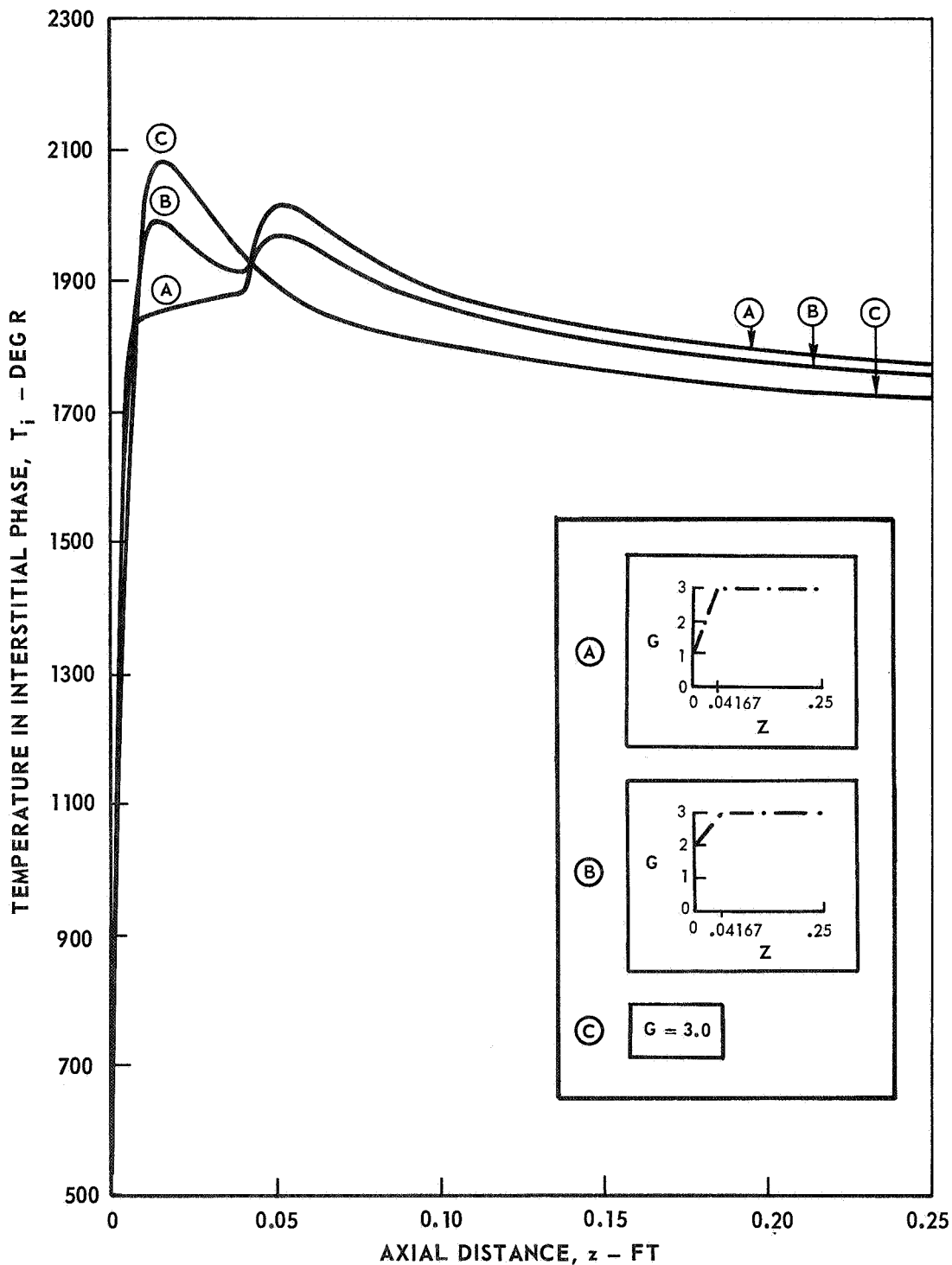
$P = 100$ PSIA

$G = 3.0$ LB/ FT² - SEC



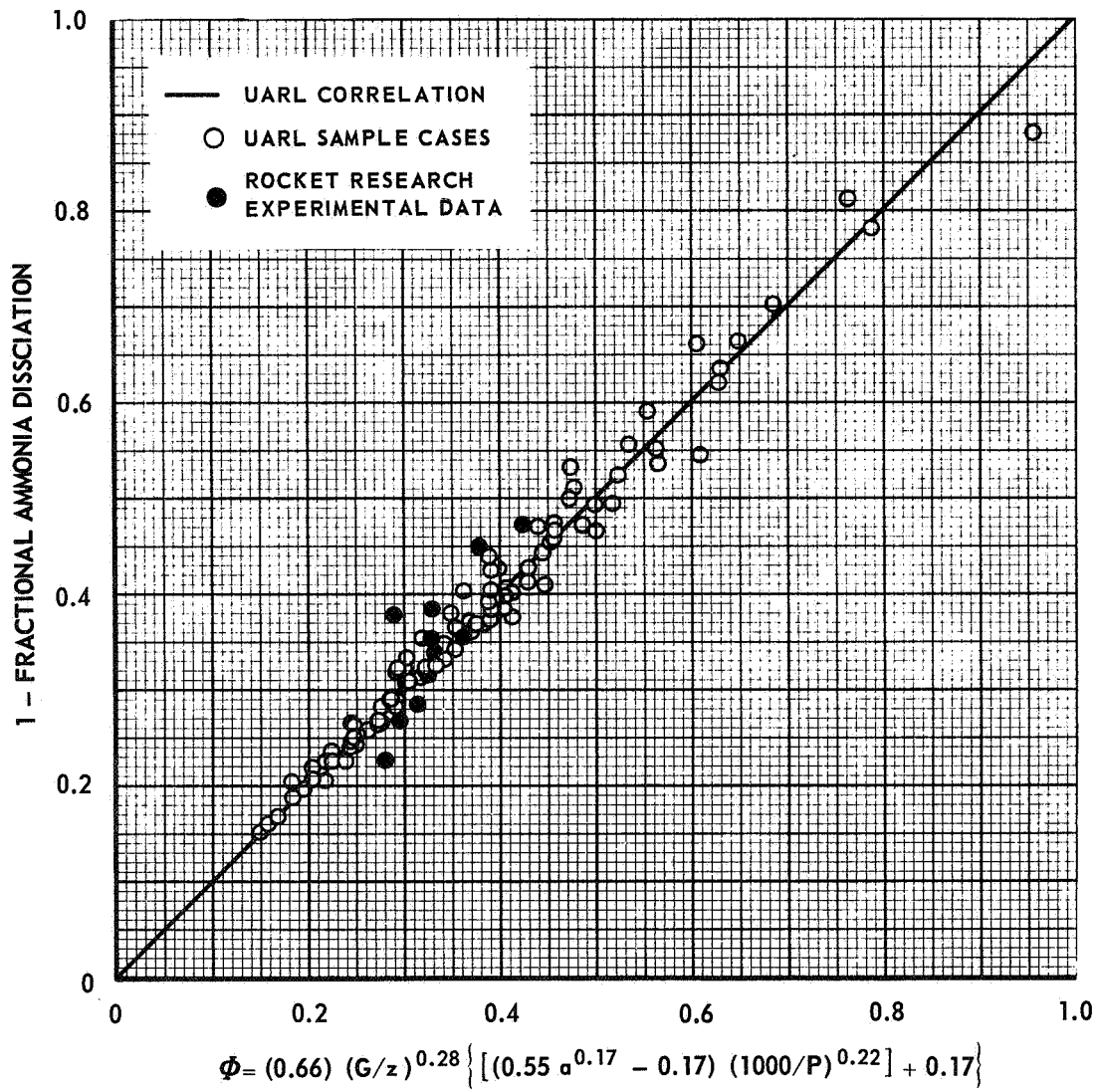
STEADY - STATE AXIAL TEMPERATURE PROFILES
 FOR VARIOUS HYDRAZINE AXIAL INJECTION PROFILES
 USING MODIFIED FILM AND PORE DIFFUSION MODEL

P = 100 PSIA
 BED CONFIGURATION : ALL 25-30 MESH GRANULES



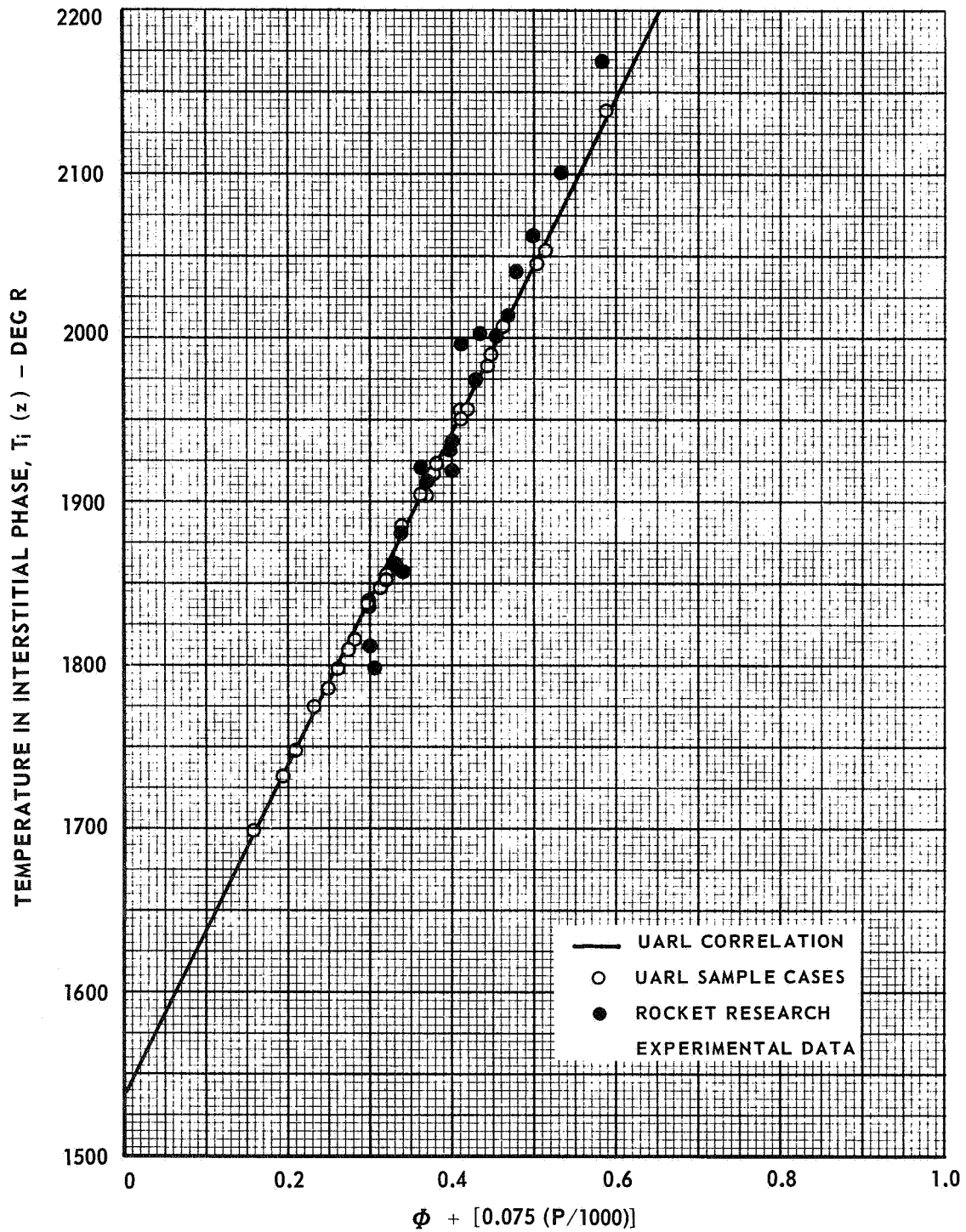
EMPIRICAL PREDICATION OF FRACTIONAL AMMONIA DISSOCIATION

SYMBOL	UNITS
z	FT
G	LB/FT ² -SEC
P	PSIA
a	FT



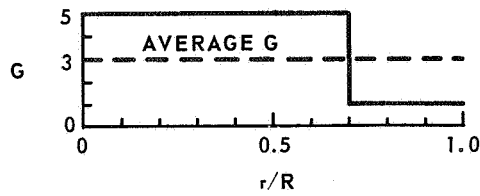
EMPIRICAL PREDICTION OF INTERSTITIAL GAS TEMPERATURE

SYMBOL	UNITS
P	PSIA
$T_i(z)$	DEG R

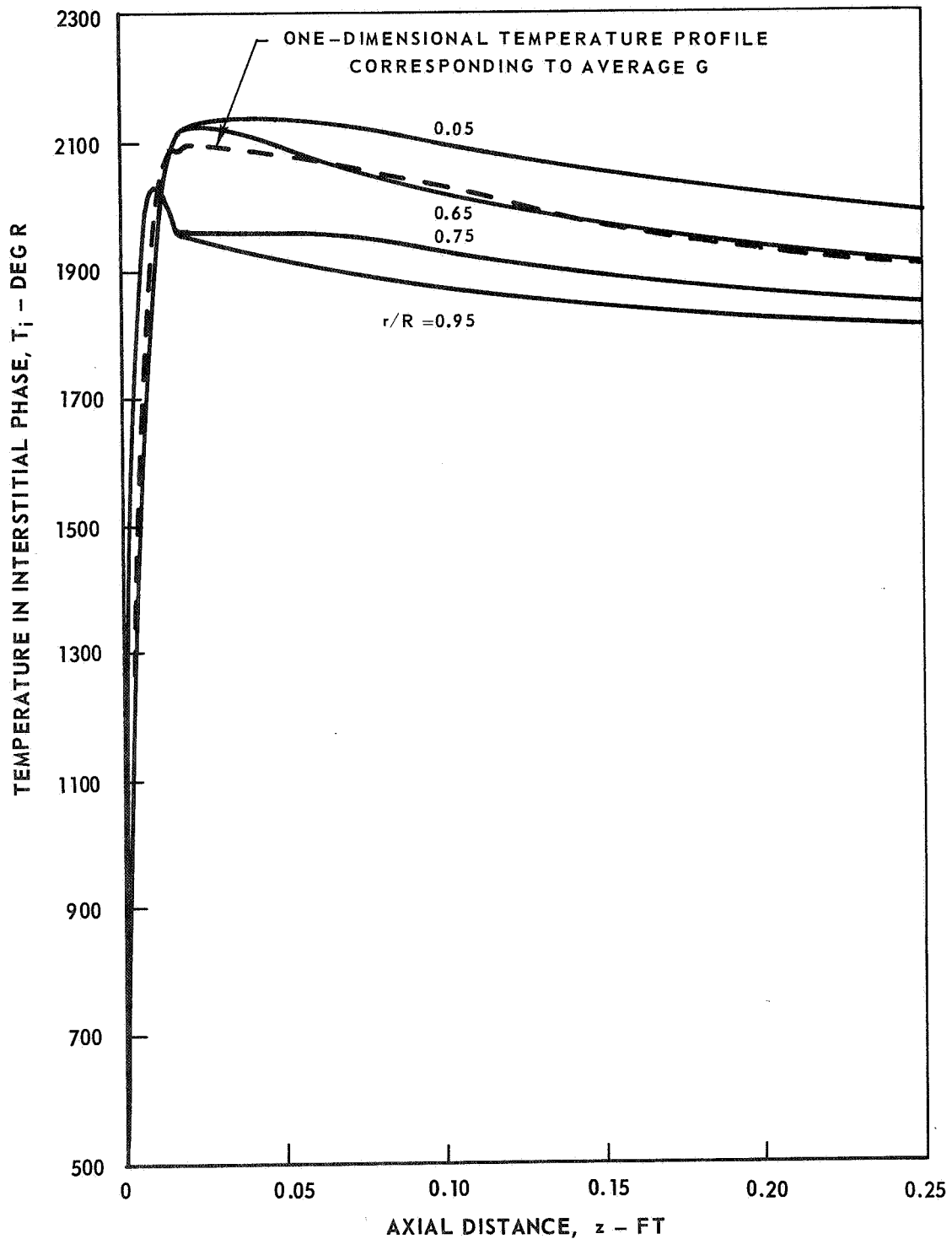


STEADY - STATE AXIAL TEMPERATURE PROFILES
AT VARIOUS RADIAL POSITIONS

P = 100 PSIA
R = 0.125 FT

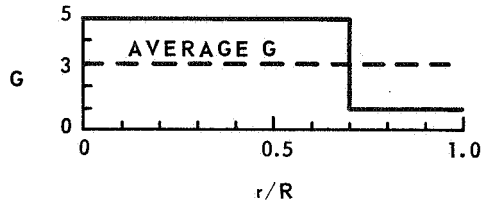


STANDARD BED
CONFIGURATION
(SEE TEXT)

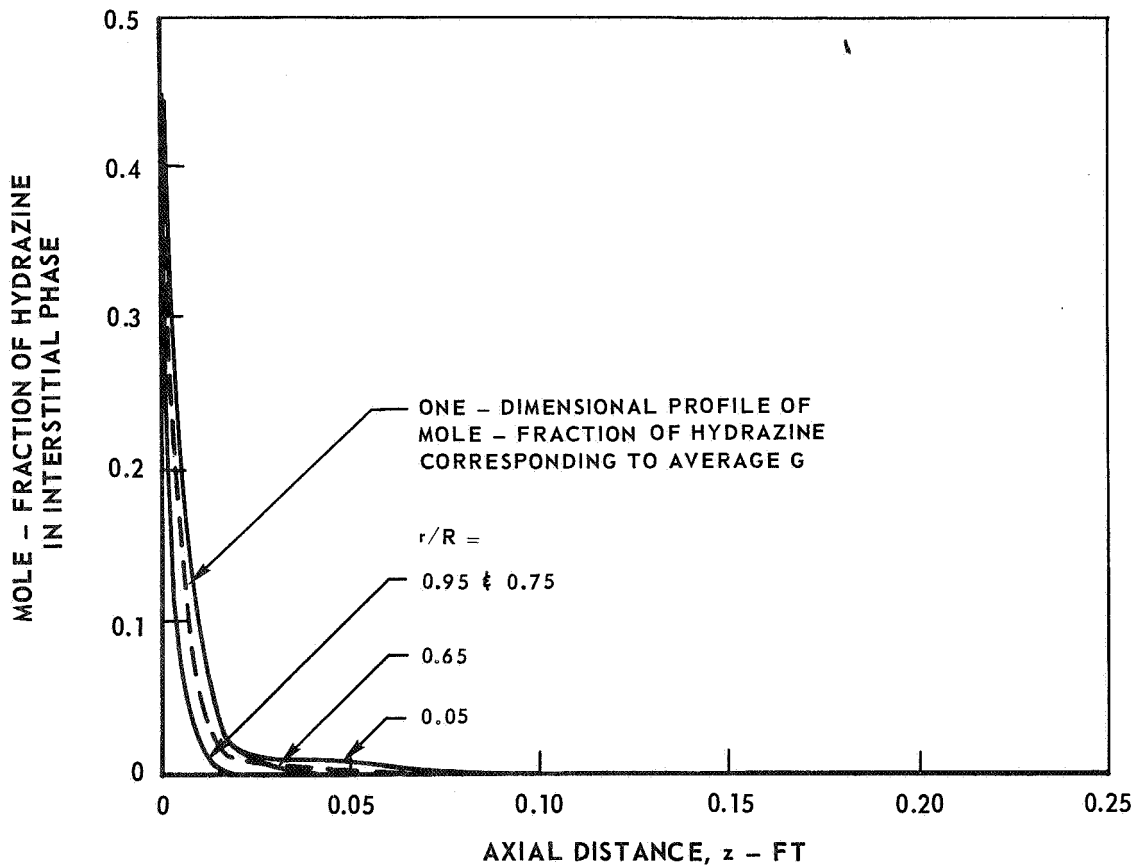


STEADY - STATE AXIAL PROFILES OF MOLE - FRACTION OF HYDRAZINE AT VARIOUS AXIAL POSITIONS

P = 100 PSIA
R = 0.125 FT

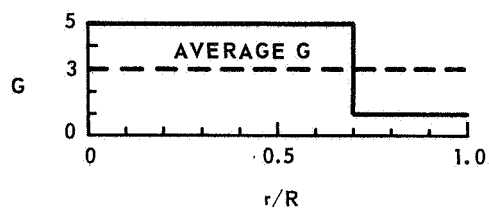


STANDARD BED
CONFIGURATION
(SEE TEXT)

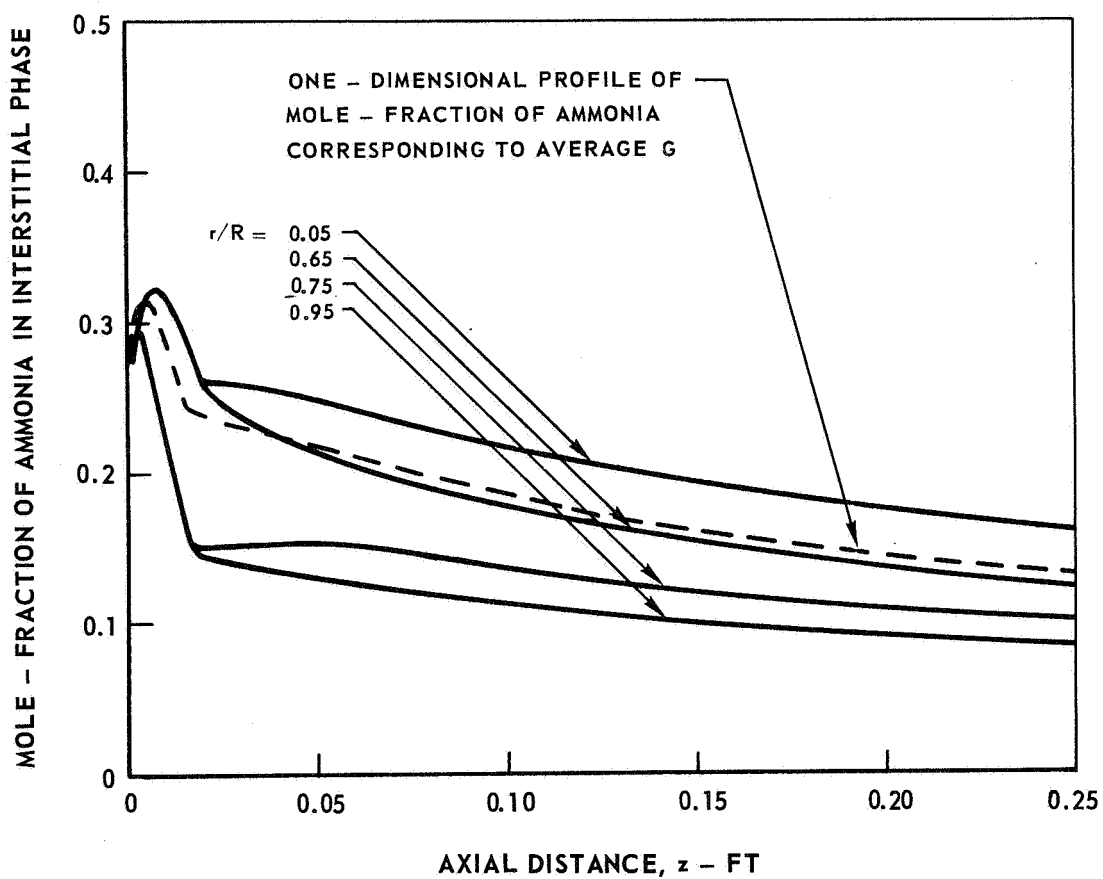


STEADY - STATE AXIAL PROFILES OF MOLE - FRACTION OF AMMONIA AT VARIOUS RADIAL POSITIONS

P = 100 PSIA
R = 0.125 FT

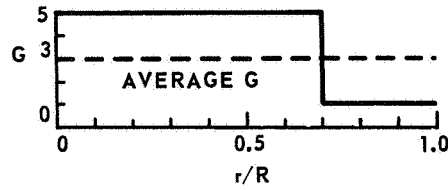


STANDARD BED
CONFIGURATION
(SEE TEXT)

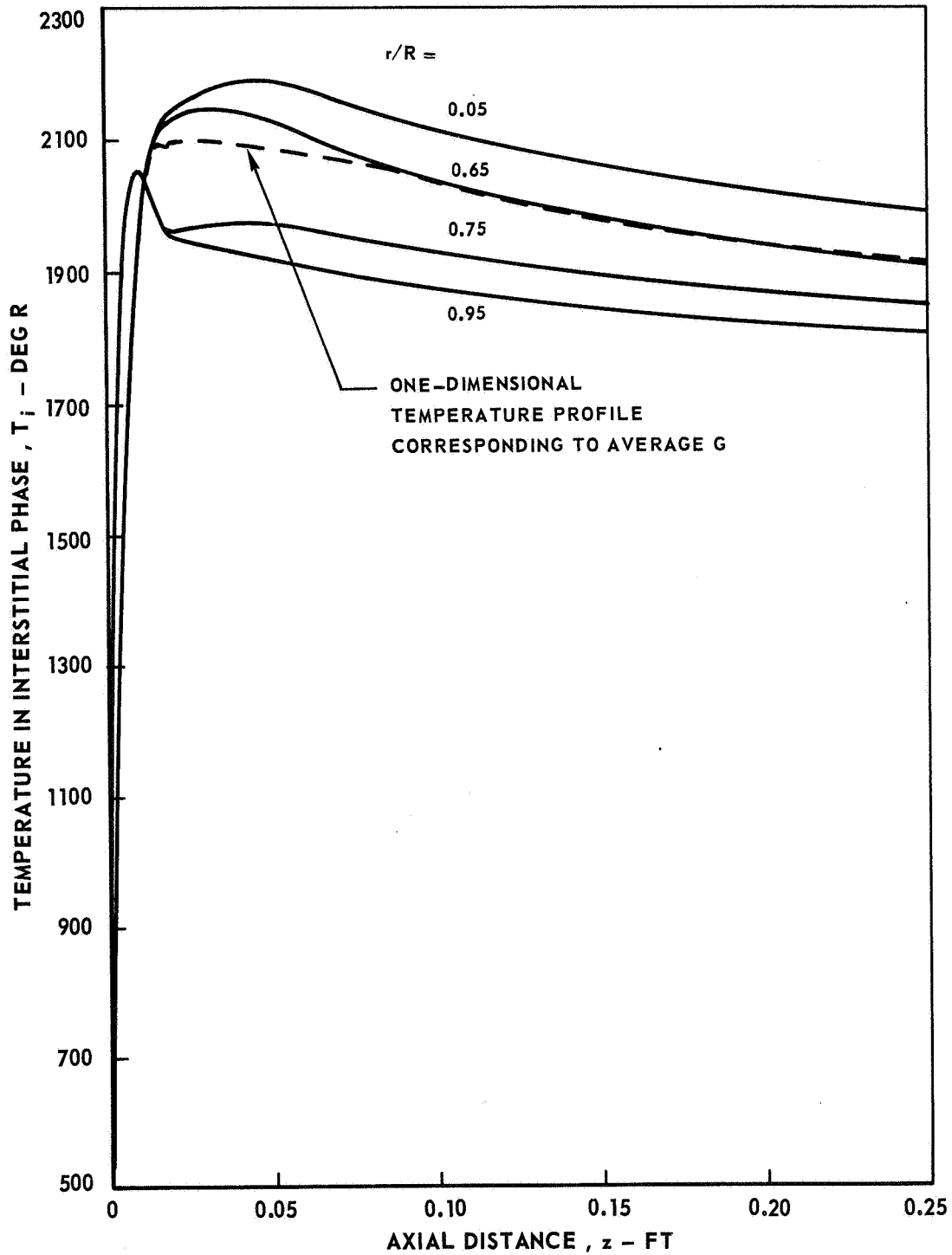


STEADY - STATE AXIAL TEMPERATURE PROFILES
AT VARIOUS RADIAL POSITIONS

P = 200 PSIA
R = 0.125 FT

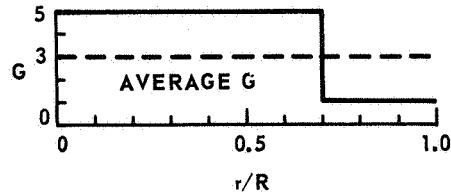


STANDARD BED
CONFIGURATION
(SEE TEXT)

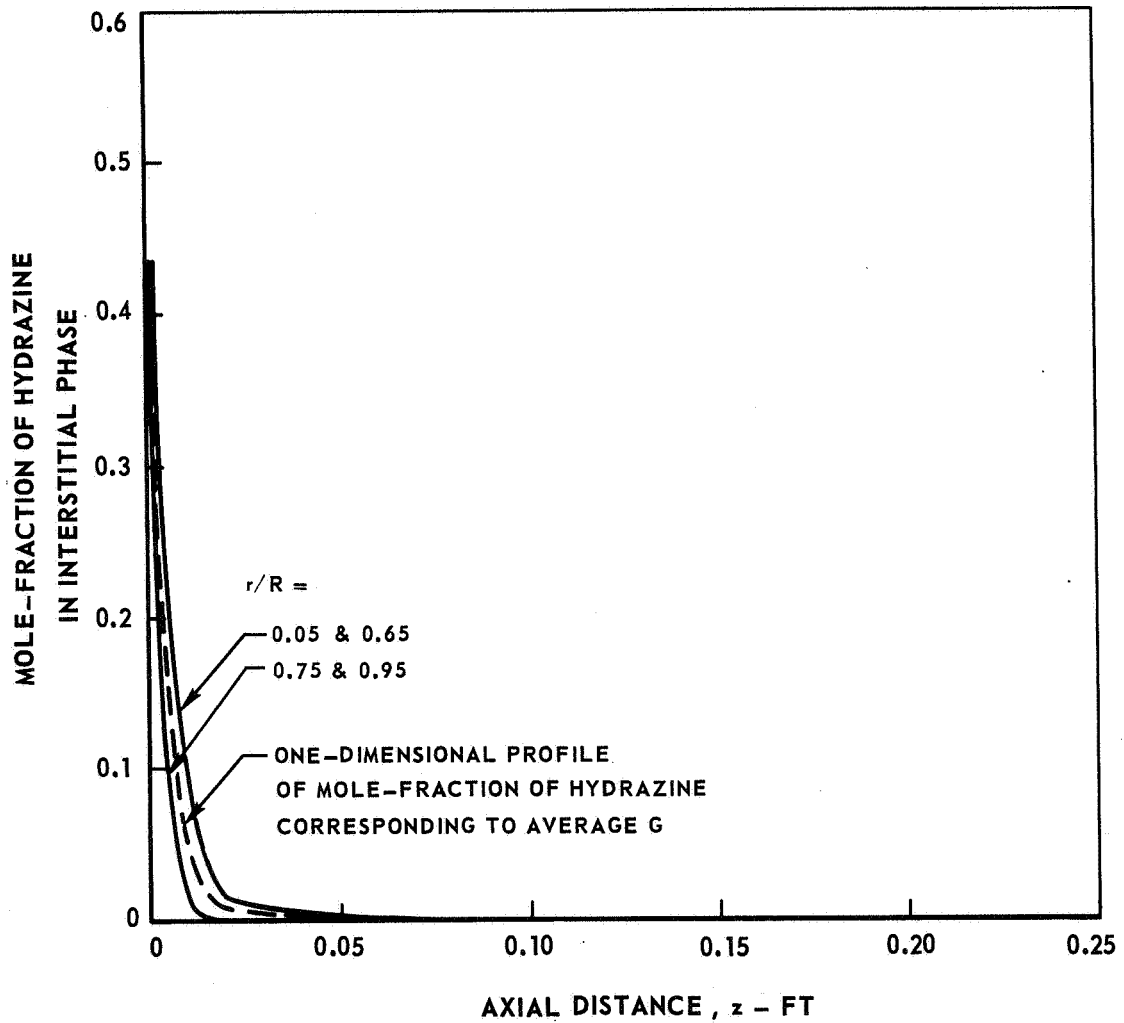


STEADY-STATE AXIAL PROFILES OF MOLE-FRACTION OF HYDRAZINE AT VARIOUS RADIAL POSITIONS

P = 200 PSIA
R = 0.125 FT

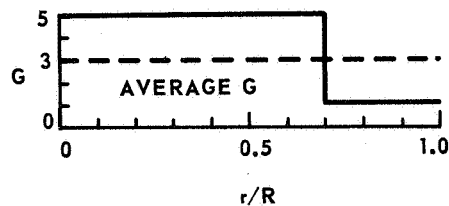


STANDARD BED
CONFIGURATION
(SEE TEXT)

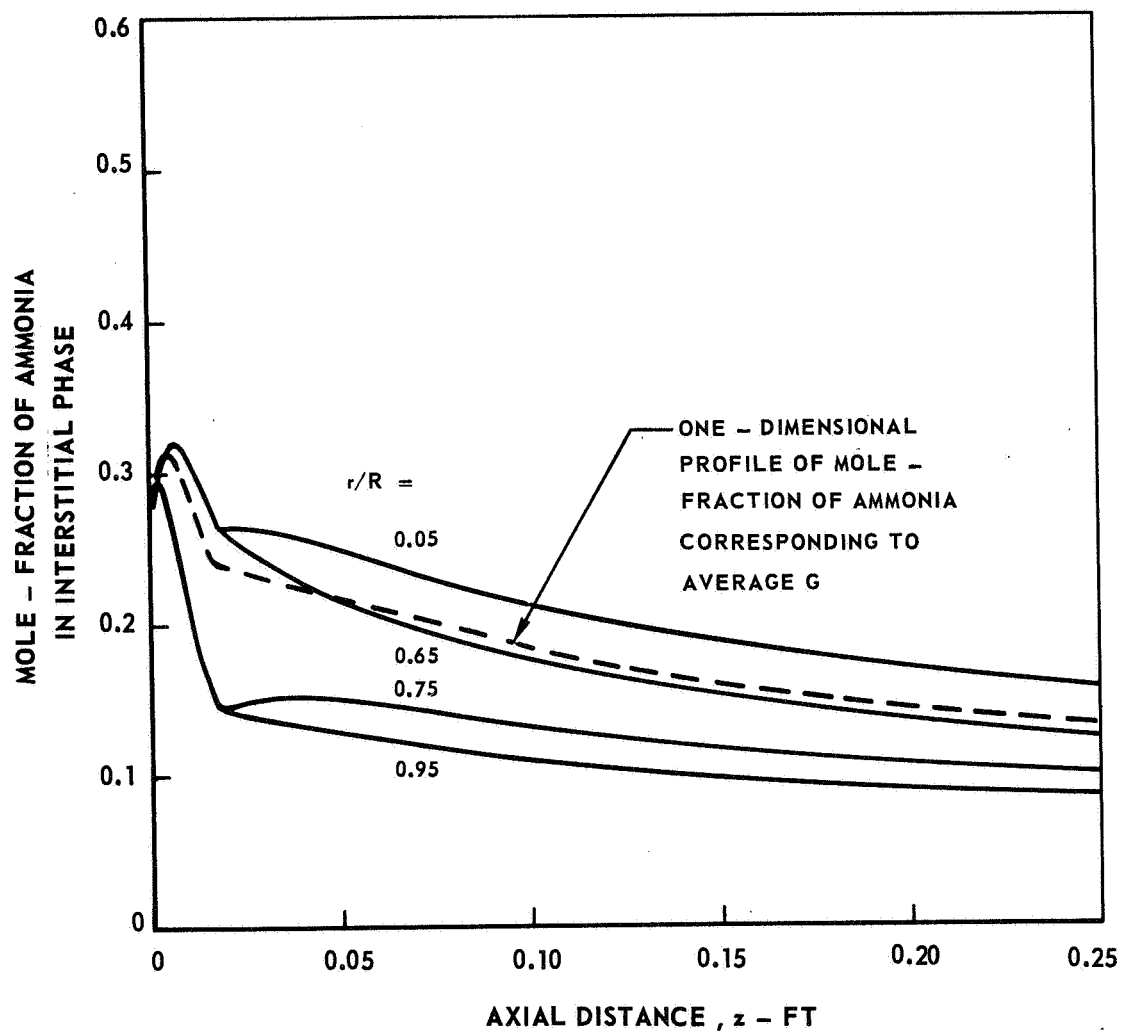


STEADY-STATE AXIAL PROFILES OF MOLE-FRACTION OF AMMONIA AT VARIOUS RADIAL POSITIONS

P = 200 PSIA
R = 0.125 FT

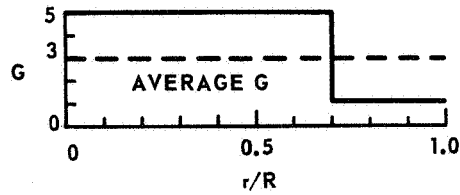


STANDARD BED
CONFIGURATION
(SEE TEXT)

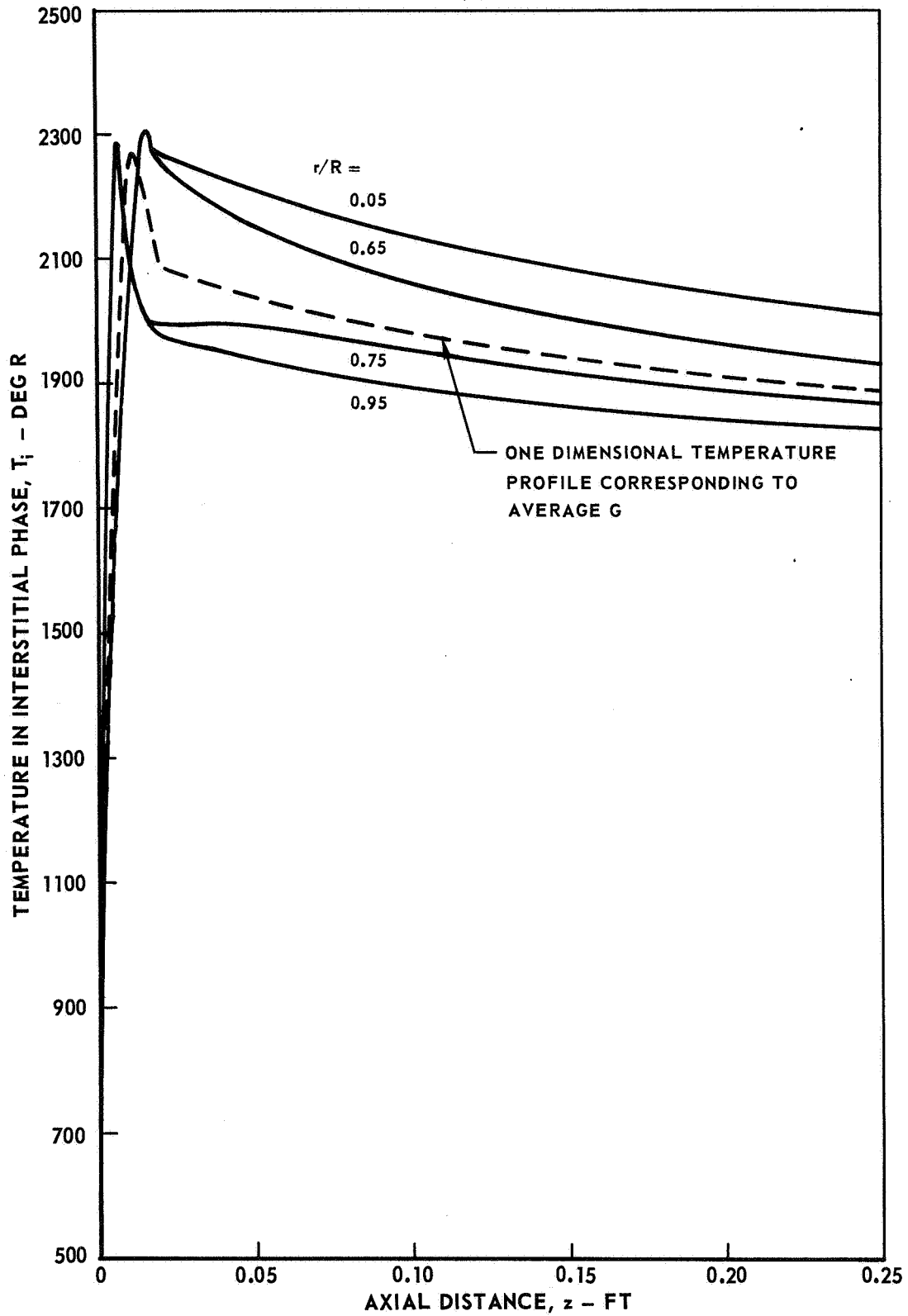


STEADY - STATE AXIAL TEMPERATURE PROFILES AT VARIOUS RADIAL POSITIONS

$P=1000$ PSIA
 $R = 0.125$ FT

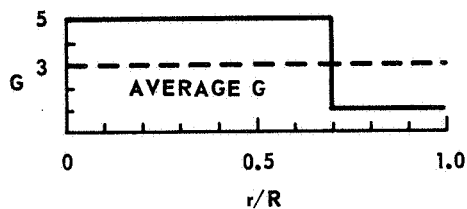


STANDARD BED
CONFIGURATION
(SEE TEXT)

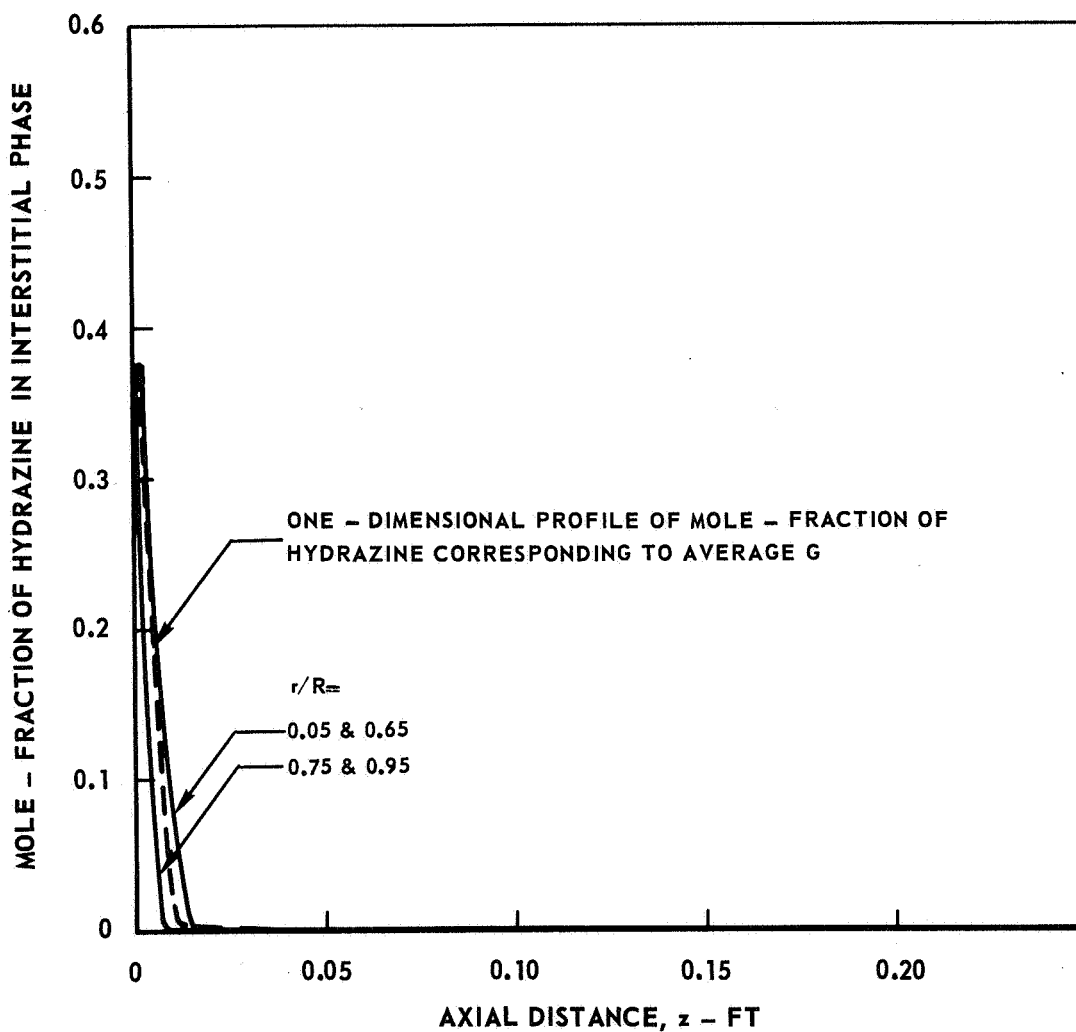


STEADY - STATE AXIAL PROFILES OF MOLE - FRACTION OF HYDRAZINE AT VARIOUS RADIAL POSITIONS

P = 1000 PSIA
R = 0.125 FT

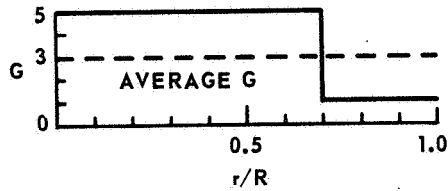


STANDARD BED
CONFIGURATION
(SEE TEXT)

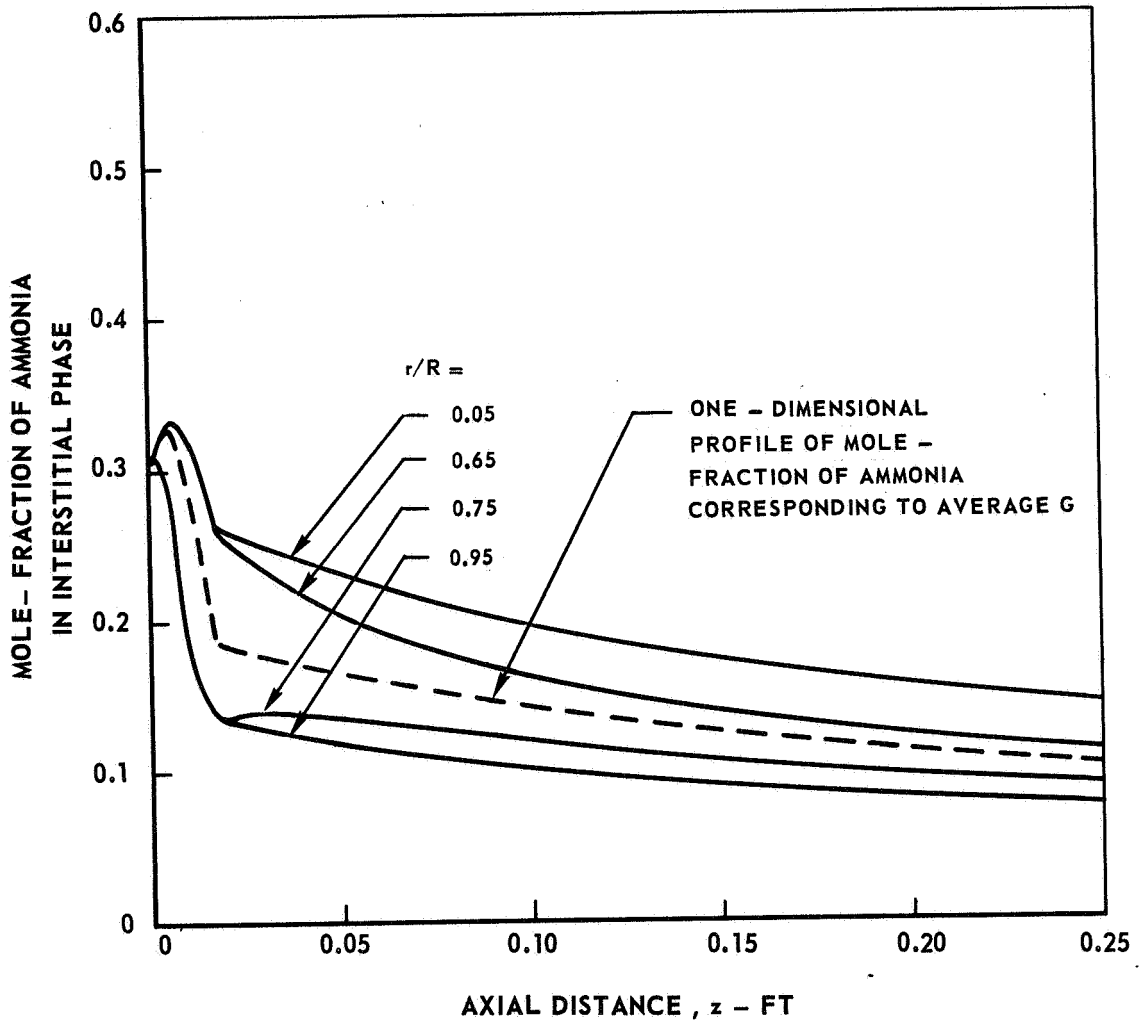


STEADY - STATE AXIAL PROFILES OF MOLE - FRACTION
OF AMMONIA AT VARIOUS RADIAL

P = 1000 PSIA
R = 0.125 FT

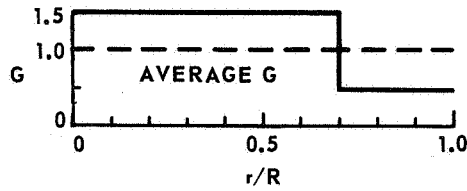


STANDARD BED
CONFIGURATION
(SEE TEXT)

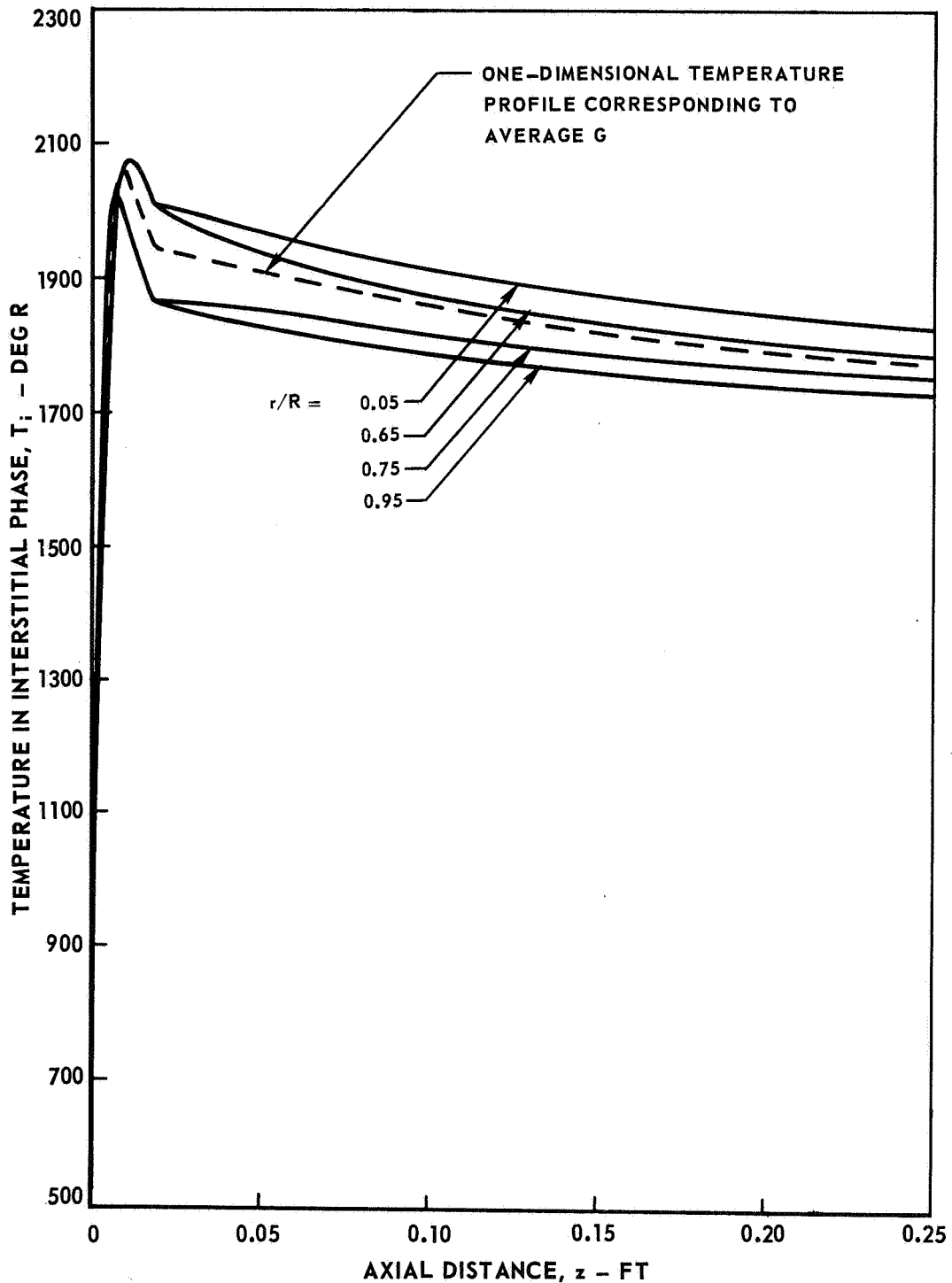


STEADY-STATE AXIAL TEMPERATURE PROFILES AT VARIOUS RADIAL POSITIONS

P = 200 PSIA
R = 0.125 FT



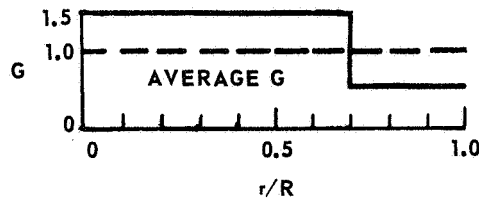
STANDARD BED
CONFIGURATION
(SEE TEXT)



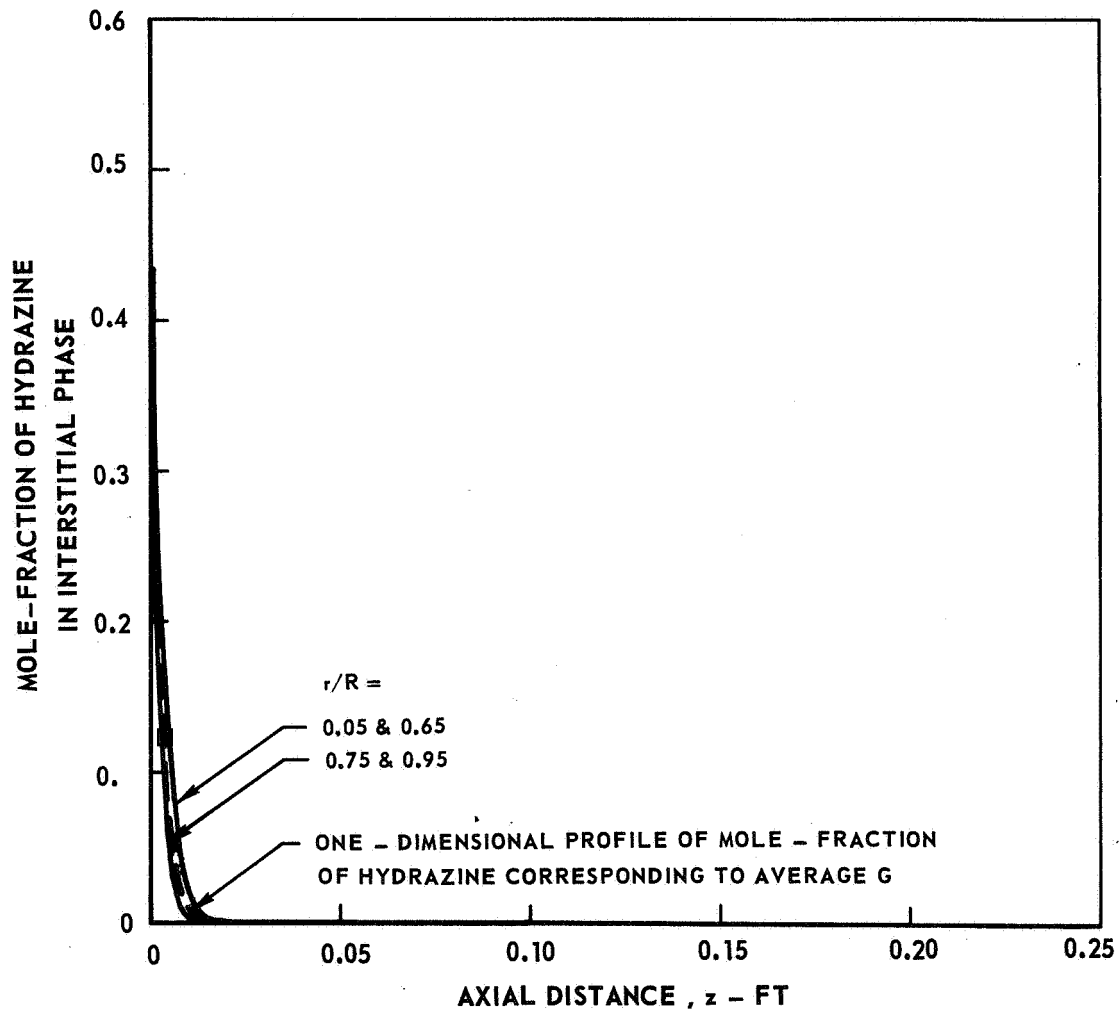
STEADY-STATE AXIAL PROFILES OF MOLE-FRACTION OF HYDRAZINE AT VARIOUS RADIAL POSITIONS

P = 200 PSIA

R = 0.125 FT

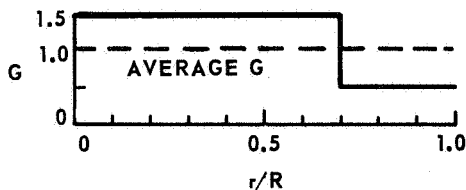


STANDARD BED CONFIGURATION
(SEE TEXT)

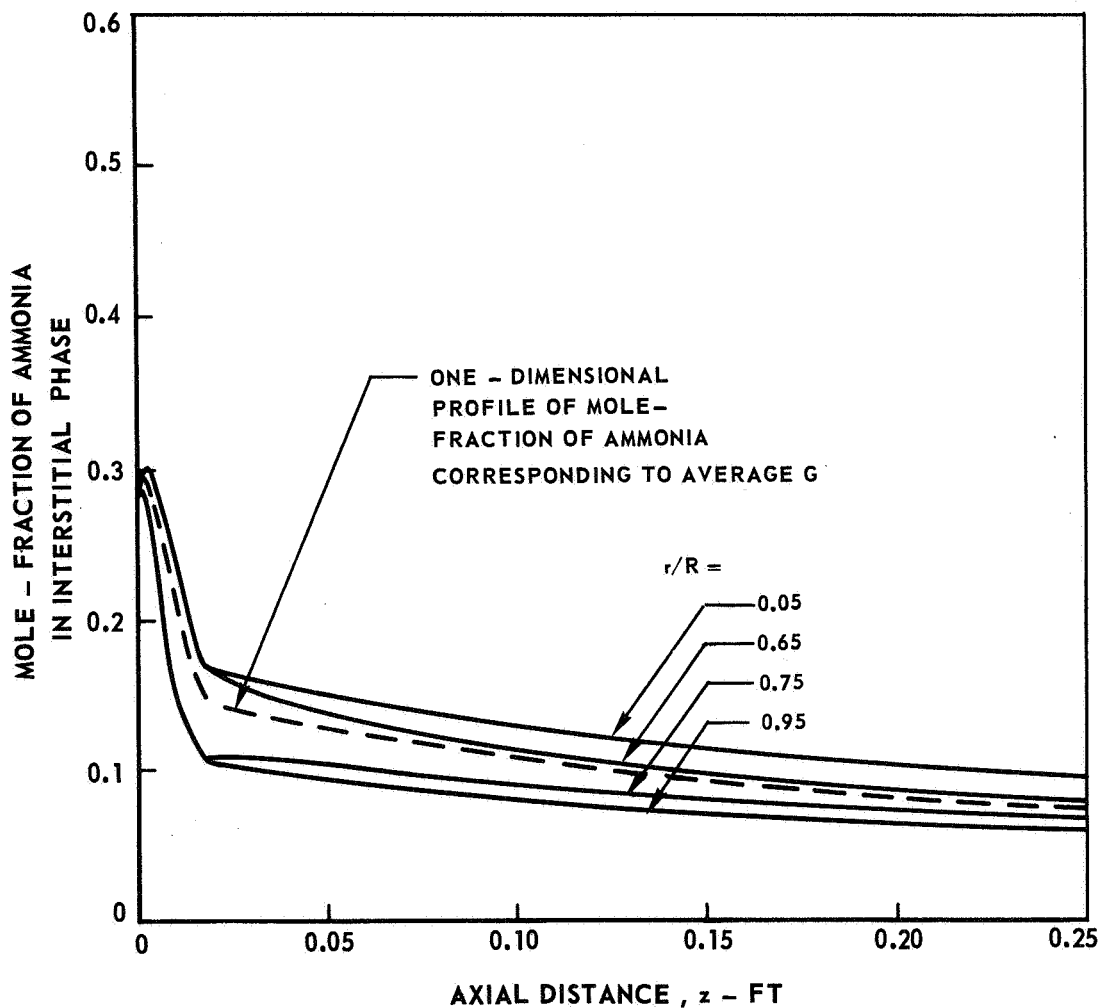


STEADY - STATE AXIAL PROFILES OF MOLE - FRACTION OF AMMONIA AT VARIOUS RADIAL POSITIONS

P = 200 PSIA
R = 0.125 FT

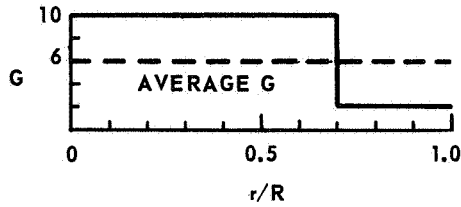


STANDARD BED CONFIGURATION
(SEE TEXT)

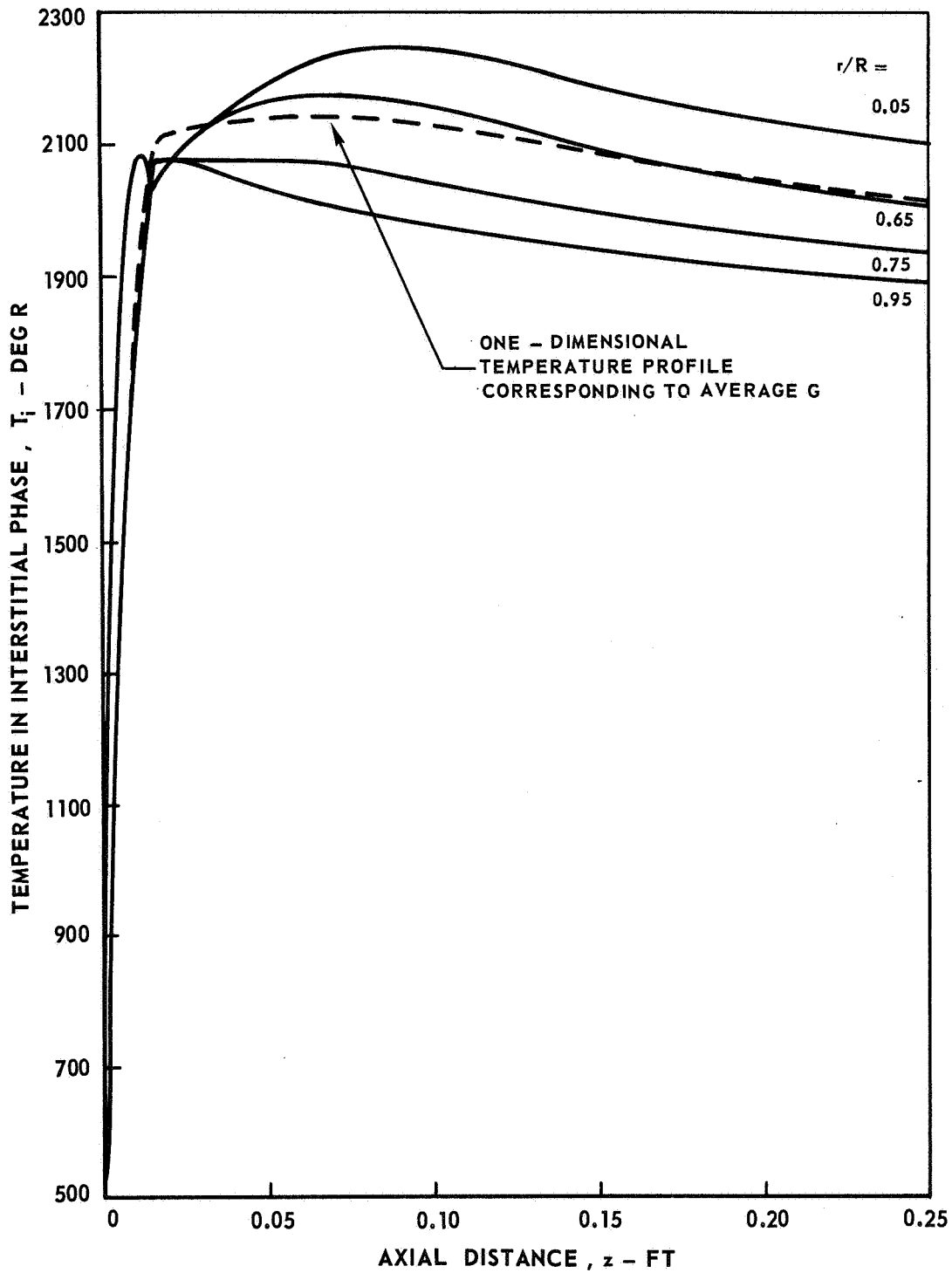


STEADY-STATE AXIAL TEMPERATURE PROFILES
AT VARIOUS RADIAL POSITIONS

P = 200 PSIA
R = 0.125 FT

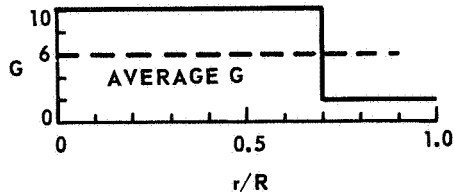


STANDARD BED
CONFIGURATION
(SEE TEXT)

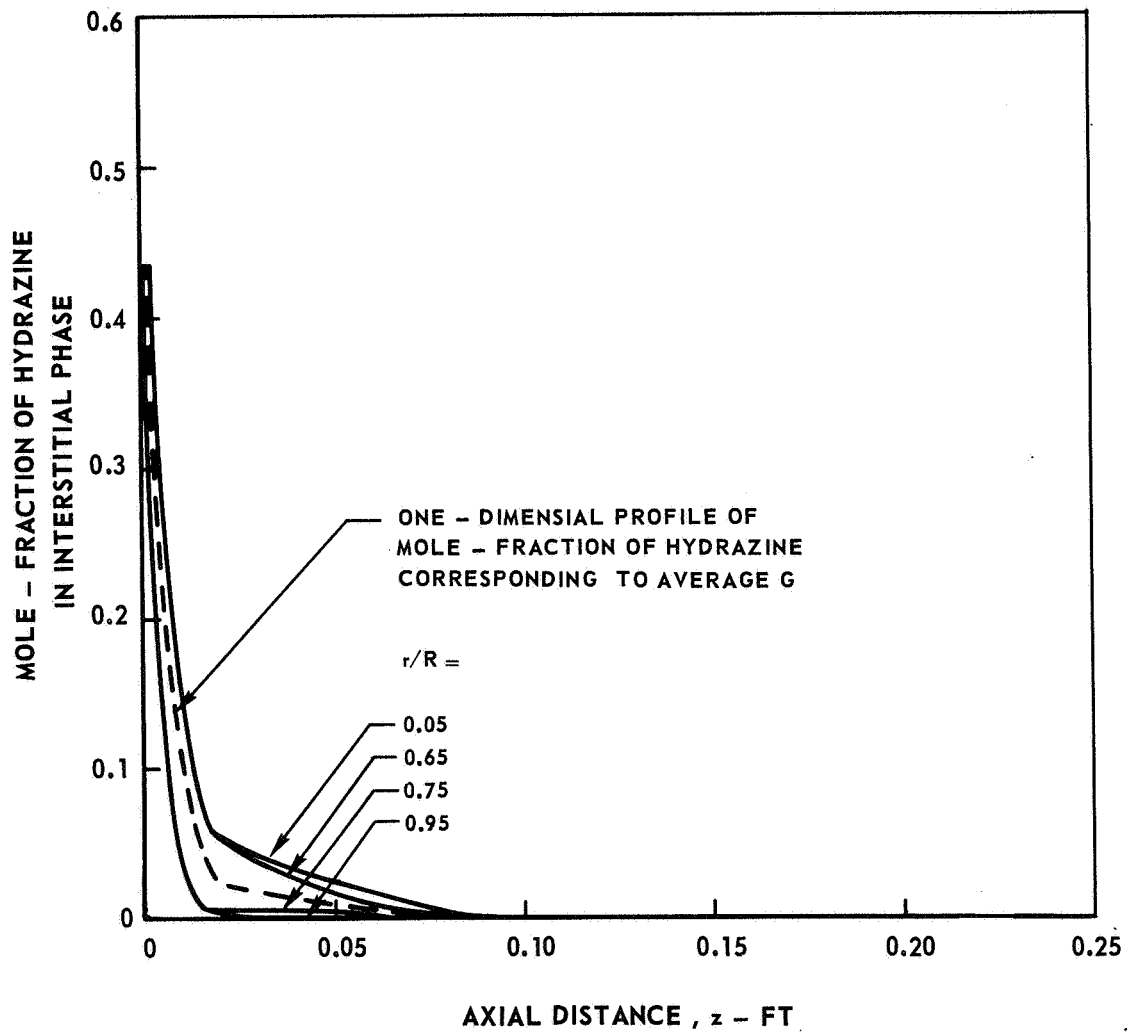


STEADY - STATE AXIAL PROFILES OF MOLE - FRACTION OF HYDRAZINE AT VARIOUS AXIAL POSITIONS

P = 200 PSIA
R = 0.125 FT

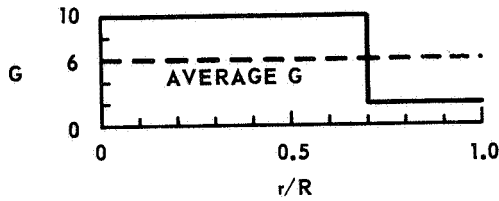


STANDARD BED CONFIGURATION
(SEE TEXT)

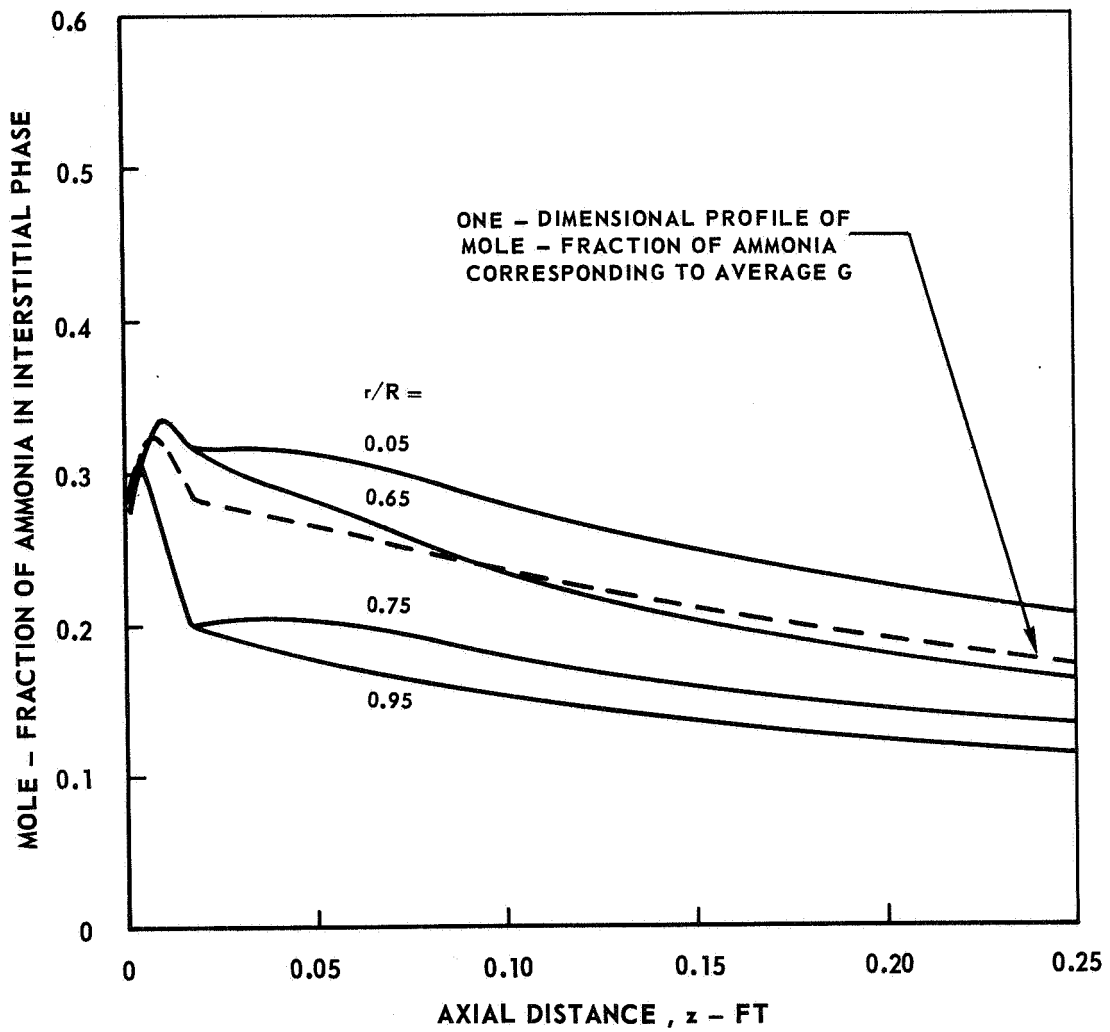


STEADY - STATE AXIAL PROFILES OF MOLE - FRACTION OF AMMONIA AT VARIOUS RADIAL POSITIONS

P = 200 PSIA
R = 0.125 FT

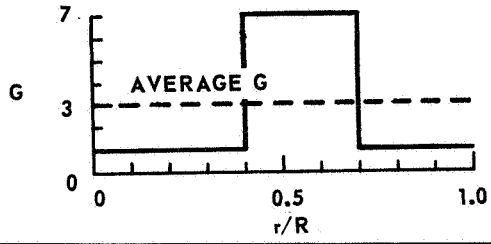


STANDARD BED CONFIGURATION
(SEE TEXT)

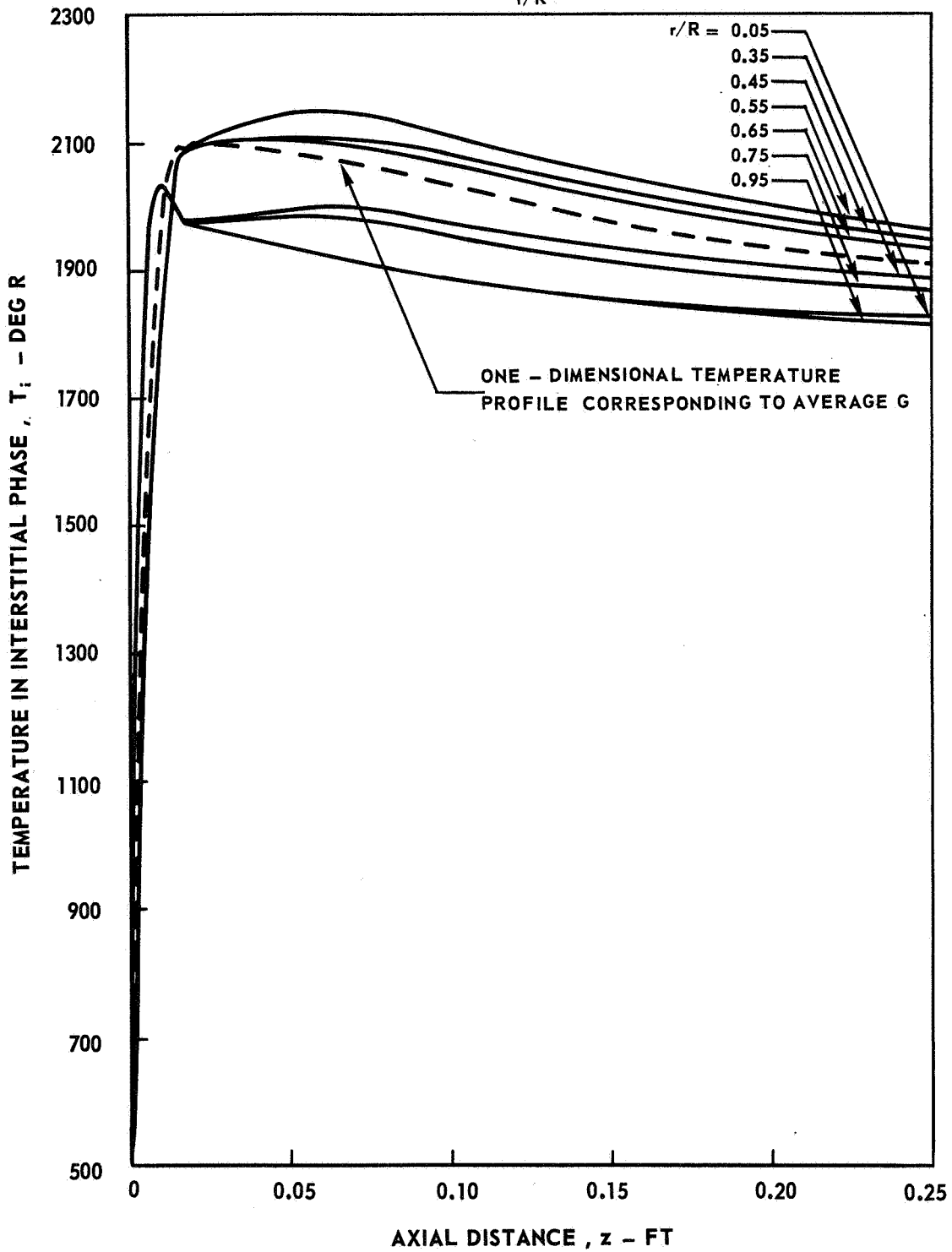


STEADY - STATE AXIAL TEMPERATURE PROFILES AT VARIOUS RADIAL POSITIONS

P = 100 PSIA
R = 0.125 FT

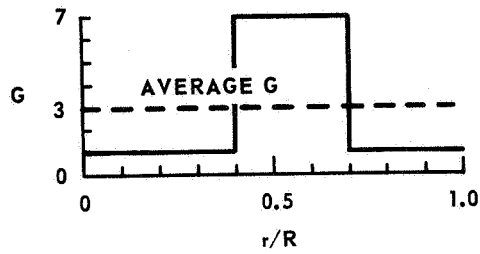


STANDARD BED
CONFIGURATION
(SEE TEXT)

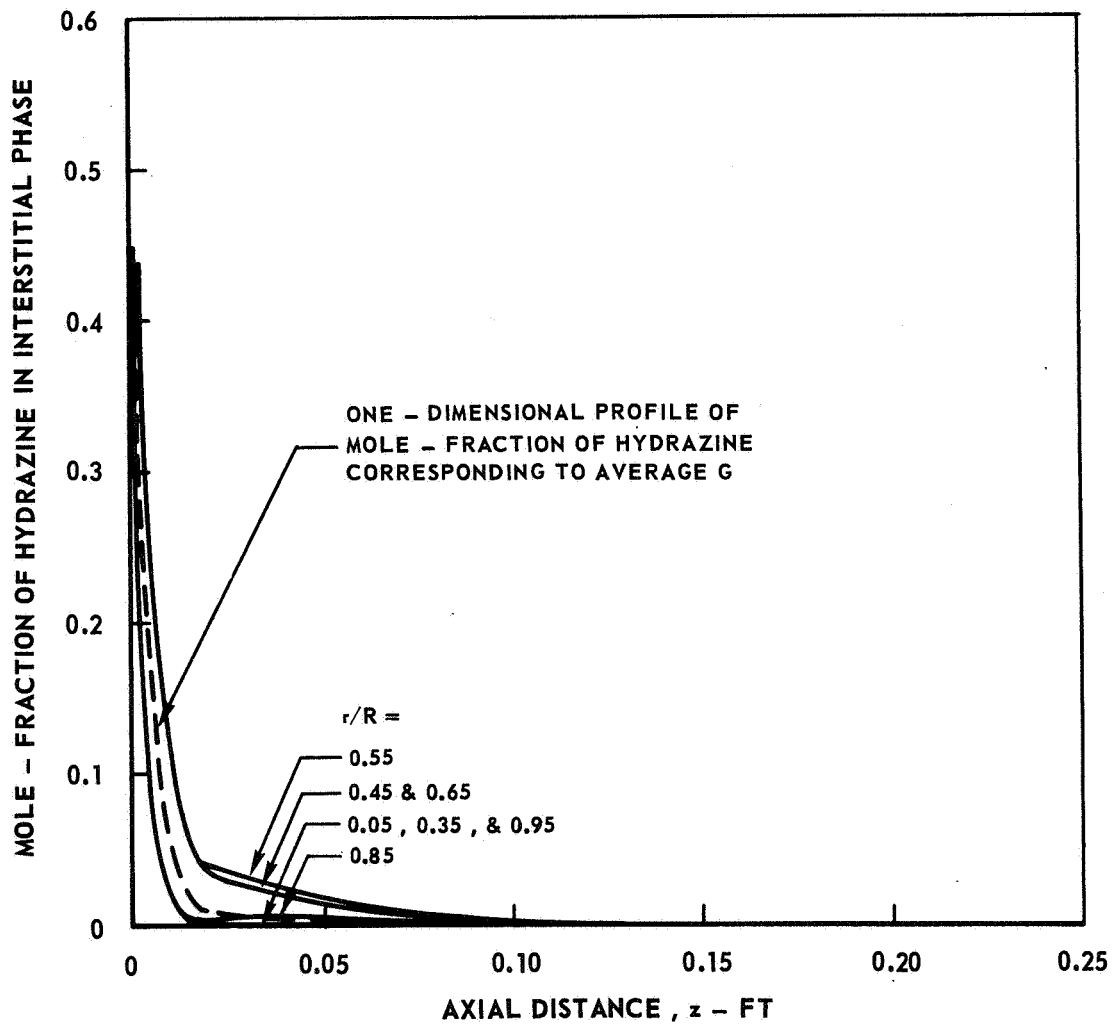


STEADY - STATE AXIAL PROFILES OF MOLE - FRACTION OF HYDRAZINE AT VARIOUS RADIAL POSITIONS

P = 100 PSIA
R = 0.125 FT

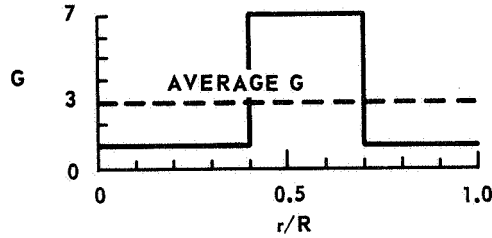


STANDARD BED CONFIGURATION
(SEE TEXT)

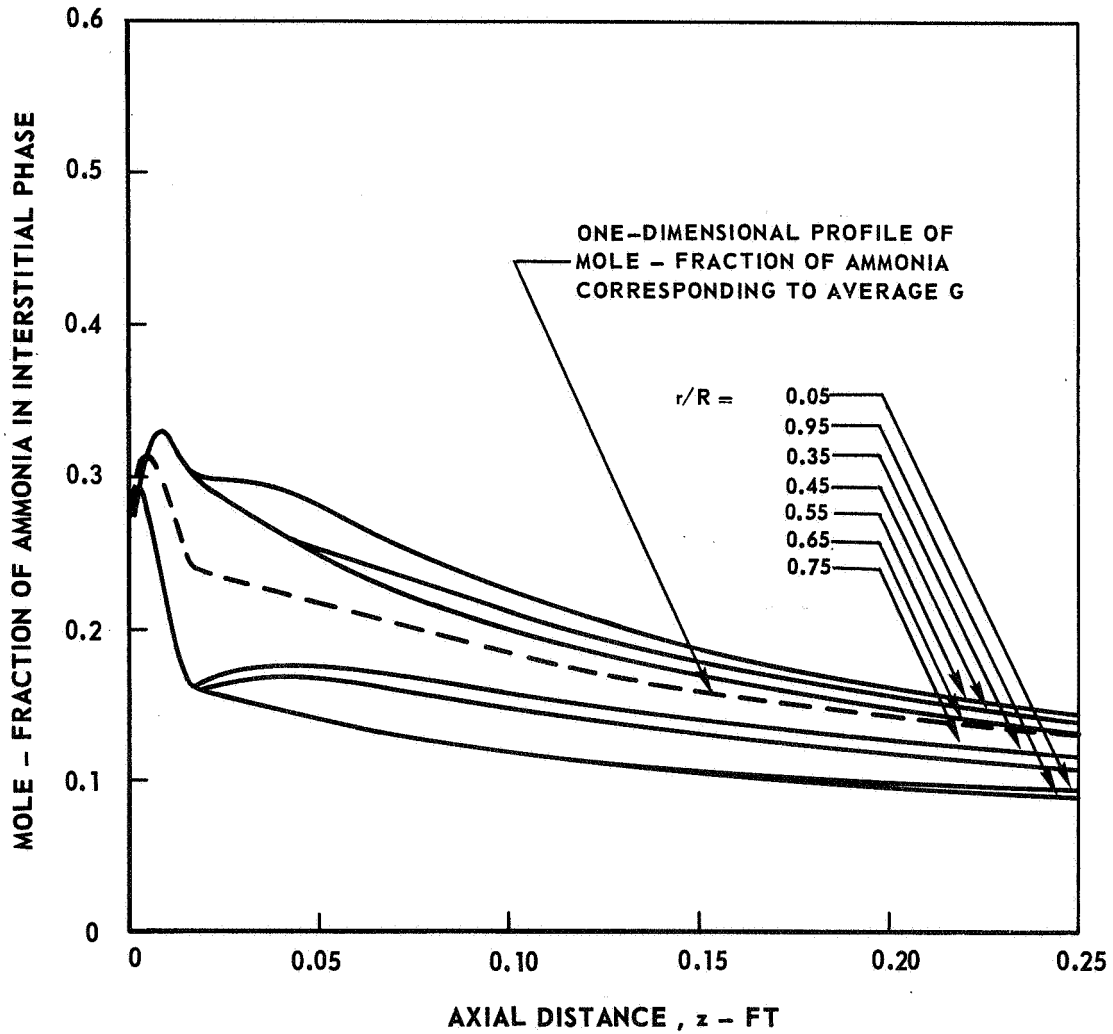


STEADY - STATE AXIAL PROFILES OF MOLE - FRACTION OF AMMONIA AT VARIOUS RADIAL POSITIONS

P = 100 PSIA
R = 0.125 FT

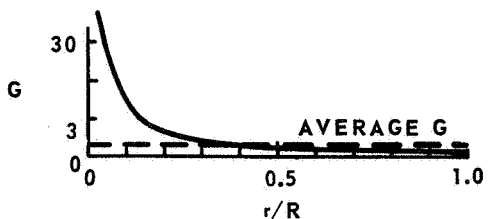


STANDARD BED CONFIGURATION
(SEE TEXT)

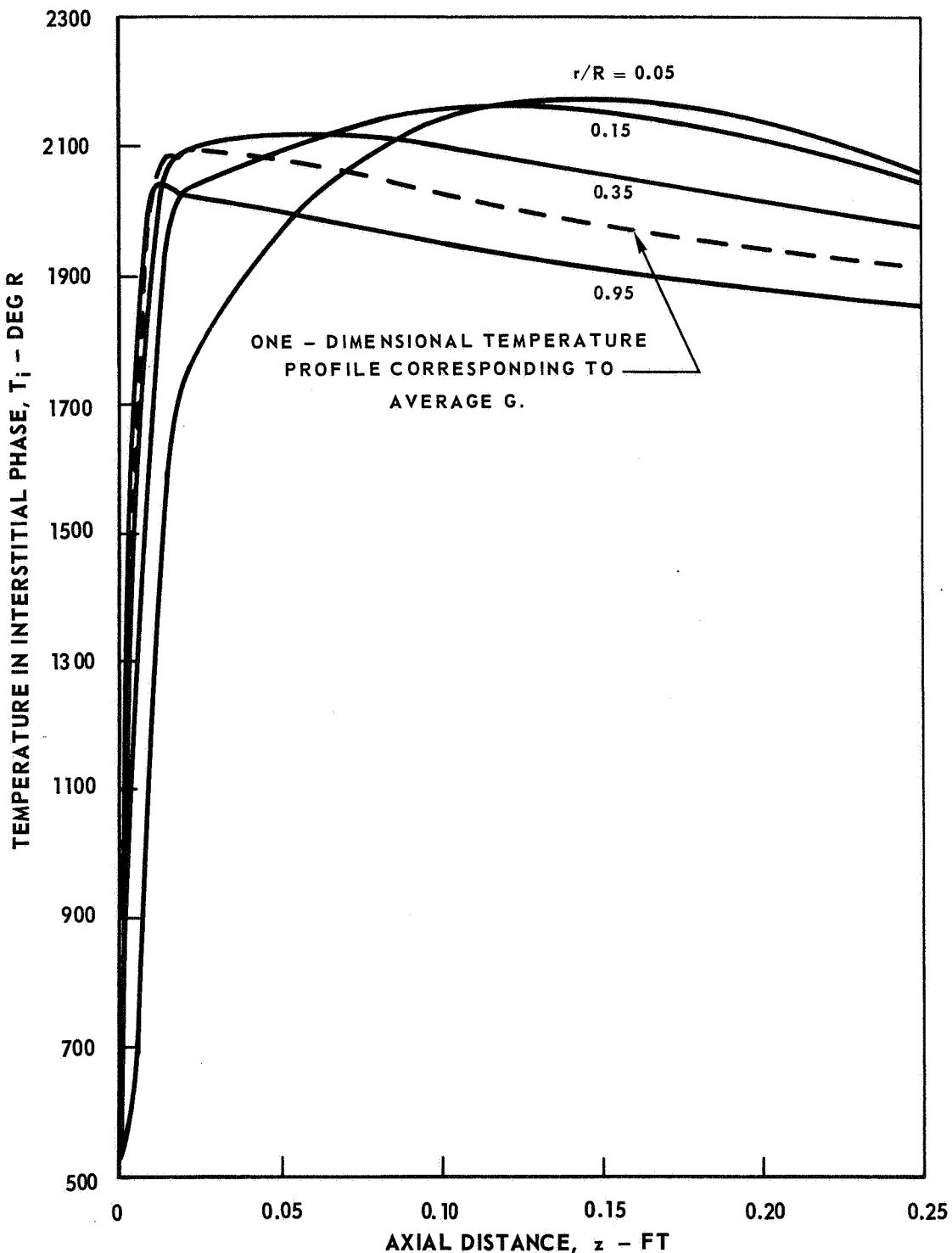


STEADY - STATE AXIAL TEMPERATURE PROFILES AT VARIOUS RADIAL POSITION

P = 100 PSIA
R = 0.125 FT

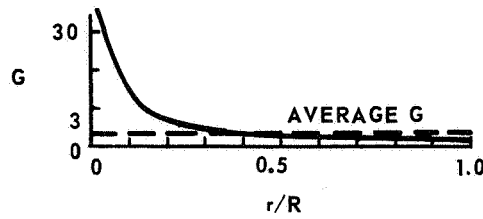


STANDARD BED
CONFIGURATION
(SEE TEXT)

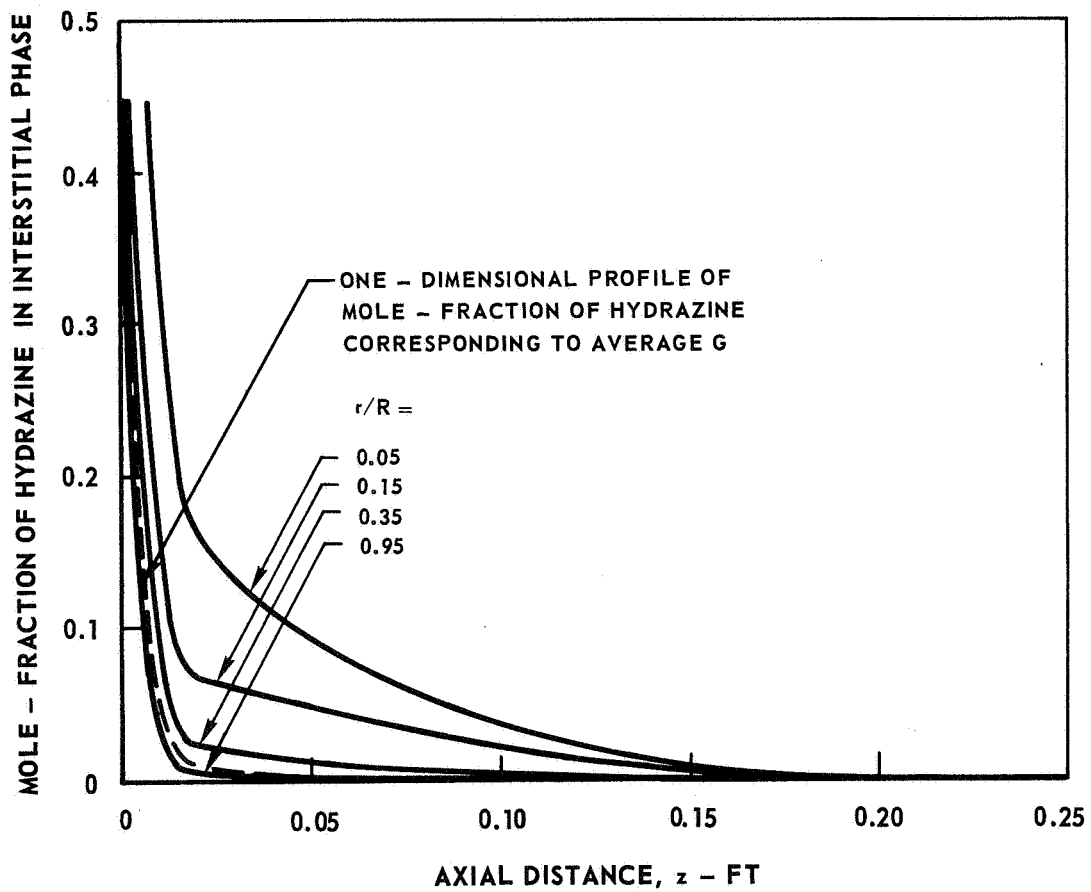


STEADY - STATE AXIAL PROFILES OF MOLE - FRACTION OF HYDRAZINE AT VARIOUS RADIAL POSITIONS

P = 100 PSIA
R = 0.125 FT

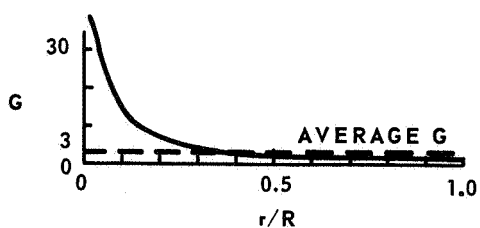


STANDARD BED CONFIGURATION
(SEE TEXT)

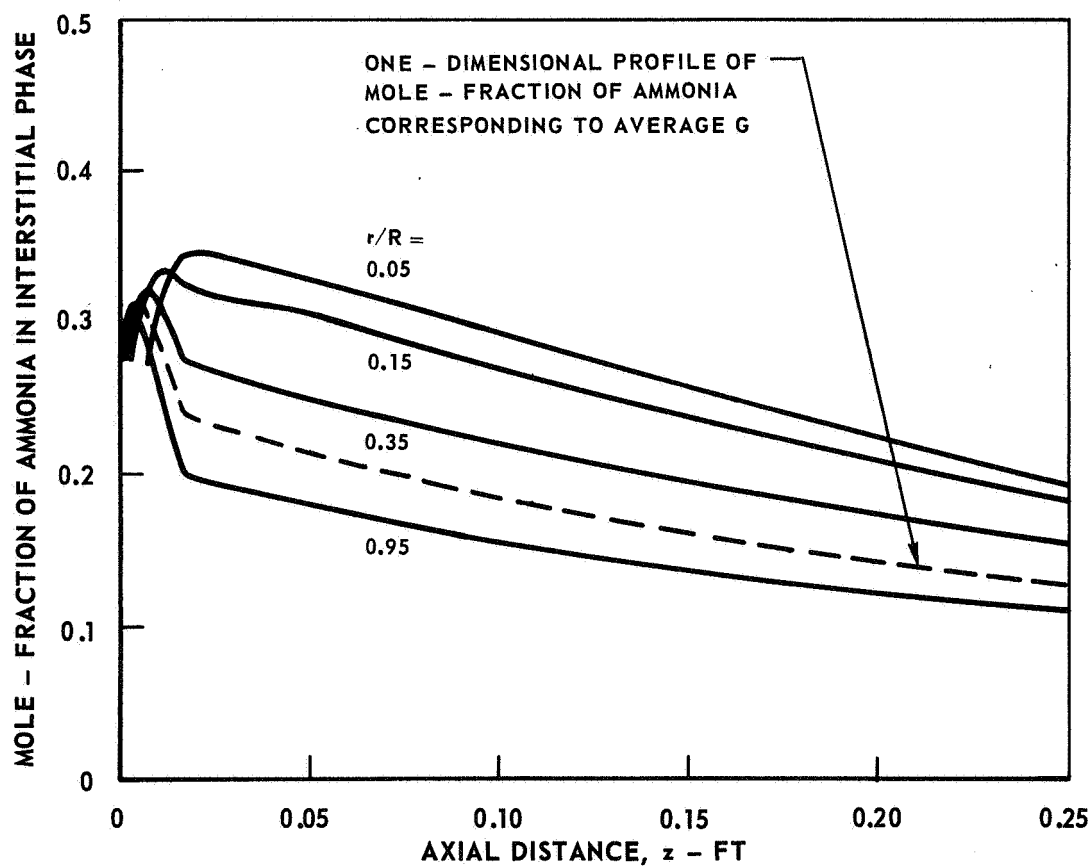


STEADY - STATE AXIAL PROFILES OF MOLE - FRACTION
OF AMMONIA AT VARIOUS RADIAL POSITIONS

P = 100 PSIA
R = 0.125 FT



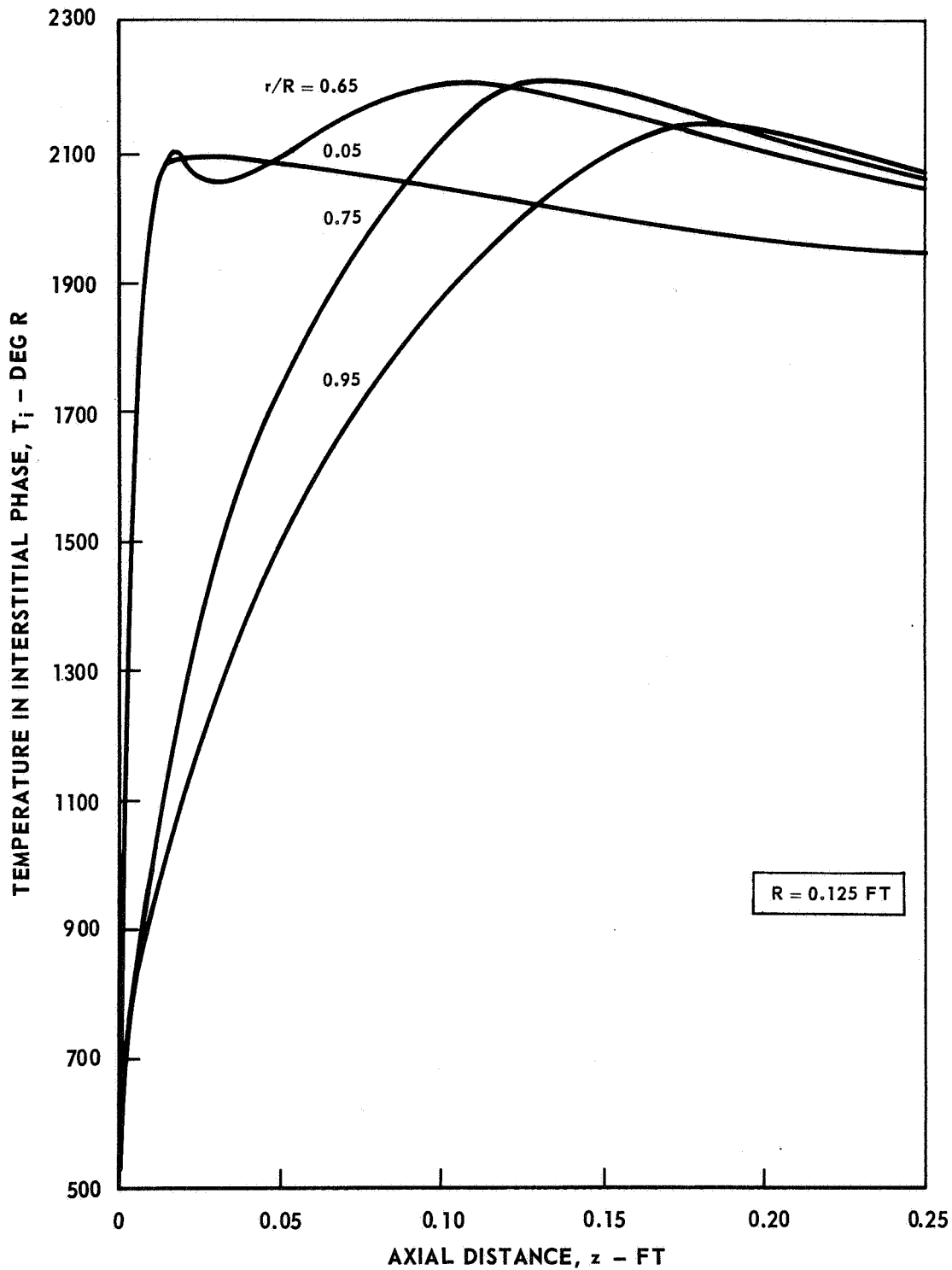
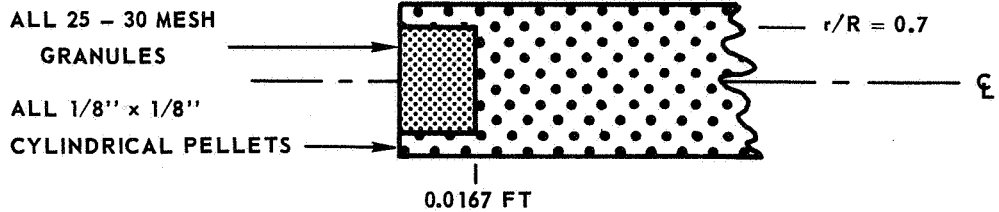
STANDARD BED
CONFIGURATION
(SEE TEXT)



STEADY - STATE AXIAL TEMPERATURE PROFILES AT VARIOUS RADIAL POSITIONS

P = 100 PSIA G = 3.0 LB/FT² - SEC

CATALYST BED CONFIGURATION:



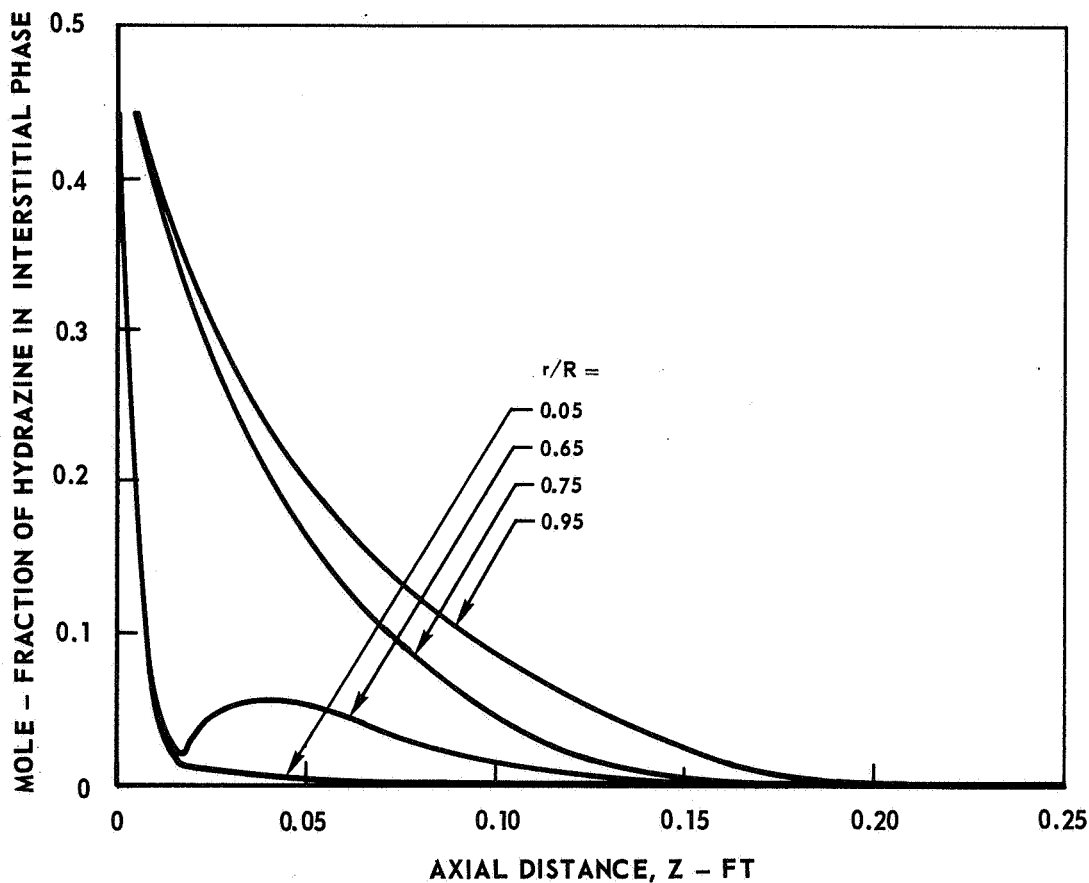
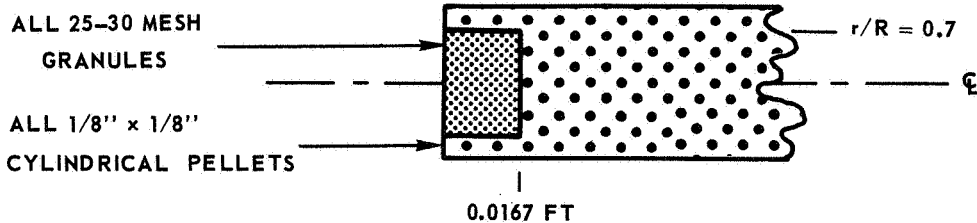
STEADY - STATE AXIAL PROFILES OF MOLE - FRACTION OF HYDRAZINE AT VARIOUS RADIAL POSITIONS

P = 100 PSIA

R = 0.125 FT

G = 3.0 LB/FT² - SEC

CATALYST BED CONFIGURATION:



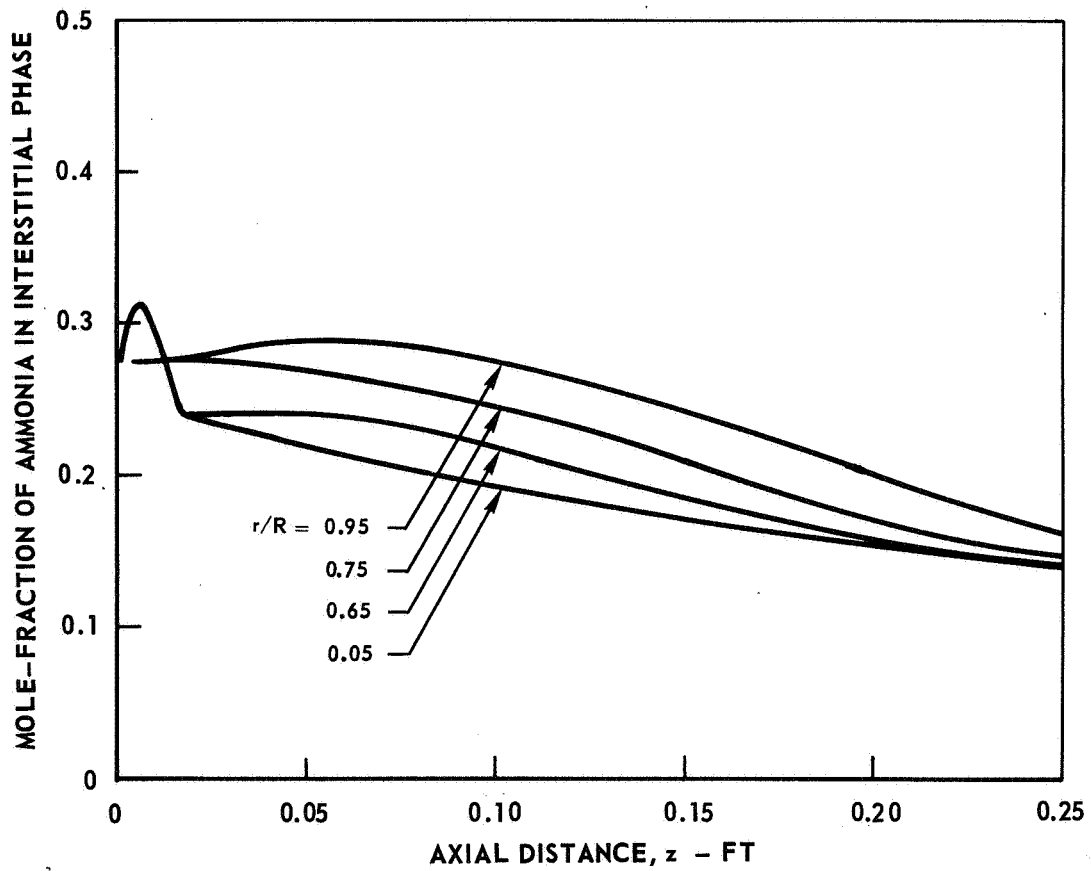
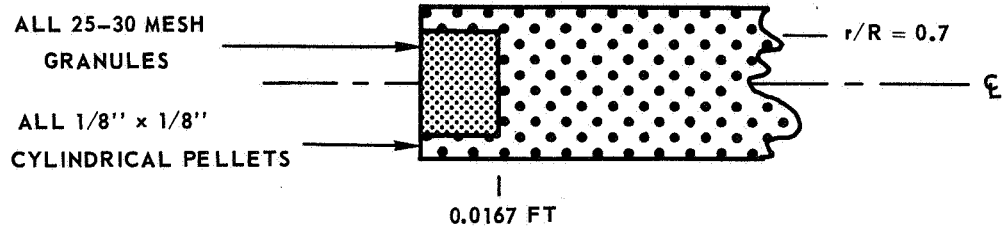
STEADY - STATE AXIAL PROFILES OF MOLE - FRACTION OF AMMONIA AT VARIOUS RADIAL POSITIONS

$P = 100 \text{ PSIA}$

$R = 0.125 \text{ FT}$

$G = 3.0 \text{ LB/FT}^2 \text{ -SEC}$

CATALYST BED CONFIGURATION:

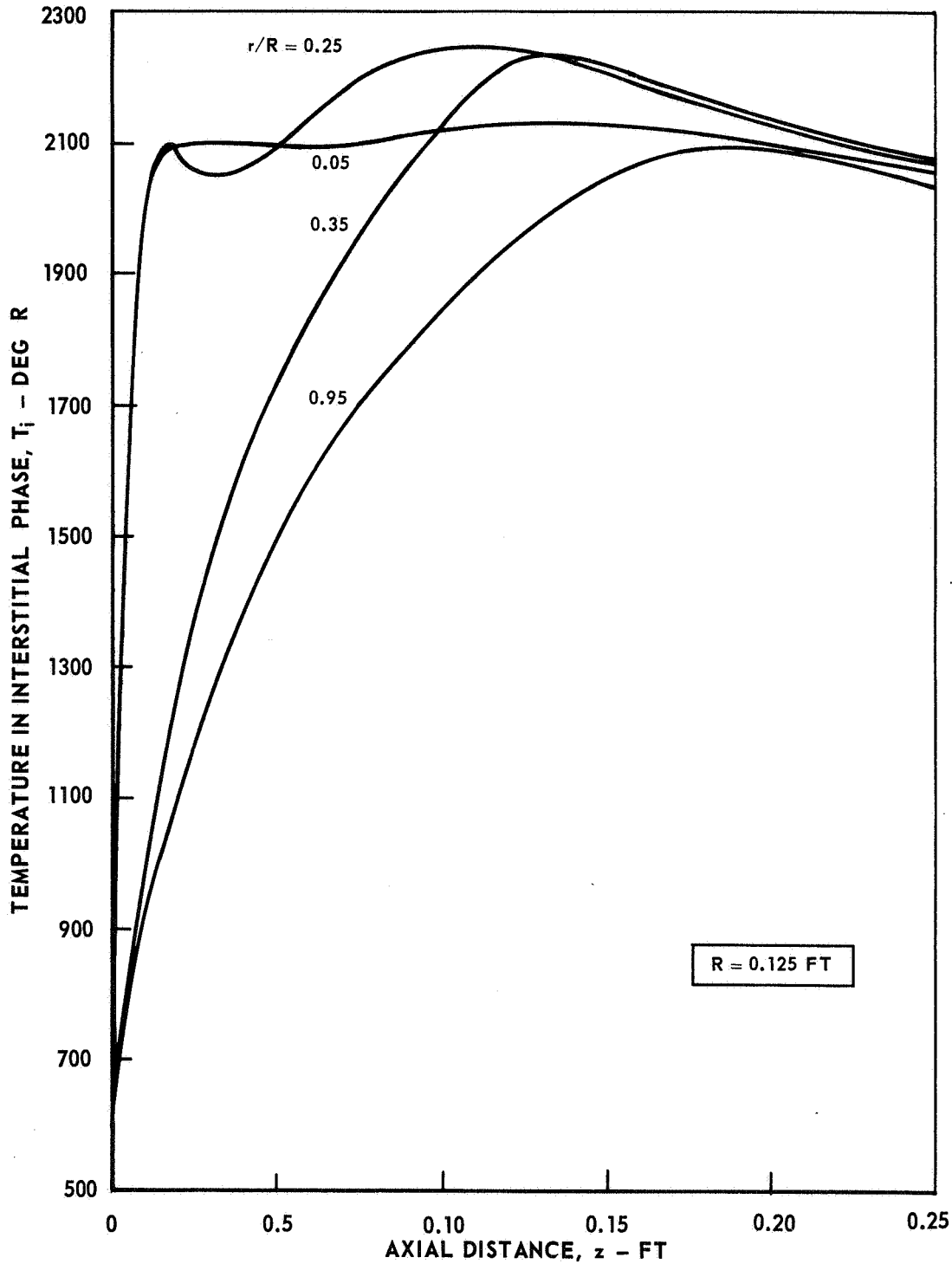
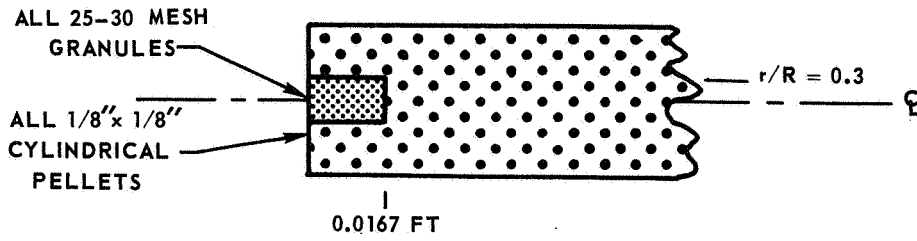


STEADY - STATE AXIAL TEMPERATURE PROFILES AT VARIOUS RADIAL POSITIONS

$P = 100 \text{ PSIA}$

$G = 3.0 \text{ LB/FT}^2\text{-SEC}$

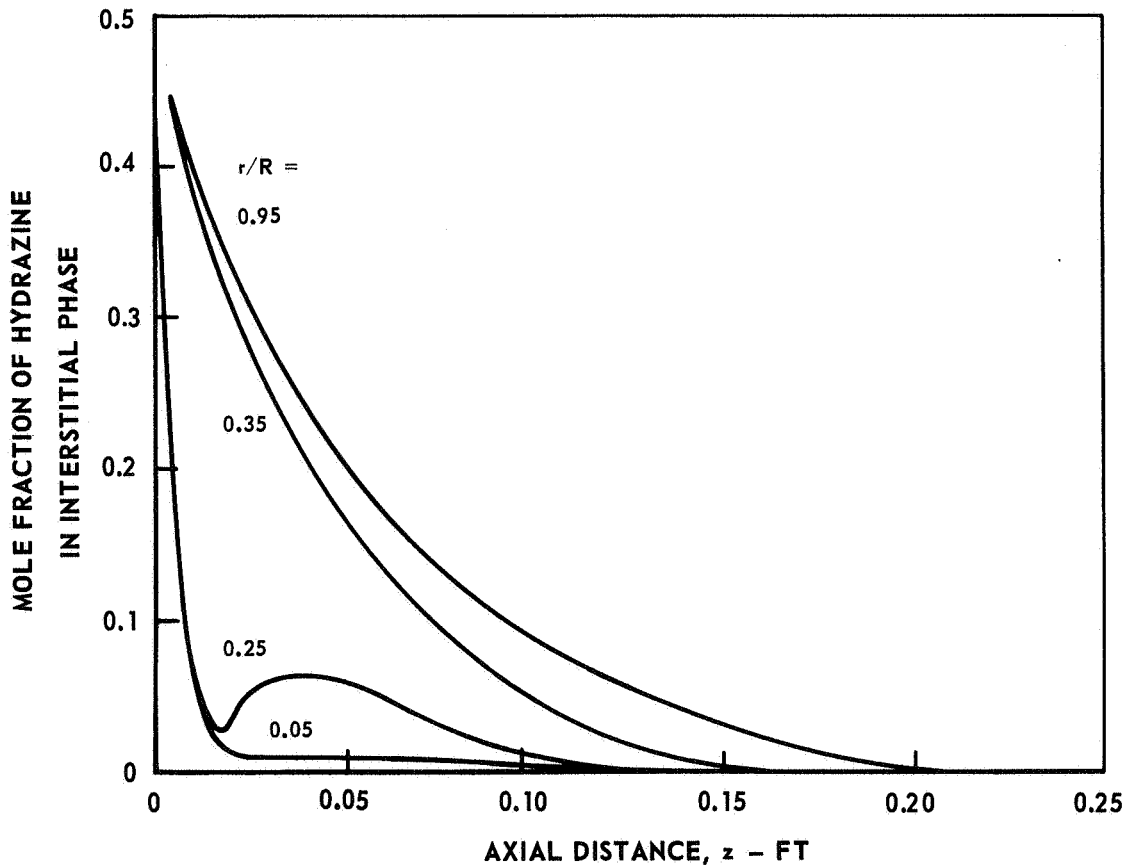
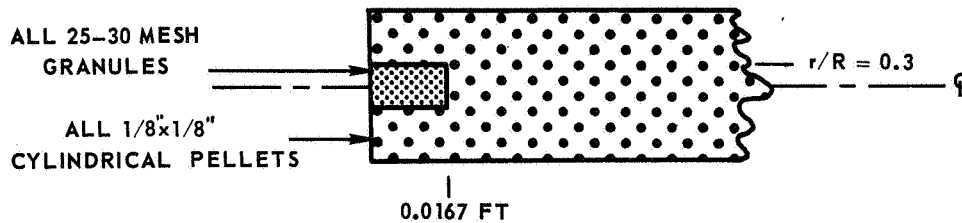
CATALYST BED CONFIGURATION:



STEADY - STATE AXIAL PROFILES OF MOLE - FRACTION OF HYDRAZINE AT VARIOUS RADIAL POSITIONS

P = 100 PSIA R = 0.125 FT G = 3.0 LB/FT² - SEC

CATALYST BED CONFIGURATION:



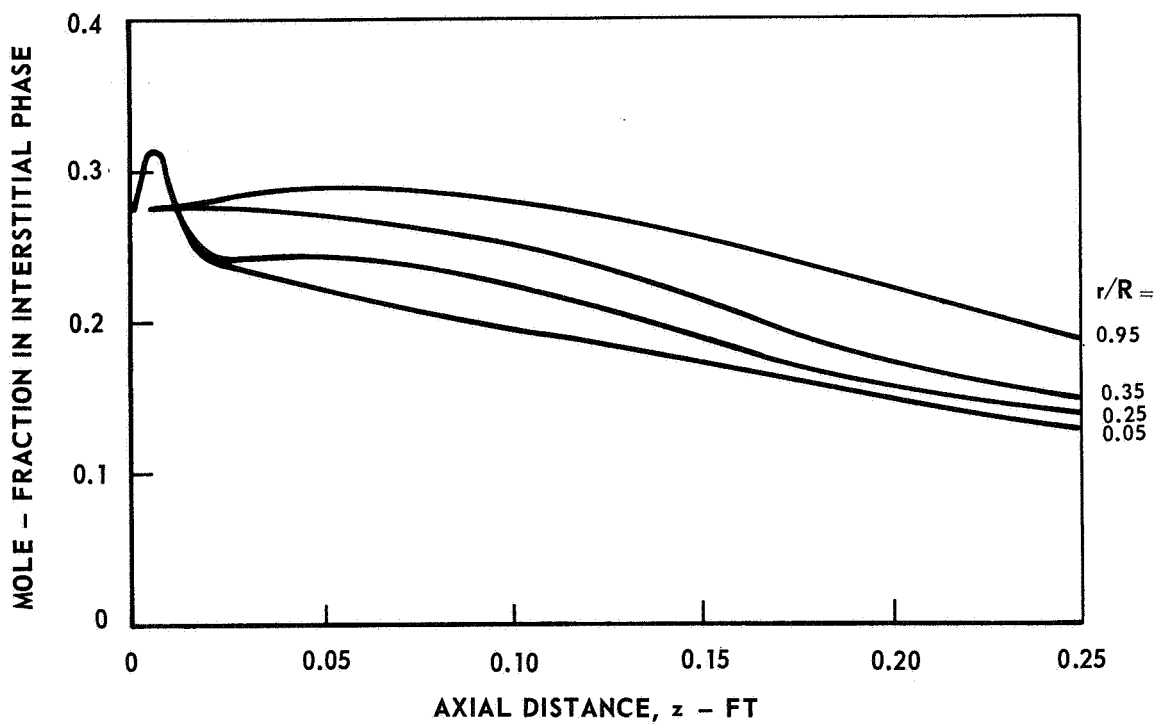
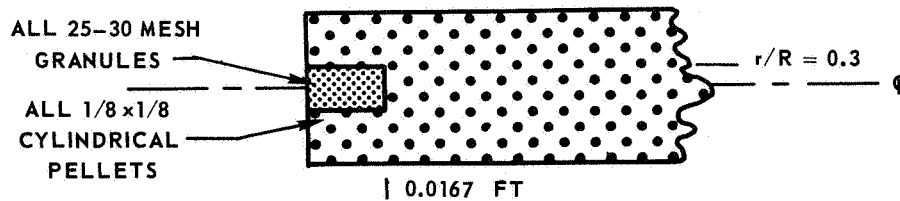
STEADY - STATE AXIAL PROFILES OF MOLE - FRACTION OF AMMONIA AT VARIOUS RADIAL POSITIONS

P = 100 PSIA

R = 0.125 FT

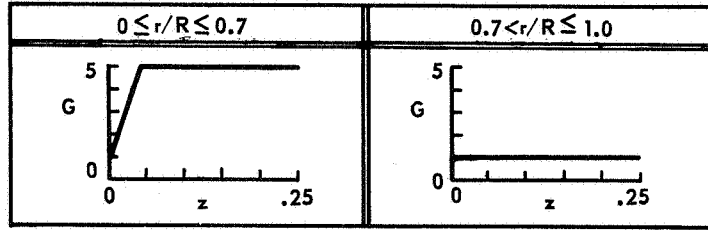
G = 3.0 LB/FT² - SEC

CATALYST BED CONFIGURATION:

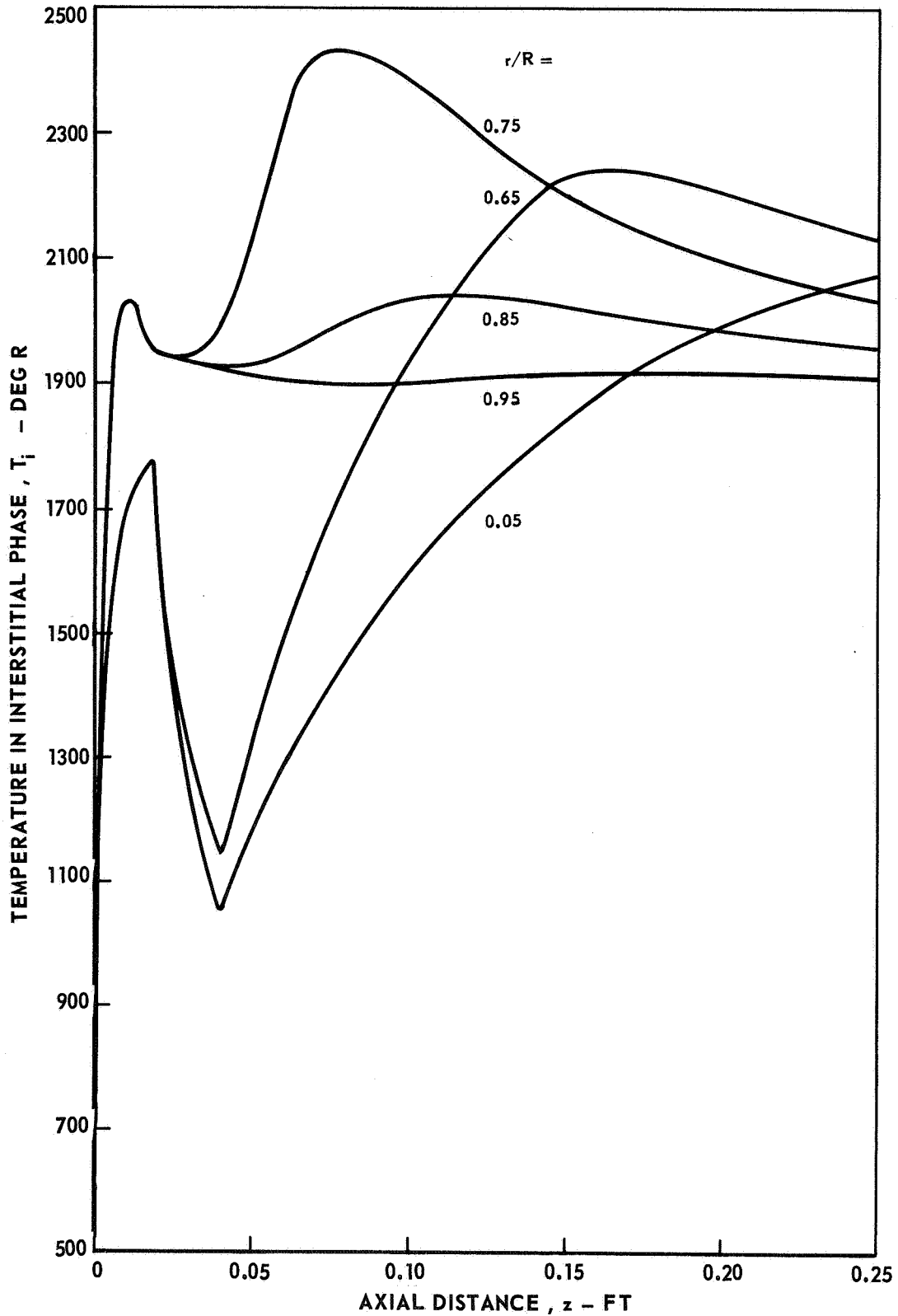


STEADY - STATE AXIAL TEMPERATURE PROFILES AT VARIOUS RADIAL POSITIONS FOR BURIED INJECTORS

P = 100 PSIA
R = 0.125 FT

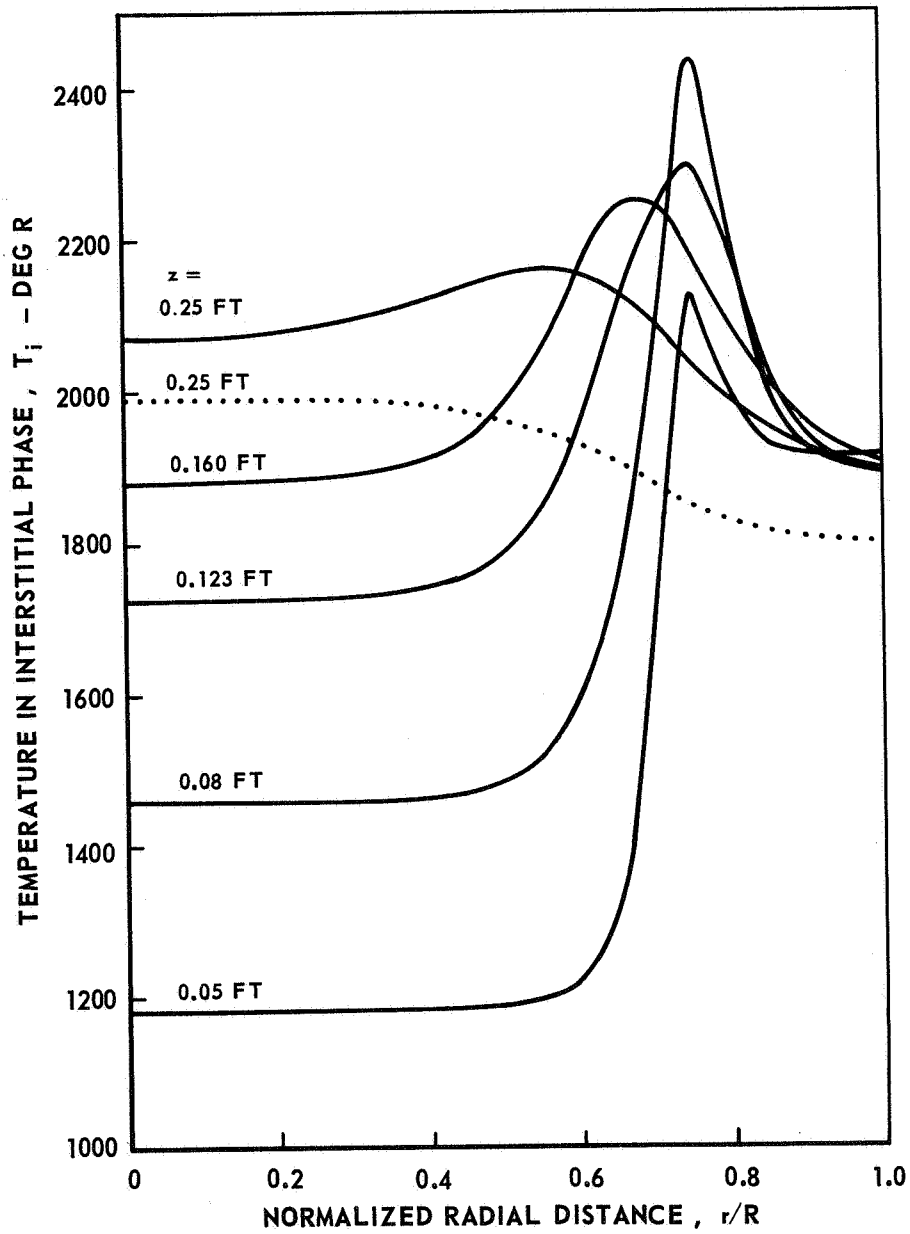
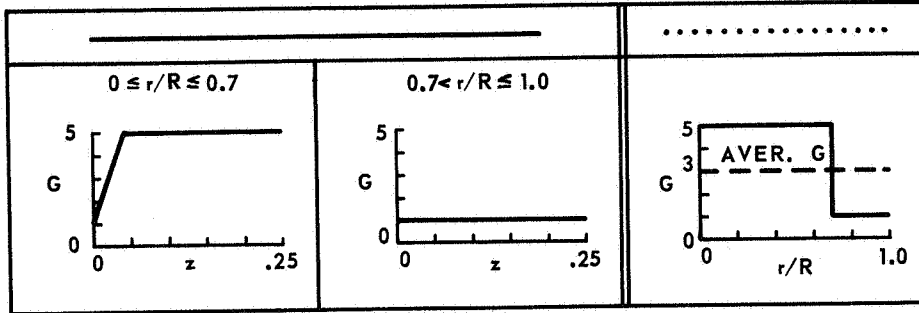


STANDARD BED CONFIGURATION
(SEE TEXT)



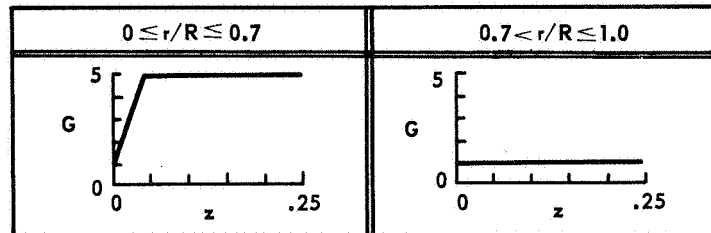
STEADY - STATE RADIAL TEMPERATURE PROFILES AT VARIOUS AXIAL POSITIONS

P = 100 PSIA R = 0.125 FT
 STANDARD BED CONFIGURATION (SEE TEXT)

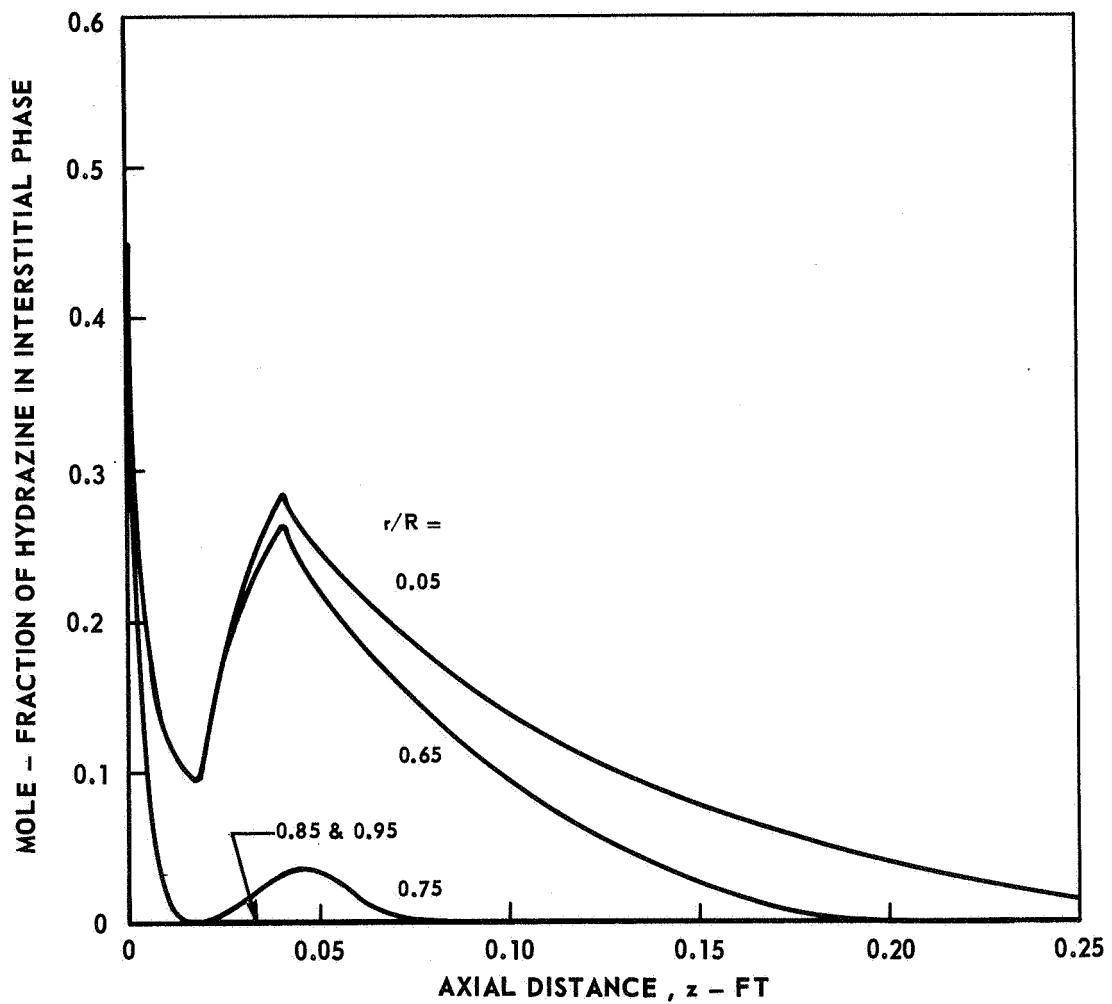


STEADY - STATE AXIAL PROFILES OF MOLE - FRACTION OF HYDRAZINE AT VARIOUS RADIAL POSITIONS FOR BURIED INJECTORS

P = 100 PSIA
R = 0.125 FT

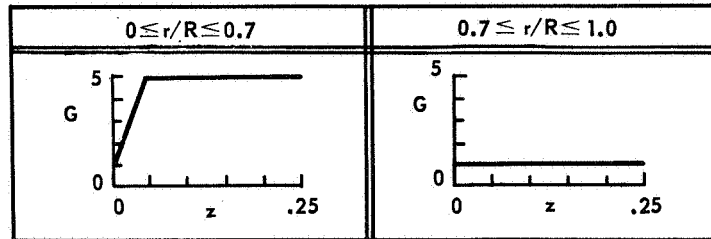


STANDARD BED
CONFIGURATION
(SEE TEXT)

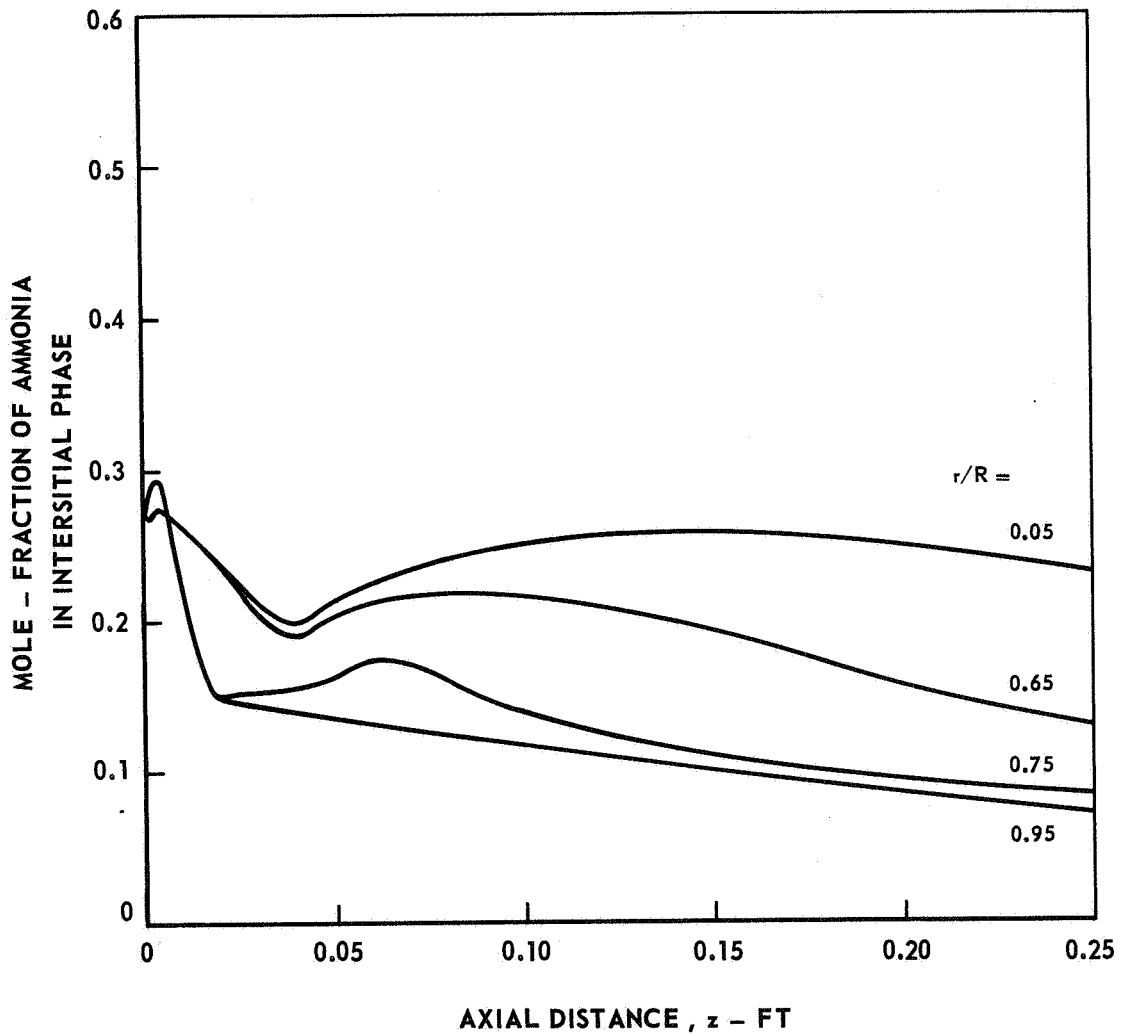


STEADY - STATE AXIAL PROFILES OF MOLE - FRACTION OF AMMONIA
AT VARIOUS RADIAL POSITIONS FOR BURIED INJECTORS

P = 100 PSIA
R = 0.125 FT

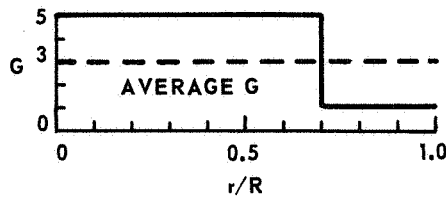


STANDARD BED
CONFIGURATION
(SEE TEXT)

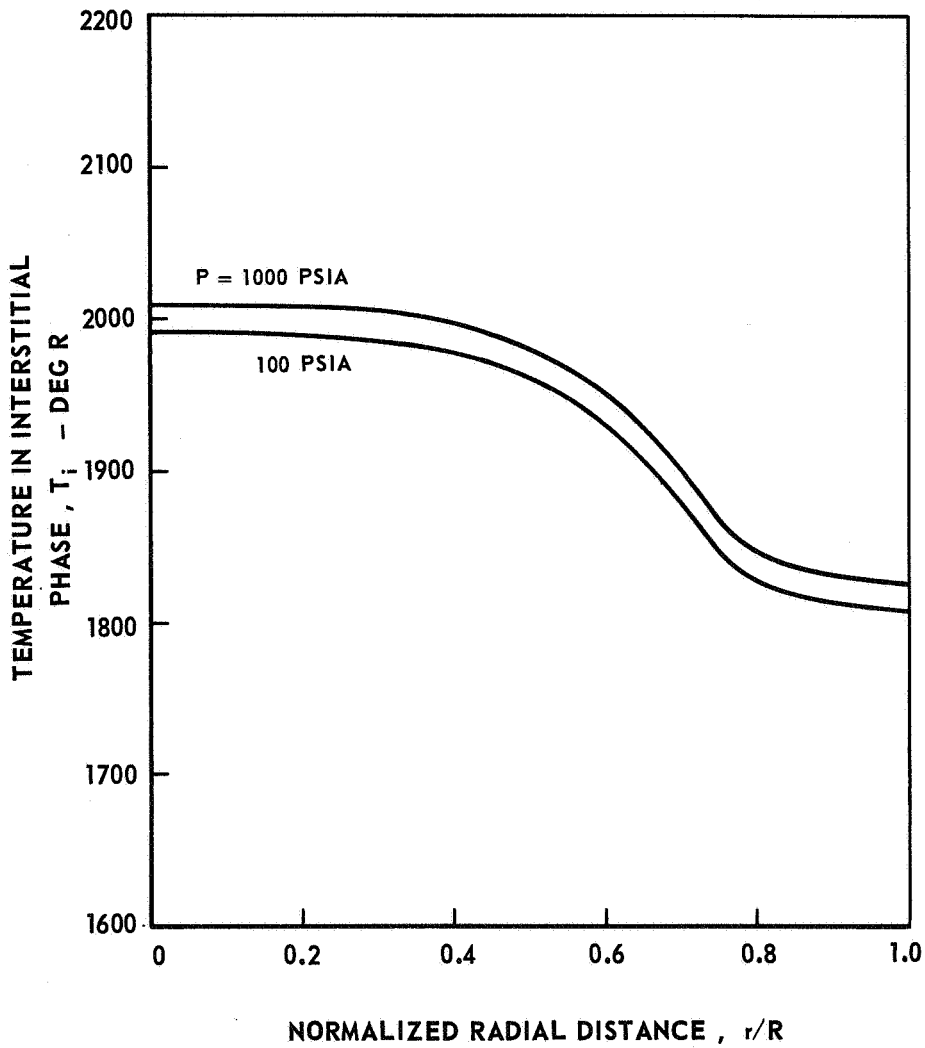


EFFECT OF PRESSURE ON STEADY - STATE RADIAL TEMPERATURE PROFILE AT EXIT OF 3 INCH BED

R = 0.125 FT

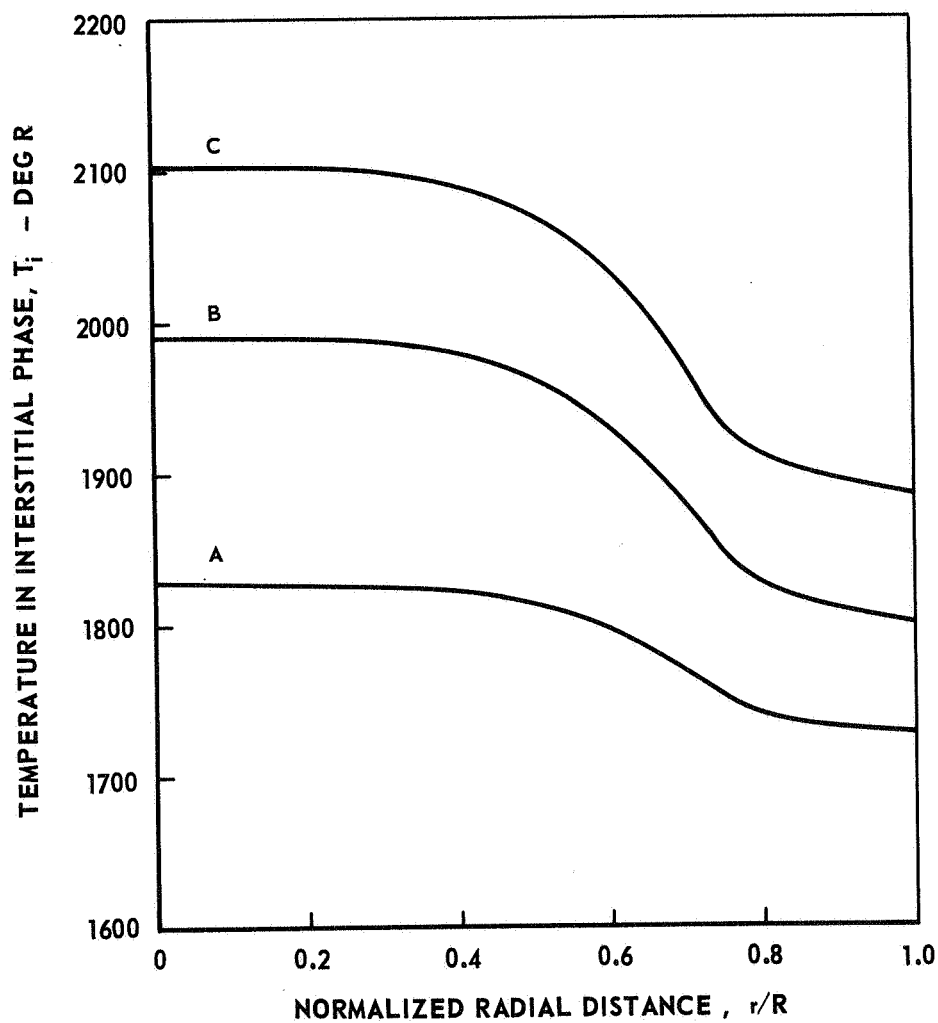
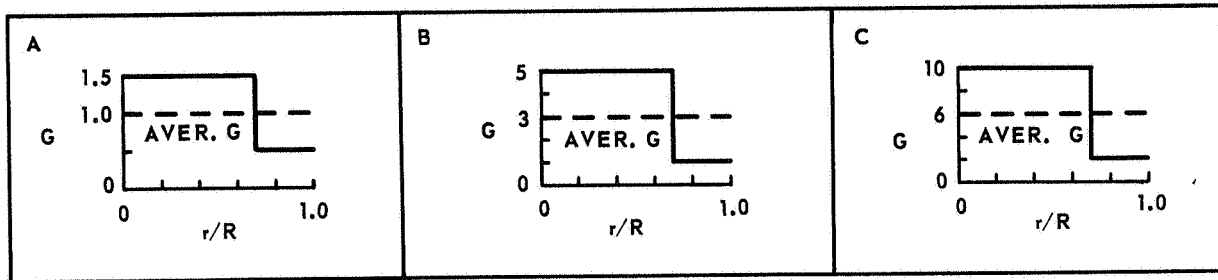


STANDARD BED CONFIGURATION (SEE TEXT)



EFFECT OF MASS FLOW RATE ON STEADY - STATE RADIAL TEMPERATURE PROFILE AT EXIT OF 3 - INCH BED FOR A GIVEN INLET INJECTION PROFILE

P = 200 PSIA R = 0.125 FT
STANDARD BED CONFIGURATION (SEE TEXT)



EFFECT OF INLET INJECTION PROFILE ON STEADY-STATE RADIAL TEMPERATURE PROFILE AT EXIT OF 3-INCH BED

P = 100 PSIA R = 0.125 FT
 STANDARD BED CONFIGURATION (SEE TEXT)

